CHEMICAL REVIEWS

pubs.acs.org/CR

Review

Gyroscopes and the Chemical Literature, 2002−2020: Approaches to a Nascent Family of Molecular Devices

Andreas Ehnbom and John A. Gladysz*

Cite This: *Chem. Rev.* 2021, 121, 3701−3750

Read Online

ACCESS | Metrics & More | Article Recommendations

ABSTRACT: Research directed toward the goal of molecular gyroscopes since the coverage of a previous review (2002) is described. Such species are a subclass of molecular rotors, which are comprised of rotators and stators. Major categories include (1) systems in which a rotator is embedded in a cage-like stator reminiscent of mechanical toy gyroscopes and (2) molecules that have been engineered to crystallize with parallel rotators and voids or other features that enable the rotator to rotate in the solid state (amphidynamic crystals). Particular attention is given to structural data and strategies for the minimization of rotational barriers. Synthetic routes are also described. Some allied types of molecules and supramolecular assemblies are also treated.

CONTENTS

1. INTRODUCTION TO GYROSCOPES

Gyroscopes are ubiquitous in everyday life[1−3] although they are often kept out of view, in part due to the general desirability of shielding moving components in mechanical assemblies. Thus,

Received: September 16, 2020
Published: February 26, 2021

https://dx.doi.org/10.1021/acs.chemrev.0c01001
Chem. Rev. 2021, 121, 3701−3750

they are less familiar to the public than other types of machines and devices. Nonetheless, many children have been introduced to toy mechanical gyroscopes, typical examples of which are illustrated in Figure 1 (panels a and b). With a little practice, these can be coaxed into a number of "tricks", such as tabletop precession or funambulism (tightrope walking). However, these phenomena do not play roles in the numerous practical applications of gyroscopes.[1−3]

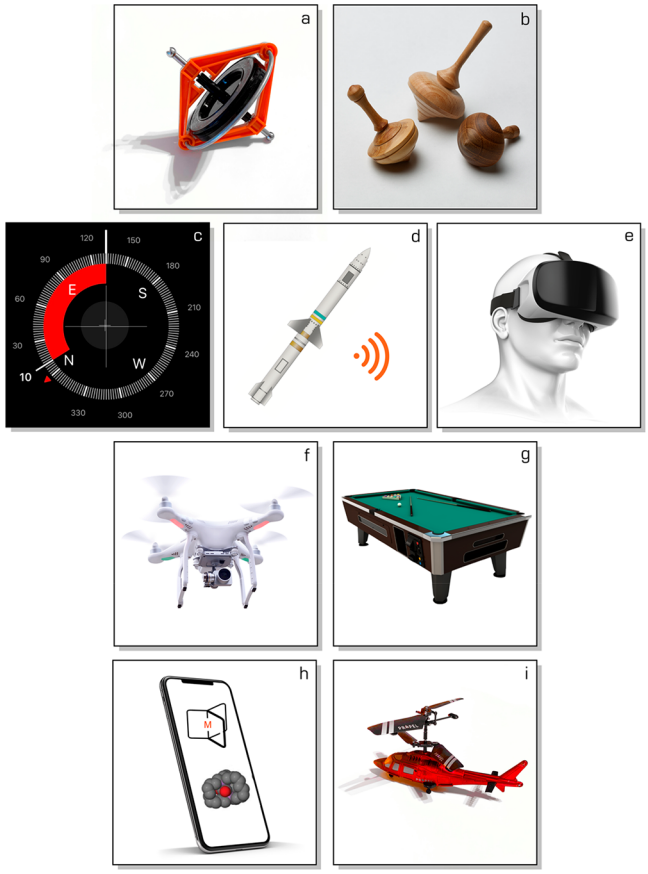

Figure 1. Toy mechanical gyroscopes (panels a and b) and some practical applications of gyroscopes (panels c−i).

The practical applications usually involve some aspect of the orientation of an object. They include antiroll stabilizers in seagoing vessels and high speed trains, railroad track occupancy monitors, automotive safety systems, gyrocompasses in drones and airplane autopilots, space station orientation and navigational systems, virtual reality headsets and other wearable technology (e.g., relating to fitness or fall protection), wireless computer pointing devices, and the display orientation and gaming controls of mobile phones (panels c−i, Figure 1).[1−11] Some non-everyday applications that underscore the broad applicability of gyroscopes include stabilizing the horizontal surfaces of pool tables[12] and Iron Man's flying suit.[13] Furthermore, properties associated with gyroscopes are exploited in various aspects of race car and motorcycle stabilization.[1,14]

The useful attributes of mechanical gyroscopes derive from the conservation of angular momentum,[15−17] and the toy version in panel a of Figure 1 provides a useful point of reference. The most critical component is the flywheel. As with many devices with rotating elements, the flywheel is typically sterically insulated with a "belt" and "spokes". However, these are not essential for function. When the rotating flywheel is tilted from the plane in which it is initially set in motion, there is a restoring force to realign the flywheel with the original plane. This can easily be felt in the wrist when so slanting a spinning toy gyroscope.

There are a variety of newer designs for gyroscopes, many of which are based upon vibrating as opposed to rotating components.[17−21] These can have exotic sounding names, such as "wine glass resonator" or "Coriolis vibrating" gyroscopes. Some can furthermore be designated as "micro-electromechanical systems" (MEMS)[22] or "quantum" gyroscopes.[23−28] Regardless of type,[29] molecular analogs remain unknown. When Steve Jobs gave his roll out presentation of the iPhone gyroscope, which controls the orientation of the screen display and enables various gaming functions, an image of a mechanical gyroscope was projected onto the screen at the rear of the stage.[30] However, in reality, one of the newer vibrating architectures was utilized.

Importantly, the physics of a mechanical gyroscope[15−17] holds at a molecular level.[31] Thus, in the ongoing quest to miniaturize devices, molecular gyroscopes would seem to be unbeatable. They also constitute a subclass of an extensive body of molecules that have been termed "molecular rotors".[31,32] Formally, rotors are comprised of rotating and nonrotating substructures. However, motion is always a function of the frame of reference. Thus, the convention is to consider the substructure with the greater moment of inertia to be stationary and hence termed the "stator". Similarly, the substructure with the lower moment of inertia is termed the "rotator". Some stators consist of two nonbonded components that cap the termini of a rotator, and these will often be referred to as "endgroups".

2. SCOPE OF REVIEW

As follows from the previous paragraph, molecular rotors are ubiquitous, with a compound as simple as ethane qualifying. Accordingly, the universe of molecules that might be able to function as gyroscopes is enormous. It is not the purpose of this review to collect all examples. Rather, the focus is on studies where the investigators have explicitly sought to access molecules or families of molecules that in their view hold promise as functional molecular gyroscopes. In most cases, these have featured sterically shielded rotators.

In an earlier review,[33] the authors sought to comprehensively cover the interface of gyroscopes and the chemical literature through 2002. This included all compounds for which any type of link to a gyroscope was claimed. As would be expected, some were more relevant than others, and a few especially germane systems are treated again below. The coverage in the present review is also quite liberal with respect to author claims. A cutoff date of 01 July 2020 is generally applied to cited literature.

In order to help readers appreciate the basis for selecting the new literature, the next section describes, in general terms, the currently most popular approaches to achieving functional molecular gyroscopes. Additional strategies have been suggested[31] but seem to have a greater number of practical obstacles.

https://dx.doi.org/10.1021/acs.chemrev.0c01001
Chem. Rev. 2021, 121, 3701−3750

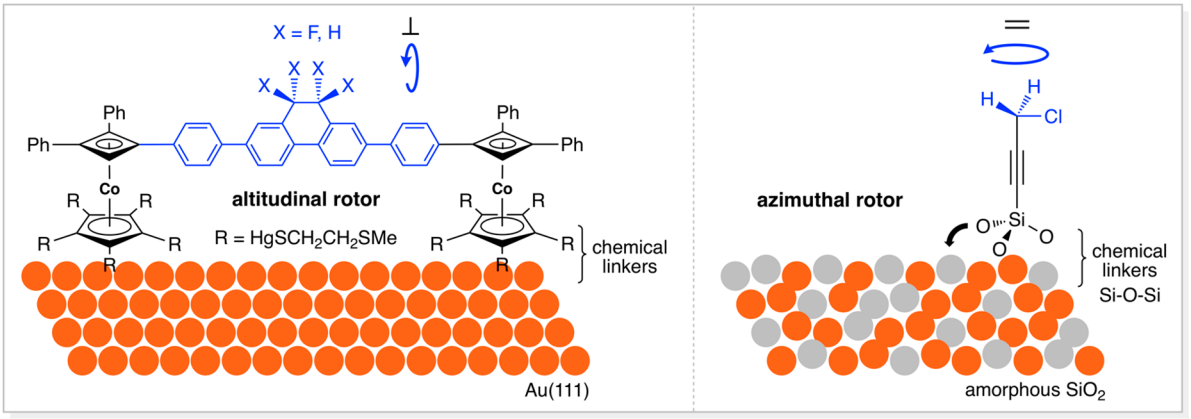

Figure 2. Limiting types of surface mounted rotors, illustrated with literature systems.

3. STRATEGIC CONSIDERATIONS: FUNCTIONAL MOLECULAR GYROSCOPES

For a molecular rotor or a suitable ensemble or bulk sample thereof to function as a gyroscope, all rotators must rotate unidirectionally, that is, clockwise or counterclockwise, as opposed to randomly (Brownian). This generates angular momentum analogously to a macroscopic mechanical gyroscope. Thus, something that will enforce non-Brownian rotation, akin to pulling the string on the toy gyroscope in panel a of Figure 1, is required.

The most frequently presented and easily visualized means of implementing such unidirectional rotation requires the introduction of a dipole moment on the rotator, giving what is termed a "dipolar rotator" or, considering the entire molecule, a "dipolar rotor".[31] A static electric field can then orient the rotator. Rotors thus treated have been termed molecular compasses.[34−37] Similarly, an electric field that rotates at an appropriate frequency can drive unidirectional rotation of the rotator.[31,38−46] However, any compound with a dipolar rotator also possesses a molecular dipole. A complication in these scenarios is that the electric field may drive "whole molecule" orientation or rotation, processes that would often be of lower energy than the rotation of a rotator embedded in a stator. Although there may be ways to exploit whole molecule rotation, this would frequently be a deal-killer. Furthermore, in many types of ensembles or bulk samples the axes of the rotators would be arrayed in different directions, leading to variable degrees of interaction with an electric field.

An alternative approach would involve immobilizing the molecules in a manner that renders all rotator axes parallel and only the rotators capable of rotating. One strategy would involve mounting the rotors on a surface.[31,38,42−51] Two limiting orientations can be envisioned, altitudinal (rotator axes parallel to the surface) and azimuthal (axes perpendicular to the surface).[38,42,43] Several elegantly designed systems have been studied by Michl,[31,38,39,42−46,49−51] both experimentally and computationally. Examples are illustrated in Figure 2. Sykes has also published a number of relevant studies.[52−57]

However, with surfaces to which multiple altitudinal rotors have been attached, there is no *a priori* means of ensuring that the rotators are mutually parallel. In contrast, the rotator axes in any ensemble of *rigorously* azimuthal rotors must be parallel (some types of surfaces and anchoring moieties may be more amenable to this idealized orientation than others).

Since the specific rotors illustrated in Figure 2 are dipolar, there are opportunities for various experiments involving electric fields. Detailed molecular dynamics simulations of the response of the azimuthal rotor in Figure 2 to rotating electric fields have been carried out, with particular attention to the effects of field strength, frequency, and temperature.[44] The altitudinal rotor in Figure 2 has been studied experimentally in static electric fields and computationally in oscillating electric fields.[46] Another goal with the altitudinal system has been to drive the rotator using a flowing stream of molecules.[38,42,43,58,59] For some of these studies, computational simulations (movies) are available.[58,59] The electrical stimulation of surface bound rotators with STM tips has also been investigated.[52−57]

A second approach to realizing ensembles of rotors with parallel rotators would involve crystallization. Naturally, molecules can crystallize in numerous ways, and substrates would need to be engineered to yield lattices not only with parallel axes, but also with voids or other features that allow the rotator to rotate with a minimal energy barrier. Both intra- and intermolecular van der Waals contacts must be avoided or minimized. Cage-like superstructures or scaffolding would be one approach to enforcing voids.

Crystals in which components or subunits of the molecules can rotate are said to be amphidynamic, a term coined by Garcia-Garibay.[34−37] Although some luck is involved in any effort to tailor a crystal lattice, there have been some notable successes in the direction of molecular gyroscopes, as described below. Furthermore, there is an ever growing body of MOFs and related species that offer geometrically well-defined scaffolding for rotators and often feature large void spaces,[60,61] as detailed below. Porous materials can also be exploited as hosts for dipolar rotors, as illustrated in section 9.3.

Some other design considerations merit emphasis. For example, nonionic compounds are preferred. Any counterions can electrostatically interact with dipolar rotators as they rotate. The resulting attractive and repulsive domains can lead to increased rotational barriers. Also, any structural or electronic modification that can lower the rotational barrier, sometimes spoken of as "intramolecular friction", is desirable. For example, if the rotating electric field were disengaged, the rotators of systems with lower barriers would continue their unidirectional trajectories for longer periods of time. Indeed, rotors that are essentially barrierless are being increasingly documented,[62] as further exemplified in section 8.3 below.

https://dx.doi.org/10.1021/acs.chemrev.0c01001
Chem. Rev. 2021, 121, 3701−3750

An additional consideration is the means by which electric fields can be applied to samples. To the authors' knowledge, there is no "off the shelf" instrumentation capable of delivering a rotating electric field, although experimental protocols have been described.[31] However, there is an established technique, dielectric spectroscopy, that delivers an oscillating electric field, that is, one that "flips" back and forth by 180°.[63−65] This instrumentation is commercially available and has numerous applications, although it is not very familiar to chemists and the review literature is geriatric.[63−65] Typically, the change in capacitance, which is a function of the molecular dipoles in the bulk sample, is measured. The resonance frequency that would be established for dipole oscillation would be correlated to the rotational frequency of an electric field necessary to drive unidirectional rotation.

Functional molecular gyroscopes would be characterized by a number of testable properties. Probably the most intuitive are associated with the conservation of angular momentum. Thus, with respect to the "flywheel" component, if this plane were to be tilted, a measurable force would be required. Similarly, there would be a comparable driving force for restoring the original orientation of the flywheel plane.

4. SELECTED BACKGROUND MOLECULES

4.1. Molecular Turnstiles

Of the types of molecules treated in the previous review,[33] one class deserves emphasis. Specifically, compound **1** in Figure 3, which was synthesized by Moore,[66] represents what is often termed a "molecular turnstile". These are now being exploited in various contexts by a vigorous community of researchers,[67−86] of which the Hosseini group is the most prolific.[73−86]

Definitions of molecular turnstiles have been given in several papers.[71,72,77,82,83,85,86] These can, in the context of this review, be paraphrased as "molecular rotors that exhibit bistability in the sense of the rotator being able to adopt what can be viewed as *open* and *closed* states". In the most common motif, exemplified by **1** and **2** in Figure 3, both the stator and rotator are roughly planar or two-dimensional.[66,67] The turnstile is "open" when these planes are perpendicular, and "closed" when they are parallel or nearly so. There are also a fair number of what might be termed "half turnstiles", as illustrated by **3** in Figure 3.[69−71] The rotators in these systems are not entirely circumnavigated by the stators but can still be perpendicular or parallel with respect to the plane of the stator.

In another variant, the stator or rotator becomes complete only when an "effector" is added. For example, **3** is prepared by combining the palladium(II) effector $(MeCN)_2PdCl_2$ with the free bis(alkynylpyridine) ligand.[70] In a more complex variant, **4** can be viewed as a half turnstile with a 4-pyridyl−C≡C−Pt−C≡C−4-pyridyl rotator and a P−Pt−P axis.[81] When the appropriate palladium species is added, **5** results. This can be viewed as a "full" turnstile with a 4-pyridyl rotator and a Pt−C≡C−4-pyridyl−Pt axis, and now with the P−Pt−P axis "locked down".

In these efforts, there have not to the authors' knowledge been any connections to the molecular gyroscope literature, although there is one study that involves the interaction of a dipolar rotator with an electric field.[72] An issue would be the lack of "steric protection" for the rotator when it is in the "open" position, with the plane perpendicular to that of the stator. Thus, molecular turnstiles are not included in the sections below detailing the main avenues of approach to molecular gyroscopes. However, there are probably ways to engineer sterically more protected systems, for example, by introducing appropriately bulky R′ groups in **1** (Figure 3), so this class of molecules merits consideration for future research.

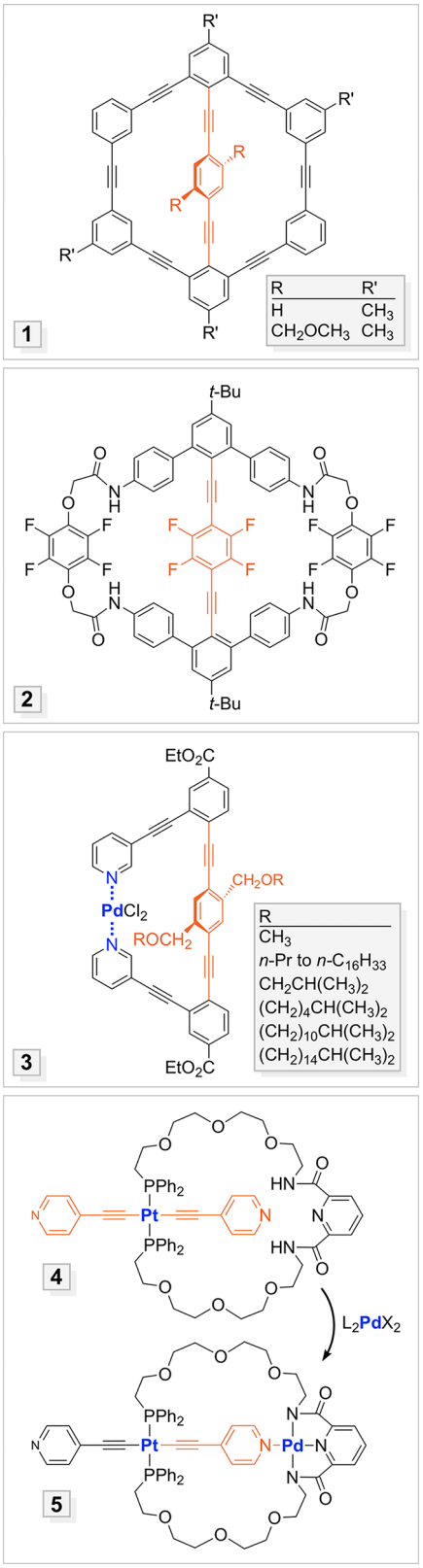

Figure 3. Representative compounds that have been described as molecular turnstiles.

https://dx.doi.org/10.1021/acs.chemrev.0c01001
Chem. Rev. 2021, 121, 3701−3750

4.2. Species with N−ML_2−N Rotators Where N Denotes a Disubstituted Pyridine Ligand

An important compound topologically related to the preceding turnstile systems was reported in 1999 by Lambert,[87] who left academia shortly thereafter. He first prepared the *trans*-palladium bis(pyridine) complex **6** shown in Figure 4 (top), in which the 2 and 6 pyridine positions (adjacent to the nitrogen atom) feature alkene containing $CH_2CH_2CH{=}CH_2$ substituents. This complex underwent 2-fold *interligand* ring closing olefin metathesis with Grubbs' first generation catalyst to yield what could be termed a pyridinophane adduct (**7**). Such ring closing metatheses commonly give *cis*/*trans* C=C mixtures, but the *cis*,*cis* isomer crystallized, and an X-ray structure could be obtained.

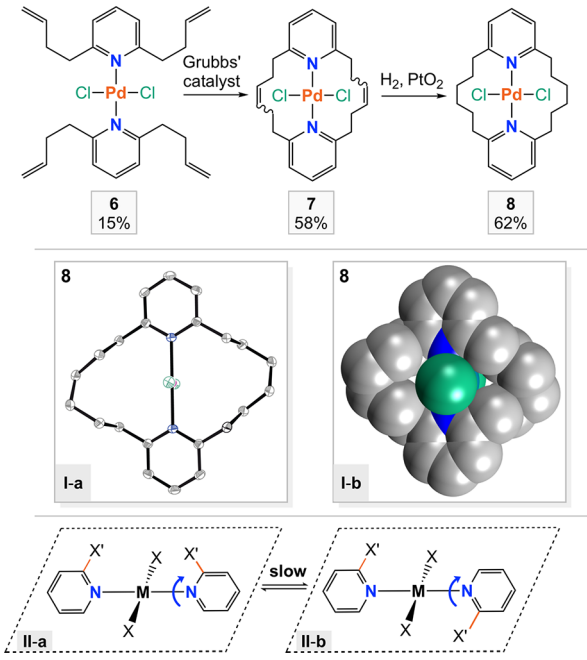

Figure 4. Ring closing metathesis reaction that connects 2,6-disubstituted *trans*-pyridine ligands (top), ORTEP and space filling representations of the hydrogenation product **8** (middle), and atropisomers arising from restricted pyr−M−pyr rotation in related square planar systems (bottom).[87,88]

In subsequent efforts in the authors' laboratory,[88] **7** was hydrogenated to give **8**. The crystal structure is shown in Figure 4 (**I-a**). As can best be appreciated from space filling models (**I-b**),[88] any 2,6-pyridine substituents effectively block $PdCl_2$ rotation. This is reflected by the perpendicular orientation of the Cl−Pd−Cl vector with respect to the pyridine ligand planes in crystalline **8** (as well as **6** and *cis*,*cis*-**7**; not depicted). Accordingly, atropisomers have been observed for a number of square planar complexes featuring two *trans*-2-monosubstituted pyridine ligands (Figure 4, bottom).[89,90]

In follow up efforts, the authors similarly prepared the dichloroplatinum pyridinophane complexes **9**−**11** shown in Figure 5.[88] In particular, **10** and **11** were viewed as attractive families of molecular rotors, as replacing 2,6-substituents by 3,5-substituents should allow $PtCl_2$ rotation. Thus, they represent functional molecular turnstiles. Also, the introduction of appropriate substituents at the 4 position ("*para*" to nitrogen) could enable surface mounting with an azimuthal rotator orientation. However, for several reasons, such as the absence of three-dimensional shielding of the rotator by the stator, these systems were not further pursued.

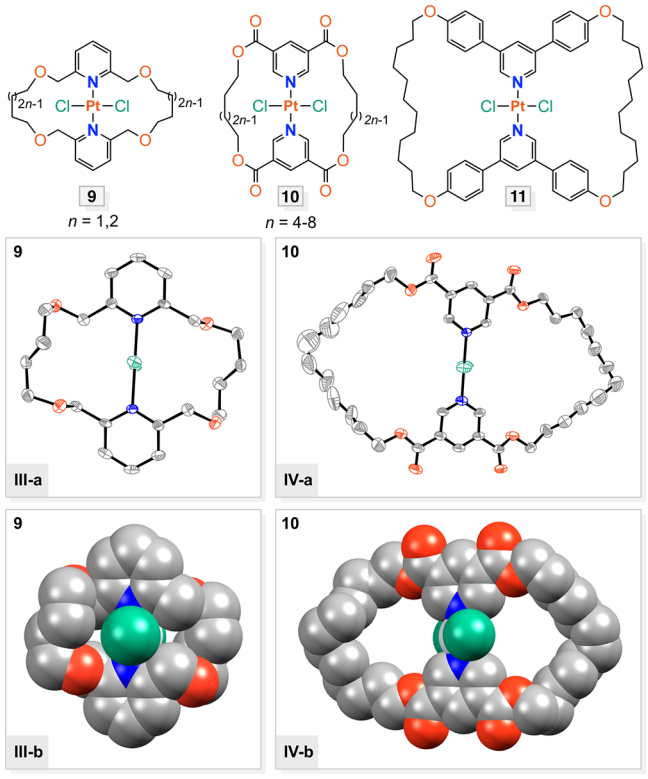

Figure 5. Additional complexes with substituted *trans*-bis(pyridine) ligands prepared by the route in Figure 4 (**9**−**11**),[88] and ORTEP and space filling representations of **9** and **10**.

4.3. Other Stators in Which Two Bridges Connect the Termini of the Rotator

With most of the compounds in Figures 3−5, the axes of the rotators terminate with sp^2 hybridized carbon or nitrogen atoms. This leaves two atoms or substituents for architectural purposes—i.e., creating the two bridges ("spokes") that comprise the stator connecting the termini of the rotator.

One can also consider the generation of two bridges between atoms that bear three substituents, which would generally have tetrahedral or (for heteroatoms with a lone pair substituent) trigonal pyramidal geometries (approximate sp^3 hybridization). Such systems have in fact been crafted, as summarized in Figures 6 and 7.[91−96] In some cases, the syntheses were carried out as intermediate feasibility studies[91] associated with the preparation of analogs with three bridges connecting the rotator termini (treated in following sections). Compounds **15** and **16**, in which the rotators, substituted *p*-phenylenes, lack a transition metal (Figure 7), were synthesized by the Setaka group.[95,96]

Note that these syntheses are capable of giving two isomeric products, as generalized in the bottom panel of Figure 6. In one, the positions of the nonbridging substituents (or lone pairs) on opposite termini are *antiperiplanar*, and in the other, they are *synperiplanar*. Usually the latter dominates, and rationales have been proposed.[91−93] Although the resulting stators have a lower degree of planarity than those in Figures 3−5, they still do not effectively shield the rotators in a three-dimensional sense. Hence, the authors have never applied the term "gyroscope-like" to these systems in their own writings.

https://dx.doi.org/10.1021/acs.chemrev.0c01001
Chem. Rev. 2021, 121, 3701−3750

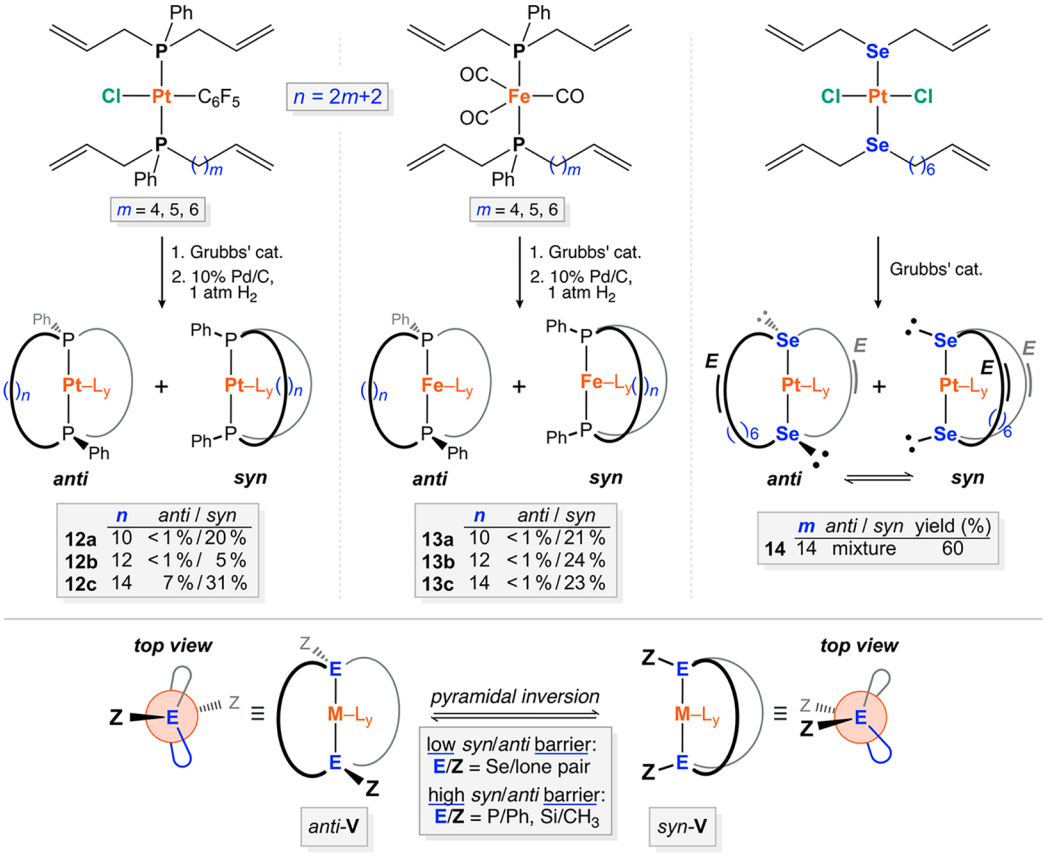

Figure 6. Molecular rotors in which the rotators terminate in tetrahedral or trigonal pyramidal atoms and the stators feature two connecting bridges.[91−94]

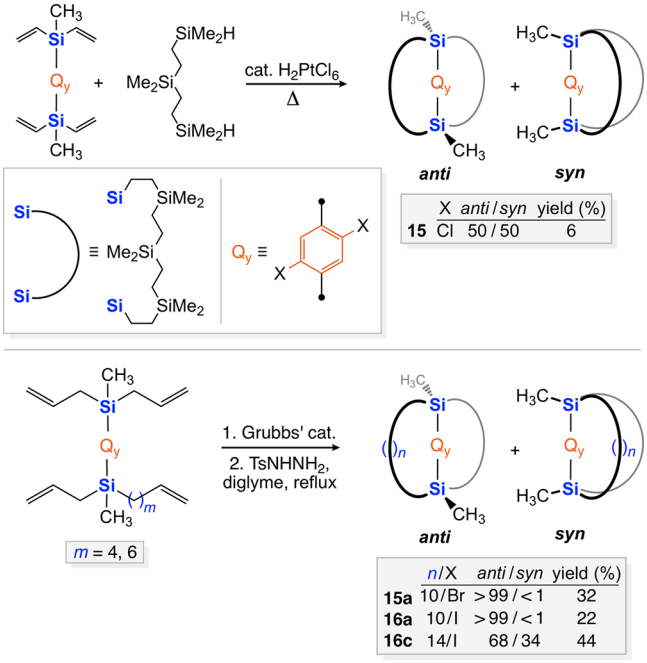

Figure 7. Additional molecular rotors in which the arylene rotators (denoted Q_y) terminate in tetrahedral atoms and the stators feature two connecting bridges.[95,96]

5. SUMMARY OF COVERAGE

In the following three sections, results from the major groups pursuing candidates for molecular gyroscopes are presented in turn. A fourth section collects relevant systems from other laboratories. In each case, the text progresses from simpler to more complex structures. At the same time, attempts are made to highlight phenomena common to substrates that do not hold adjacent positions in this hierarchy.

Coverage begins with studies from the authors' laboratory.[97−113] All of the underlying syntheses involve olefin metatheses, as first communicated in 2004.[97] These were preceded by investigations of other modes of olefin metathesis in metal coordination spheres.[114−119] A more detailed description of the chemical phenomena associated with this work will be provided in a later review.[120] Also, the broader topic of multifold ring closing metatheses in metal coordination spheres has been separately reviewed.[121]

Efforts from the Setaka laboratory are then treated.[122] This group has also made extensive use of olefin metathesis in their syntheses,[122−138] but has employed other macrocyclizations as well (e.g., Figure 7, top).[94,139−141] Attention is then turned to the Garcia-Garibay laboratory.[34−37] This ordering does not do justice to the intellectual and experimental leadership that has distinguished this group. However, it was felt that the data could best be highlighted and analyzed in this position. As noted above, systems where other researchers have attempted connections to molecular gyroscopes are presented in a subsequent section.

Finally, mention should be made of the Michl group, which has had a marked influence upon the field of molecular rotors.[31] In addition to the surface mounted systems described above (Figure 2), Michl (sometimes in collaborations) has studied a wide variety of dipolar rotors in numerous contexts. However,

https://dx.doi.org/10.1021/acs.chemrev.0c01001
Chem. Rev. 2021, 121, 3701−3750

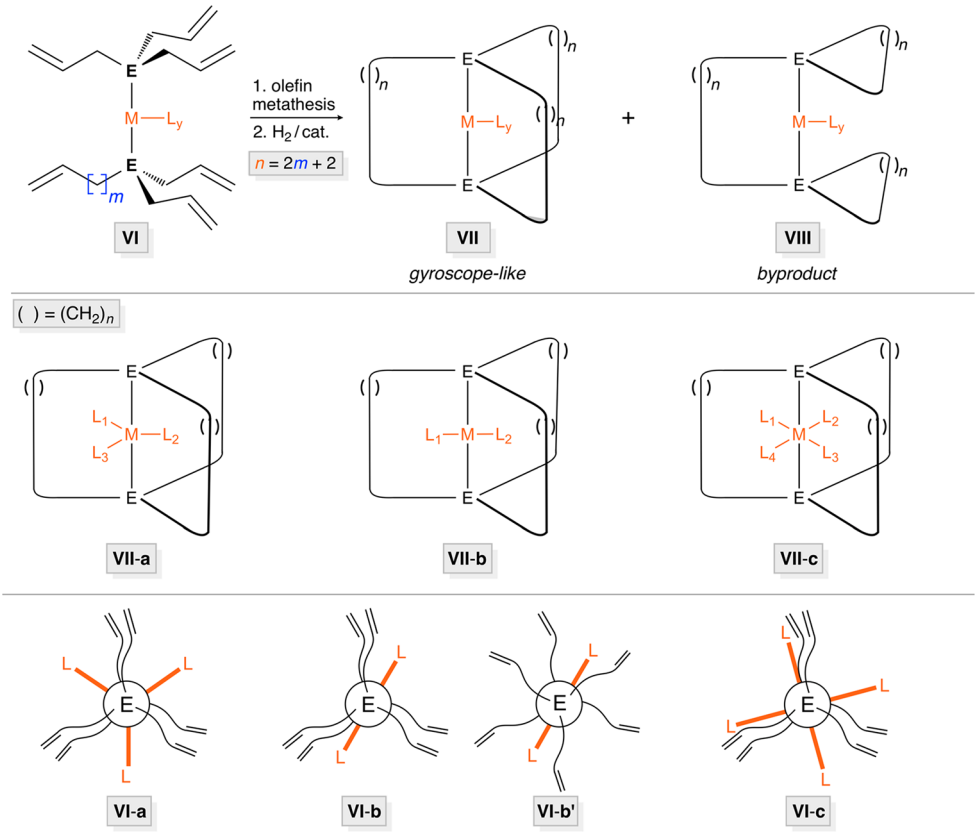

Figure 8. Three-fold intramolecular ring closing olefin metatheses involving *trans* heteroatom donor ligands $E(CH_2)_mCH{=}CH_2$ (top; E usually = P), applications to different metal coordination geometries (middle), and relevant reactant conformations (bottom).

none of these studies have targeted molecular gyroscopes per se. As a result, descriptions of relevant studies are dispersed throughout the text.

6. SYSTEMS FROM THE GLADYSZ GROUP

6.1. Syntheses Involving Olefin Metathesis

The signature reaction sequence of the authors' group is depicted in Figure 8 (top). The starting materials are usually metal complexes with two alkene containing *trans* phosphine ligands of the formula $P((CH_2)_mCH{=}CH_2)_3$ (see **VI**).[103] Analogous arsine and stibine adducts can also be employed. Then 3-fold intramolecular and interligand ring closing olefin metatheses are carried out, most commonly with Grubbs' first generation catalyst. To avoid dealing with mixtures of *cis*/*trans* C=C isomers, these are followed by hydrogenations to give the cage-like products **VII**.

To minimize side reactions, spectator ligands in the equatorial plane of the substrates must be "small", meaning monatomic and linear diatomic species such as halides, CN, and CO. High overall yields of products have been obtained with trigonal bipyramidal (**VII-a**, Figure 8), square planar (**VII-b**), and octahedral coordination geometries (**VII-c**). The number of methylene groups in the chains connecting the *trans* phosphorus atoms, *n*, is related to the number of methylene groups in each substituent of the phosphine ligand, *m*, by the equation $n = 2m + 2$. The authors commonly refer to such complexes as "gyroscope-like". The conservative phrasing reflects that functional molecular gyroscopes have yet to be realized.

The alternative monometallic products in Figure 8, **VIII**, are derived from mixtures of interligand and intraligand ring closing metatheses. While such species are sometimes observed with square planar and octahedral coordination geometries, they are seldom the major product. Any other byproducts are presumed to be oligomers or polymers. In the case of square planar products, authentic samples of some *cis* isomers have been synthesized.[112,113] However, in all systems studied to date, *cis*/*trans* isomerization only takes place at elevated temperatures, with the *trans* isomers being more stable.[112,113] Thus, it is believed that *cis*/*trans* isomerization plays no role in any of the phenomena described below.

The sequence in Figure 8 will first be analyzed as a function of coordination geometry. In subsequent sections, ligand substitution, addition, and elimination reactions will be examined. The last two increase and decrease the coordination numbers, respectively. Thus, there is more than one pathway to any given coordination geometry.

To date, the only phosphine based trigonal bipyramidal complexes accessed via the sequence in Figure 8 (**VII-a**, E = P) are the $Fe(CO)_3$ adducts **17** shown in Figure 9.[106] The overall yields (47−64%) are higher than those obtained with square planar or octahedral substrates (*vide infra*). In fact, **17a** and **17b** are the only complexes so far accessed with shorter $(CH_2)_{10}$ and $(CH_2)_{12}$ connecting bridges. The enhanced yields may be due to unique conformational properties of the reactants. By analogy to the energy minima of ethane or other species with $C_{sp^3}-C_{sp^3}$ linkages, the three olefinic phosphine substituents should stagger with respect to the three iron−carbon bonds of the $Fe(CO)_3$ fragment, as shown in **VI-a** in Figure 8. This P−

https://dx.doi.org/10.1021/acs.chemrev.0c01001
Chem. Rev. 2021, 121, 3701−3750

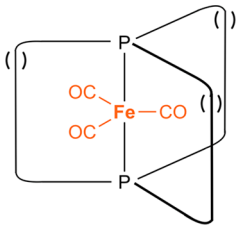

	n	yield (%)
17a	10	50 64*
17b	12	63
17c	14	64 62*
17e	18	47

Figure 9. Trigonal bipyramidal $Fe(CO)_3$ complexes prepared according to Figure 8. An asterisk indicates a yield obtained with Grubbs' second generation catalyst [() indicates $(CH_2)_n$].[106]

Fe−P conformation "preorganizes" the $CH{=}CH_2$ groups that are required to undergo ring closing metathesis.

Crystal structures provide visual clues as to how these systems would behave as molecular rotors. Two representations of the complex with three $(CH_2)_{14}$ bridges (**17c**) are shown in Figure 10 (**IX-a,b**). Counting the P−Fe−P linkages, this makes for three 17-membered macrocycles. It is a simple matter to calculate the van der Waals radius of $Fe(CO)_3$ as well as other ML_y rotators (see section 6.6). The macrocycles indeed offer sufficient lateral or horizontal "clearance" for $Fe(CO)_3$ rotation, although top/bottom or vertical interactions are tighter.

In contrast, the opposite conclusion is easily reached when viewing the crystal structure of a related complex with three 10-carbon bridges (**X-a,b** in Figure 10; 13-membered macrocycles). Actually, this structure is that of the precursor to **17a** prior to hydrogenation, with three E-$(CH_2)_4CH{=}CH(CH_2)_4$ bridges. In any case, the $Fe(CO)_3$ rotator is clearly held in a "straight jacket" that only allows a back and forth oscillation over a few degrees. Phosphite analogs of **17** have been synthesized, but these were obtained as oils and could not be rigorously purified.[102]

Analogous sequences can be carried out with square planar *trans*-phosphine adducts of $PtCl_2$, $PdCl_2$, and Rh(CO)Cl.[98,100,104,112] The resulting products are shown in Figure 11. In these cases, the reactants lack P−M−P conformations that "preorganize" the $CH{=}CH_2$ groups as in **VI-a** in Figure 8. Although **VI-b** depicts a conformation that is favorable for the desired 3-fold ring closing metathesis, an alternative in which one P−M bond is rotated by 180° (**VI-b′**) would have approximately the same energy and a greater propensity for side reactions. In any case, the overall yields are diminished relative to those for the trigonal bipyramidal complexes, and phosphine ligands $P((CH_2)_mCH{=}CH_2)_3$ with $m \geq 6$ (corresponding to $n \geq 14$) are required. Otherwise only oligomeric and polymeric products are obtained. A crystal structure of the $PtCl_2$ complex with n = 14 (**18c**) is shown in Figure 12 (**XI-a,b**). This molecule features the same macrocycle size (17-membered) as **17c** in Figure 10.

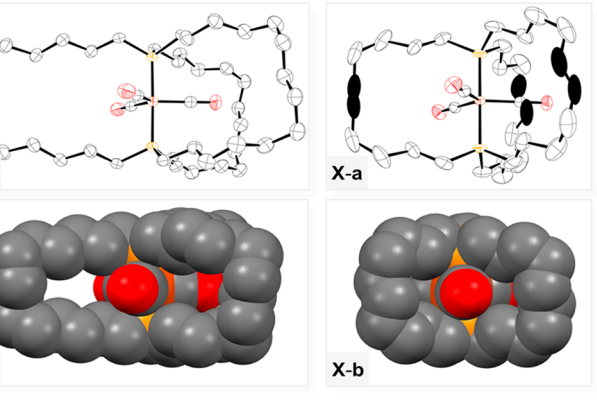

Figure 10. Thermal ellipsoid and space filling representations of complexes from Figure 9 or close relatives thereof (left, **17c**; right, *E,E,E*-tris(olefinic) precursor of **17a** with C=C linkages darkened).[106]

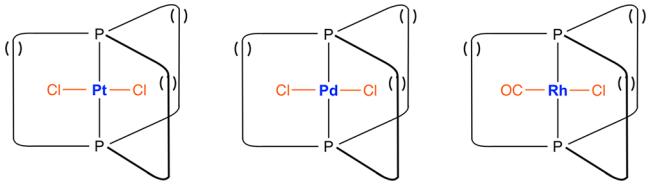

	n	yield (%)
18c	14	43
18d	16	4
18e	18	23
18f	20	3
18g	22	19
18k	30	8*

	n	yield (%)
19c	14	36
19e	18	15

	n	yield (%)
20c	14	41

Figure 11. Square planar complexes prepared according to Figure 8. An asterisk indicates a yield obtained with the second generation Hoveyda−Grubbs catalyst [() indicates $(CH_2)_n$].[98,100,104,112]

So far no upper bound on m has been reached with the square planar precursors. Phosphine adducts of $PtCl_2$ with m = 10 and 14 have been successfully employed, leading to complexes with n = 22 (**18g**) and 30 (**18k**), or 25- and 33-membered macrocycles. The crystal structure of the former is depicted in Figure 12 (**XII-a,b**). This represents the complex with the longest $(CH_2)_n$ bridges that has been structurally characterized to date.

The Rh(CO)Cl adduct **20c** in Figure 11 constitutes the first complex in this section with a dipolar rotator. This sequence has been extended to precursors with *trans*-triarylphosphine ligands of the formula $P(p\text{-}C_6H_4O(CH_2)_mCH{=}CH_2)_3$.[99] The complexes **21b,c** in Figure 13 (top), which feature 25- and 27-membered macrocycles, can be isolated in 41−26% overall yields. The crystal structures of both have been determined, and the latter is depicted in Figure 13. The interior of the cage-like stator is clearly much more spacious than in the aliphatic systems (cf. **XIII-b** vs **XIb**), although in the solid state neighboring molecules interdigitate as treated in greater detail below.

To the authors' initial surprise, it also proved possible to conduct analogous olefin metatheses with octahedral complexes, as reflected by the rhenium and osmium adducts in Figure 14.[110,111] This requires the six $(CH_2)_mCH{=}CH_2$ groups to "wrap" around an equatorial coordination plane that contains four ligands. Again, m must be at least 6, but substrates with $m \geq 9$ have not yet been studied. Since the yields of byproducts of the type **VIII** in Figure 8 are often comparable (and in a few cases higher), both are tabulated in Figure 14. A crystal structure of a representative complex with n = 14 (**22c**) is provided in Figure 15.

Finally, the iron tricarbonyl diphosphine systems in Figure 9 have been extended to the diarsine complexes **26a−c** in Figure 16.[107] The overall yields are slightly lower. X-ray diffraction

https://dx.doi.org/10.1021/acs.chemrev.0c01001
Chem. Rev. 2021, 121, 3701−3750

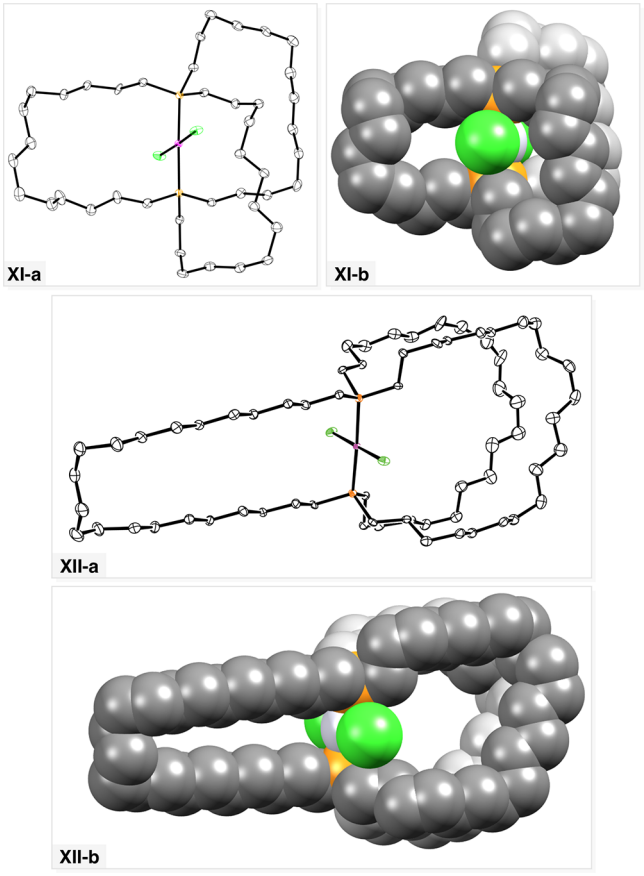

Figure 12. Thermal ellipsoid and space filling representations of the $PtCl_2$ complexes **18c** (top) and **18g** (bottom) from Figure 11.[104,112]

shows the adduct with n = 14 to be isostructural with the diphosphine homologue in Figure 10. The volume of the unit cell is only 0.7% greater, but the iron−heteroatom bonds are 4.0% longer, which will have consequences as seen below.

6.2. Reactions That Alter the Coordination Number

The metathesis/hydrogenation sequences in the previous section provide only a fraction of the molecular rotors of interest to the authors' group. Importantly, they can be elaborated to a variety of other rotors, some of which are viewed as particularly attractive candidates for molecular gyroscopes. Addition and elimination reactions that alter the coordination numbers of the complexes are treated in this section. Substitution reactions that modify the rotators but retain the coordination numbers are summarized in the following section.

As shown in Figure 17 (top), the octahedral osmium(II) dicarbonyl dichloride ($Os(CO)_2Cl_2$) complex **24c** prepared in Figure 14 can be reduced with potassium graphite under a CO atmosphere to give the trigonal bipyramidal osmium(0) tricarbonyl ($Os(CO)_3$) complex **27c**.[110] The corresponding dibromide complex, as well as higher homologues, reacts similarly. X-ray diffraction establishes that this complex is isostructural with the iron analog depicted in Figure 10. As would be expected from the longer osmium−phosphorus versus iron−phosphorus bond (Os−P 2.3626(6) Å, Fe−P 2.2056(5) Å), the unit cell volume is slightly larger (4693.71(16) vs 4633.5(3) $Å^3$, or 1.3%). However, it cannot (yet) be analogously synthesized, as the authors have never been able

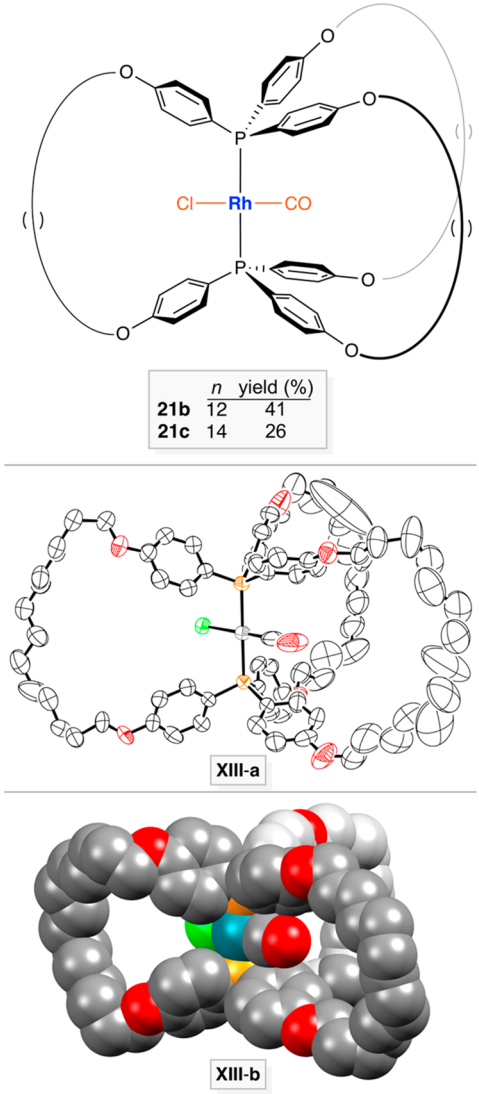

Figure 13. Square planar Rh(CO)Cl complexes with 25- or 27-membered macrocycles derived from olefinic triarylphosphine ligands [() indicates $(CH_2)_n$]. Thermal ellipsoid and space filling representations of **21c** (center and bottom).[99]

to access the necessary precursor *trans*-$Os(CO)_3(P((CH_2)_6CH{=}CH_2)_3)_2$.

Trigonal bipyramidal complexes can also be generated by additions to square planar species. Several bis(phosphine) rhodium(I) carbonyl iodide complexes, *trans*-$Rh(CO)I(PR_3)_2$, have been noted to (reversibly) add a second carbonyl ligand to give *trans*-$Rh(CO)_2I(PR_3)_2$.[142,143] As shown in Figure 17 (bottom), the gyroscope-like carbonyl iodide complex **28c** can be generated by a chloride ligand substitution of **20c**.[100] When **28c** is treated with CO (1 atm), the trigonal bipyramidal dicarbonyl addition product **29c** is quantitatively generated. It was possible to crystallize **29c**, but the CO addition is readily reversed under a nitrogen stream.

Reactions that convert square planar d^8 complexes to octahedral d^6 complexes are ubiquitous. Thus, as shown in Figure 18 (top), the rhodium carbonyl chloride complex and $CBrCl_3$ combine to give the rhodium(III) oxidative addition product **30c**.[100] In unpublished work, several platinum(IV) adducts have been synthesized and crystallographically characterized.

https://dx.doi.org/10.1021/acs.chemrev.0c01001
Chem. Rev. 2021, 121, 3701−3750

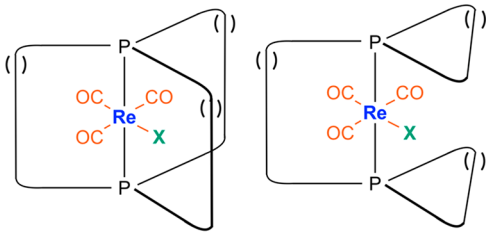

	X	n	yield (%)
22c/22'c	Cl	14	61/6
22d/22'd	Cl	16	*/27
22e/22'e	Cl	18	25/11
23c/23'c	Br	14	37/–
23d/23'd	Br	16	–/20
23e/23'e	Br	18	18/*

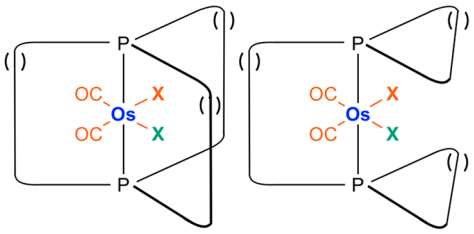

	X	n	yield (%)
24c/24'c	Cl	14	28/13
24d/24'd	Cl	16	5/51
24e/24'e	Cl	18	23/12
25c/25'c	Br	14	31/18
25d/25'd	Br	16	5/40
25e/25'e	Br	18	27/24

Figure 14. Octahedral complexes prepared according to Figure 8. An asterisk indicates that traces of the product were detected by NMR [() indicates $(CH_2)_n$].[110,111]

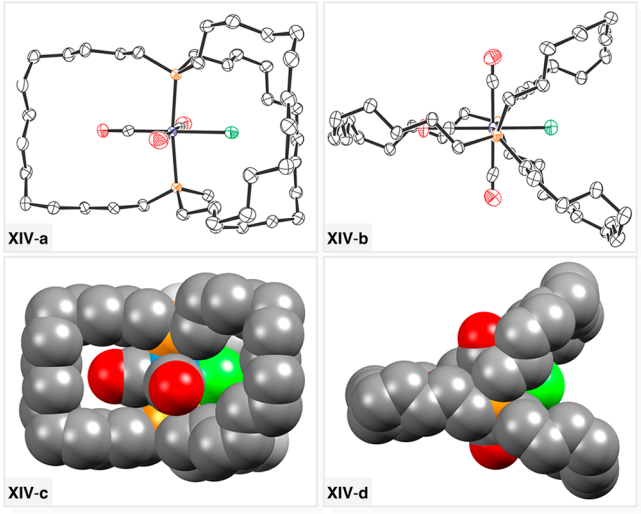

Figure 15. Thermal ellipsoid and space filling representations of **22c** from Figure 14 with the P–Re–P axis in (left) and perpendicular to (right) the plane of the image.[111]

Some protonation reactions that convert trigonal bipyramidal complexes described above to cationic octahedral complexes have been reported. For example, the iron and osmium $M(CO)_3$ species shown in Figure 18 (bottom) have been treated with the strong acids CF_3SO_3H and/or $[H(OEt_2)]^+$

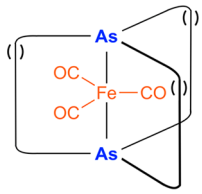

	n	yield (%)
26a	10	41
26b	12	54
26c	14	59

Figure 16. Trigonal bipyramidal $Fe(CO)_3$ complexes prepared according to Figure 8, but with arsenic in place of phosphorus [() indicates $(CH_2)_n$].[107]

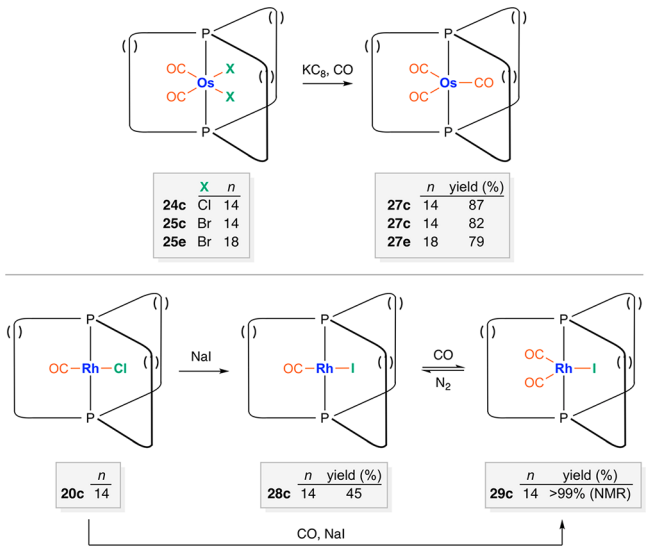

	X	n
24c	Cl	14
25c	Br	14
25e	Br	18

	n	yield (%)
27c	14	87
27c	14	82
27e	18	79

	n
20c	14

	n	yield (%)
28c	14	45

	n	yield (%)
29c	14	>99% (NMR)

Figure 17. Syntheses of trigonal bipyramidal complexes from precursors with different coordination geometries [() indicates $(CH_2)_n$].[100,110]

BAr_f^-.[106,110] The corresponding iron or osmium hydride salts $\mathbf{31}^+ X^-$ are obtained in high yields.

6.3. Substitution Reactions

6.3.1. Replacements of Chloride Ligands. The syntheses described above afford a variety of square planar and octahedral chloride complexes. This has helped to develop a rich substitution chemistry that will be fully described in a future review.[120] There are also tantalizing mechanistic questions. For example, how can such displacement reactions occur within the confines of the stator cages?

The chloride ligands can be replaced by a variety of halide and pseudohalide nucleophiles such as Br^-, I^-, CN^-, and NCS^- (Figure 19).[98,100,104,111] Both linkage isomers have been obtained with NCS^-. It has never been problematic to use aryl (e.g., $ZnPh_2$)[98,104,105,110,111] or alkynyl ($MC{\equiv}CR$)[99,100] nucleophiles. In contrast, methyl groups are easily introduced in some systems[105,110,111] but this requires extensive optimization in others. Complexes with hydride ligands have not yet been generated, but a rhodium $H-BH_2-H$ chelate derived from $NaBH_4$ has been isolated (**33c**, Figure 19).[105] A few substitution reactions of analogous bromide complexes have been reported,[104,111] but they are much less developed.

With dichloride complexes such as the $PtCl_2$ species **18** in Figure 11, there is interest in monosubstitution reactions. These would yield dipolar rotators. To date, all efforts in the authors'

https://dx.doi.org/10.1021/acs.chemrev.0c01001
Chem. Rev. 2021, 121, 3701–3750

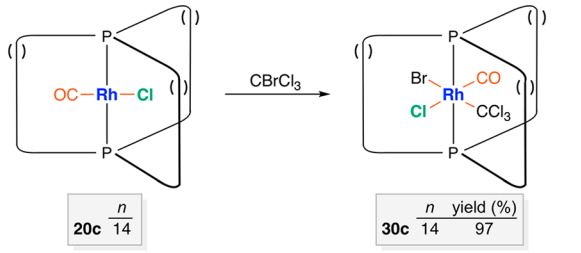

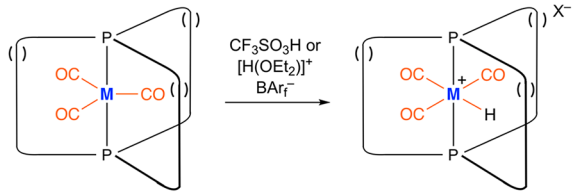

	M	n
17a	Fe	10
17b	Fe	12
17c	Fe	14
17e	Fe	18
17a	Fe	10
17b	Fe	12
17c	Fe	14
27c	Os	14
27e	Os	18

	M	n	yield (%)
31a+ $CF_3SO_3^-$	Fe	10	99*
31b+ $CF_3SO_3^-$	Fe	12	99
31c+ $CF_3SO_3^-$	Fe	14	98*
31e+ $CF_3SO_3^-$	Fe	18	99
31a+ BAr_f^-	Fe	10	99
31b+ BAr_f^-	Fe	12	99
31c+ BAr_f^-	Fe	14	98
32c+ BAr_f^-	Os	14	80
32e+ BAr_f^-	Os	18	80

Figure 18. Syntheses of octahedral complexes from precursors with different coordination geometries [() indicates $(CH_2)_n$]. An asterisk indicates an NMR yield for a species generated *in situ*.[100,106,110]

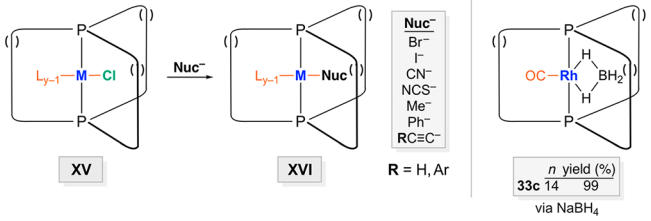

Figure 19. Reactions of chloride complexes of various coordination geometries with nucleophiles [() indicates $(CH_2)_n$].[104−106]

laboratory have yielded difficultly separable mixtures of products. Part of the problem is that the rate constant for the first substitution often appears to be similar to the second. However, alternative routes can sometimes be developed. For example, Figure 20 shows an initial disubstitution of the chloride ligands in **18c,e** by phenyl ligands.[104] When the diphenyl complexes **34c,e** are then treated with HCl, the phenyl chloride complexes **35c,e** can be isolated in 93−98% yields.[109] Presumably, the introduction of the first electron withdrawing chloride ligand diminishes the rate of further electrophilic attack by HCl.

The variation of the sizes of the ligands on the rotator, or alternatively the radius of the rotator, allows the rotational barrier to be modulated. Some might state that the substitution of a chloride ligand by a large (or "long") ligand introduces a "brake". However, the authors prefer to reserve this term for ligands that can be reversibly introduced by addition reactions. Although rotational barriers are treated more quantitatively below, some brief remarks here may be helpful.

First, for any square planar PtX_2 adduct, not all of the $(CH_2)_n$ bridges or stator spokes are equivalent. By symmetry, two sets of ^{13}C NMR signals would be expected (2:1 ratio). However,

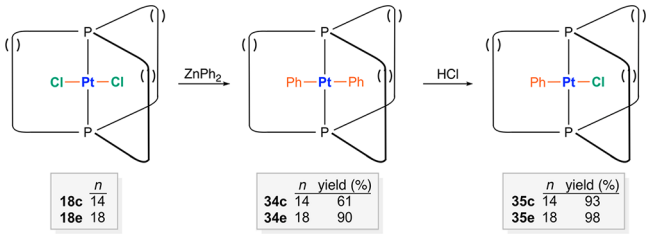

	n
18c	14
18e	18

	n	yield (%)
34c	14	61
34e	18	90

	n	yield (%)
35c	14	93
35e	18	98

Figure 20. Syntheses of complexes with dipolar PhPtCl rotators from precursors with $PtCl_2$ rotators [() indicates $(CH_2)_n$].[104,109]

for the $PtCl_2$ complex with n = 14 (**18c**), only one set is observed, even at temperatures as low as −120 °C.[104] This indicates rapid rotation of the $PtCl_2$ rotator, often qualified as "on the NMR time scale". The same limiting spectra are obtained with the $PtBr_2$, PtI_2, and $Pt(CN)_2$ analogs, at least at room temperature. However, multiple signals can be observed with longer pseudohalide ligands, such as NCS adducts.[104,105]

Similar scenarios are encountered with other complexes. For example, when the chloride ligand in the RhCl(CO) adduct **21b** (Figure 13) is replaced with the phenylethynyl ligand C≡CC_6H_5, the number of ^{13}C NMR signals (room temperature) is unaffected.[99] However, when the chloride ligand is replaced by the slightly more extended *p*-tolylethynyl ligand, C≡C−*p*-$C_6H_4CH_3$, multiple sets of signals are observed.

6.3.2. Replacements of Carbonyl Ligands. Although the photochemical substitution of carbonyl ligands has abundant precedent, all attempts to effect well-defined reactions with any of the preceding carbonyl complexes have been unsuccessful. However, with all $Fe(CO)_3$ (but not $Os(CO)_3$) complexes, the addition of NO^+ BF_4^- leads to CO/NO^+ exchange as shown in Figure 21.[106,107] The cations of the resulting salts, **36a−c**$^+$ BF_4^-, and **37a−c**$^+$ BF_4^- are isoelectronic and isostructural with their precursors, and the NMR properties are further detailed below.

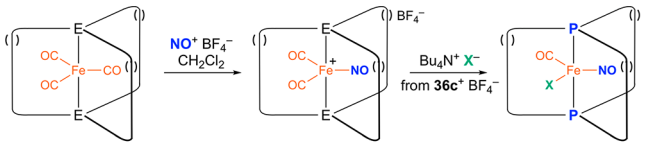

	E	n
17a	P	10
17b	P	12
17c	P	14
17e	P	18
26a	As	10
26b	As	12
26c	As	14

	E	n	yield (%)
36a+ BF_4^-	P	10	98
36b+ BF_4^-	P	12	89
36c+ BF_4^-	P	14	81
37a+ BF_4^-	As	10	95
37b+ BF_4^-	As	12	89
37c+ BF_4^-	As	14	93

	X	n	yield (%)
38c	Cl	14	81
39c	Br	14	79
40c	I	14	75
41c	CN	14	83

Figure 21. Substitution reactions of carbonyl ligands in iron complexes [() indicates $(CH_2)_n$].[106−108]

The dipolar rotators in **36a−c**$^+$ BF_4^- and **37a−c**$^+$ BF_4^- are potentially useful, but as noted above there are complications with molecular gyroscopes derived from ionic systems. However, with the diphosphine complexes **36a−c**$^+$ BF_4^-, halide and pseudohalide nucleophiles (Cl^-, Br^-, I^-, CN^-) readily displace one of the remaining carbonyl ligands, giving neutral complexes with Fe(CO)(NO)(X) rotators as shown in Figure 21 (**38c−41c**).[108] This sequence has not yet been attempted with the diarsine complexes **37a−c**$^+$ BF_4^-, but parallel chemistry is anticipated.

With this series of complexes, it was studied whether carrying out CO ligand substitution prior to the metathesis/hydrogenation sequence in Figure 8 might be advantageous.[108] In all

https://dx.doi.org/10.1021/acs.chemrev.0c01001
Chem. Rev. 2021, 121, 3701−3750

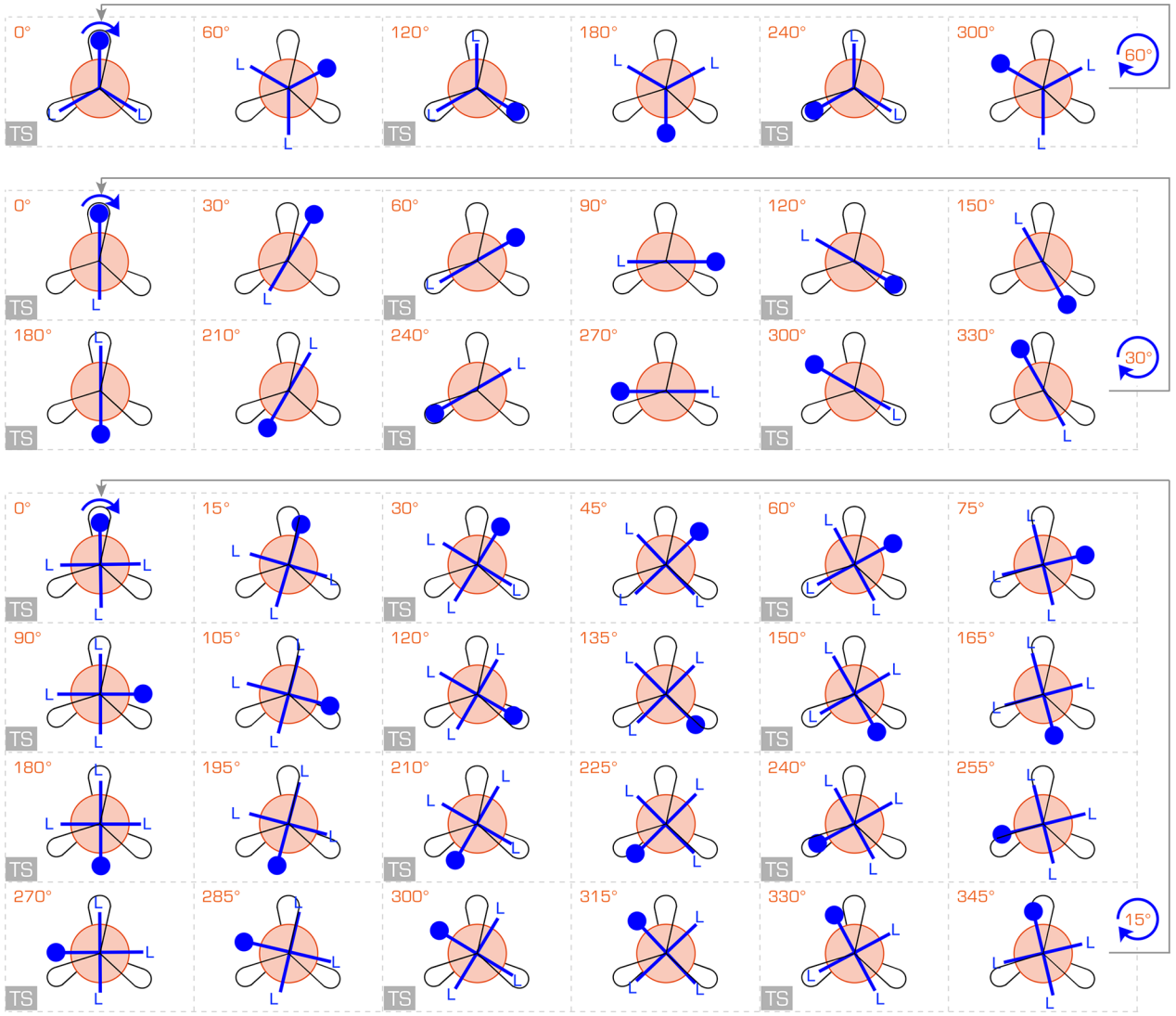

Figure 22. Energy maxima and minima as the rotators in trigonal bipyramidal (top panel), square planar (middle panel), and octahedral complexes (bottom panel) in Figure 8 are rotated by 360°. The blue dot represents a marker to help track rotation (and can also be visualized as a unique ligand).

cases, it proved better to effect substitution after installing the dibridgehead diphosphine ligand, per Figure 21.

6.4. Dynamic Properties: General Concepts

As mentioned above, some aspects of the dynamic behavior of the rotators in the preceding complexes can be gleaned from routine NMR spectra. In this context, one should note that trigonal bipyramidal complexes in which all rotator ligands are identical should adopt ground state conformations in which the three M−L bonds are staggered with respect to the P−C bonds. As depicted in the top panel of Figure 22, these would have idealized D_3 or D_{3h} symmetry in which all three $P(CH_2)_nP$ bridges are homotopic (i.e., interchangeable by a C_n rotational axis).

Square planar and octahedral complexes can be similarly considered, as illustrated in the middle and bottom panels of Figure 22. There are no ML_y conformations in which all three $P(CH_2)_nP$ bridges are related by symmetry. However, for each energy minimum, two bridges qualify as homotopic.

These situations of course change when the rotator ligands are not identical. In the case of trigonal bipyramidal complexes, there will be two homotopic $P(CH_2)_nP$ bridges for rotators of the type ML_2L', and none for $MLL'L''$ rotators. The former case is easily visualized by treating the blue marker or dot in the top panel of Figure 22 as L′. There are no homotopic bridges for square planar complexes with MLL′ rotators or octahedral complexes with ML_3L' rotators.

In any case, if only one set of $P(CH_2)_nP$ ^{13}C NMR signals is observed for a square planar or octahedral complex, there must be a mechanism for exchange of the $P(CH_2)_nP$ units that is rapid on the NMR time scale. The most intuitive would involve a simple rotation of the rotator. Other possibilities, such as multistep processes involving ligand dissociation, can be ruled out by NMR or other data.

As a point of calibration, one can consider the most intensively studied cage size with n = 14, corresponding to 17-membered macrocycles. In brief, rotators bearing only halide, cyanide, CO, NO^+, and CH_3 ligands generally remain in the fast exchange limit, even at −100 °C, regardless of coordination geometry. However, the introduction of phenyl substituents usually supplies sufficient bulk to "brake" rotation, as evidenced by two or more sets of $P(CH_2)_{14}P$ signals.[98,105] Also, the slow exchange regime is easier to reach with trigonal

https://dx.doi.org/10.1021/acs.chemrev.0c01001
Chem. Rev. 2021, 121, 3701−3750

Table 1. Activation Parameters for Fe(CO)(NO)(X) or $Fe(CO)_3H$ Rotation within $E((CH_2)_n)_3E$ Cages in Solution As Determined by Variable Temperature $^{13}C\{^1H\}$ NMR [() Indicates $(CH_2)_n$]

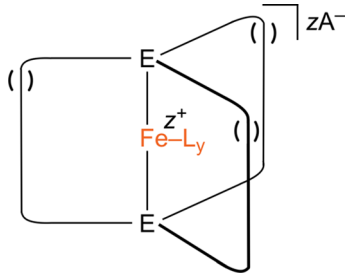

complex	L_y	E	n	zA^-	$\Delta H^{\ddagger}$ (kcal mol^{-1})	$\Delta S^{\ddagger}$ (eu)[a]	$\Delta G^{\ddagger}_{298K}$ (kcal mol^{-1})	$\Delta G^{\ddagger}_{383K}$ (kcal mol^{-1})	ref
38c[b]	CO, NO, Cl	P	14	0	5.9	−20.4	11.9	13.6	108
40c[c]	CO, NO, I	P	14	0	7.6	−23.9	14.7	16.8	108
36b$^+$ BF_4^-[c]	$(CO)_2$, NO	P	12	$1BF_4^-$	8.3	−28.4	16.7	19.2	106
36c$^+$ BF_4^-[d]	$(CO)_2$, NO	P	14	$1BF_4^-$	9.5	−6.5	11.4	11.9	106
37a$^+$ BF_4^-[c]	$(CO)_2$, NO	As	10	$1BF_4^-$				>19.4	107
37b$^+$ BF_4^-[b]	$(CO)_2$, NO	As	12	$1BF_4^-$	7.7	−22.1	14.2	16.2	107
31b$^+$ BAr_f^-[b]	$(CO)_3$, H	P	12	$1BAr_f^-$	6.1	−23.5	13.0	15.1	107
42a$^+$ BAr_f^-[c]	$(CO)_3$, H	As	10	$1BAr_f^-$				>18.9	107
42b$^+$ BAr_f^-[b]	$(CO)_3$, H	As	12	$1BAr_f^-$	5.4	−22.7	12.2	14.1	107

[a]Units of cal·mol^{-1}·K^{-1}. [b]CD_2Cl_2 solution. [c]C_6D_5Cl solution. [d]$CDFCl_2$ solution.

bipyramidal complexes (i.e., T_{coal} at less negative (higher) temperatures), for example, with a Fe(CO)(NO)Cl rotator[108] as opposed to a $Re(CO)_3Cl$ rotator.[111] How can this be understood?

First, return to the trigonal bipyramidal species in the top panel of Figure 22. The transition state for rotator rotation entails a 3-fold ligand/$P(CH_2)_nP$ (L−M−P−C) eclipsing interaction. Furthermore, as the rotator passes through 360°, three minima and three maxima are encountered. Their idealized L−M−P−C torsion angles are 60° and 0°, respectively (considering only the nearest L/$P(CH_2)_nP$ moieties). Although each set of three is degenerate, it remains instructive to view the entire coordinate as in Figure 22, where the blue dot aids the tracking of rotation. As noted above, it can also be regarded as a unique ligand, facilitating recognition of the two types of symmetry-inequivalent $P(CH_2)_nP$ bridges.

As the ML_2 rotator of a square planar complex passes through 360° (middle panel, Figure 22), six degenerate maxima and six degenerate minima are encountered. Now there is only one L−M−P−C eclipsing interaction present in each transition state. Furthermore, in the minima, the idealized L−M−P−C torsion angles associated with the nearest L/$P(CH_2)_nP$ moieties are only 30°, increasing the possibility of van der Waals interactions that would slightly destabilize the ground state. Thus, intrinsically lower rotational barriers as compared to trigonal bipyramidal analogs would be expected.

The considerations raised with the square planar complexes become more pronounced with the octahedral complexes. As shown in the bottom panel of Figure 22, there are 12 degenerate maxima and 12 degenerate minima as the rotator passes through 360°. Again, there is only one eclipsing interaction associated with each transition state, with idealized L−M−P−C torsion angles of 0°, 2 × 30°, and 60° for the nearest L/$P(CH_2)_nP$ moieties. The minima feature idealized L−M−P−C torsion angles of 2 × 15° and 2 × 45° for the nearest L/$P(CH_2)_nP$ moieties. The compressed 15° torsion angles are likely to introduce van der Waals interactions that would contribute to ground state strain. Hence, the rotational barriers should be further reduced relative to the cases above.

The preceding concepts are well recognized in the physical organic literature,[144,145] where it is common to refer to the foldedness, N, of a rotational barrier about a covalent bond A−B

$$N = (p \cdot q)/w$$

in which p is the foldedness of the fragment A (often corresponding to a C_n axis), q is the foldedness of the fragment B, and w is the number of eclipsed bonds in the transition state.

As N becomes larger, rotational barriers tend to diminish. Another way to view this trend is that for a higher fold system to have a rotational barrier comparable to a lower fold system, a similar energy change must take place over a much more restricted range of torsion angles. Accordingly, the trigonal bipyramidal systems exhibit 3-fold barriers [(3 × 3)/3] whereas the square planar and octahedral systems exhibit 6- and 12-fold barriers, respectively.

In qualitative agreement with the preceding analysis, low temperature ^{13}C NMR spectra of the trigonal bipyramidal $Rh(CO)_2I$ complex **29c** exhibit two sets of $P(CH_2)_nP$ signals (ca. 2:1 area ratio; −25 °C, CD_2Cl_2), but spectra of the square planar Rh(CO)I complex **28c** exhibit only one ($CDFCl_2$, −120 °C).[100] When the former sample is warmed, the signals coalesce. In this case, other data suggest that the mechanism by which the $P(CH_2)_nP$ bridges become equivalent involves CO dissociation, Nonetheless, it can be concluded that the $Rh(CO)_2I$ rotational barrier is higher than that for Rh(CO)I. With the other carbonyl complexes studied, the maintenance of certain couplings precludes dissociative processes.

6.5. Measured or Bounded Rotational Barriers

As summarized in Table 1, a number of barriers to rotator rotation in the preceding complexes have been measured or bounded using variable temperature ^{13}C NMR data. Note that to exchange the positions of all of the $P(CH_2)_nP$ bridges in a trigonal bipyramidal complex with a ML_2L' or MLL′L″ rotator, a 240° rotation is necessary (corresponding to the structures

https://dx.doi.org/10.1021/acs.chemrev.0c01001
Chem. Rev. 2021, 121, 3701−3750

labeled 60° and 300° in the top panel of Figure 22). However, to exchange the positions of all the $P(CH_2)_nP$ bridges in a square planar complex with a ML_2 rotator, only a 120° rotation is necessary (see structures labeled 30° and 150° in the middle panel of Figure 22). With a MLL′ rotator, a 300° rotation becomes necessary (structures labeled 30° and 330°). For octahedral complexes with ML_4 or ML_3L' rotators, the equivalent values are 60° and 330°, respectively. Thus, the rate constants employed in the Eyring plots used to generate the activation parameters can represent varying degrees of rotation.

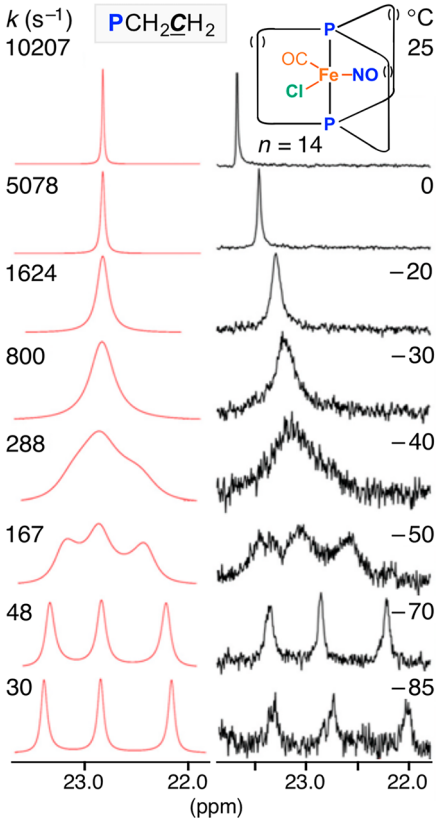

Figure 23. Partial $^{13}C\{^1H\}$ NMR spectra of the Fe(CO)(NO)Cl complex **38c** as a function of temperature (CD_2Cl_2, right) and simulated line shapes with rate constants (left).[108]

A typical series of spectra used to generate the data in Table 1 is shown in Figure 23. At each temperature, the line shapes are simulated with standard programs, and the rate constants are extrapolated. The negative $\Delta S^{\ddagger}$ values in Table 1 suggest quite ordered transition states, consistent with ligands traversing through the otherwise unoccupied macrocycle cavities. Also, consistent with expectations involving barrier foldedness, the trigonal pyramidal complexes with $Fe(CO)_2(NO)^+$ rotators exhibit higher $\Delta G^{\ddagger}$ values than the corresponding octahedral complexes with $Fe(CO)_3H^+$ rotators (e.g., at 383 K, 19.2 vs 15.1 kcal/mol for **36b**$^+$ BF_4^- and **31b**$^+$ BAr_f^-, or 16.2 vs 14.1 kcal/mol for **37b**$^+$ BF_4^- and **42b**$^+$ BAr_f^-). Other trends in Table 1 are interpreted below.

6.6. Key Solid State Properties

The authors have determined the crystal structures of large numbers of the preceding complexes. In some cases, there is disorder in the $(CH_2)_n$ segments, but well over half the time, this can be modeled. The authors have also made frequent use of geometric analyses of the types illustrated in Figure 24.[104,106−108,110,111] Various features of these diagrams are examined in turn.

The first step with each crystal structure is to calculate the radius (or "horizontal steric demand") of the rotator. One simply takes the distance from the metal to the terminal atom of each ligand and adds the van der Waals radius of the terminal atom. The largest of these values is considered the radius. As would be expected, the radius of any ML_y rotator or individual M−L bond length does not significantly vary with the lengths of the $P(CH_2)_nP$ moieties (and could often in theory be taken from appropriate model compounds in the literature).

Next, the "horizontal clearance" provided by the three $P(CH_2)_nP$ bridges is considered. The syntheses in Figure 8 always give an even number for *n*, which places the midpoint between two atoms. Hence, the authors have focused on the two innermost CH_2 groups (Figure 24, left), for example, the seventh and eighth from either terminus in a $P(CH_2)_{14}P$ bridge. Thus, the distances of six carbon atoms from the metal are calculated, and the van der Waals radius of a carbon atom (1.70 Å) is subtracted from each. Although a number of ways to treat these data can be considered, the authors have always taken (as the most conservative estimate) the shortest of the resulting distances as the "clearance" (while also tabulating the average distance). When this value is greater than the radius of the rotator, rotation is always rapid on the NMR time scale and only a single set of $P(CH_2)_nP$ ^{13}C NMR signals are observed.

The qualitative nature of the preceding analysis deserves emphasis. First, in the crystal lattice, the three $P(CH_2)_nP$ units usually exhibit different conformations. However, in solution, they all have the same ensemble of conformations available. Furthermore, these conformations will change during the course of rotator rotation. Second, this treatment also ignores the hydrogen atoms of the stator. However, it is often found that hydrogen atoms can be neglected when evaluating the feasibility of dynamic processes from space filling models.

Similar analyses of the "vertical" or "top/bottom" clearance can be carried out.[106,107] Several approaches with largely equivalent results have been taken. The first step is to consider the *trans*-CH_2−P−M−P−CH_2 linkages or $(CH_2)_3P$−M−$P(CH_2)_3$ units. The distances between the closest CH_2 groups on opposite termini can then be calculated. These are not quite eclipsed, as is evident from the views shown in the crystal structure in Figure 25 (bottom panel). Alternatively, the distance between the two planes defined by the three $P(CH_2)_3$ carbon atoms can be calculated (Figure 24, right; these are often parallel due to crystallographic symmetry). In either case, the van der Waals radii of two carbon atoms are then subtracted to give a clearance. The values are then compared to the van der Waals *diameter* (or "vertical steric demand" or "fatness") of the atoms bound to the rotator.

Consider the structurally characterized neutral iron complexes with dipolar rotators, Fe(CO)(NO)(X) (**38c**, **39c**, **41c**).[108] In the case of the chloride complex **38c**, diameters of the ligating atoms are 3.10 Å (NO), 3.40 Å (CO), and 3.50 Å (Cl) versus a vertical clearance of ≥2.62 Å. In the case of the bromide complex **39c**, the vertical clearance is nearly unchanged (≥2.68 Å), but the bromide ligand has a larger diameter (3.70 Å) than chloride. In the case of the cyanide complex **41c**, the diameters of the ligating atoms are all ≤3.40 Å, while the clearance is little changed (≥2.58 Å). Despite the pronounced van der Waals interactions that clearly must

https://dx.doi.org/10.1021/acs.chemrev.0c01001
Chem. Rev. 2021, 121, 3701−3750

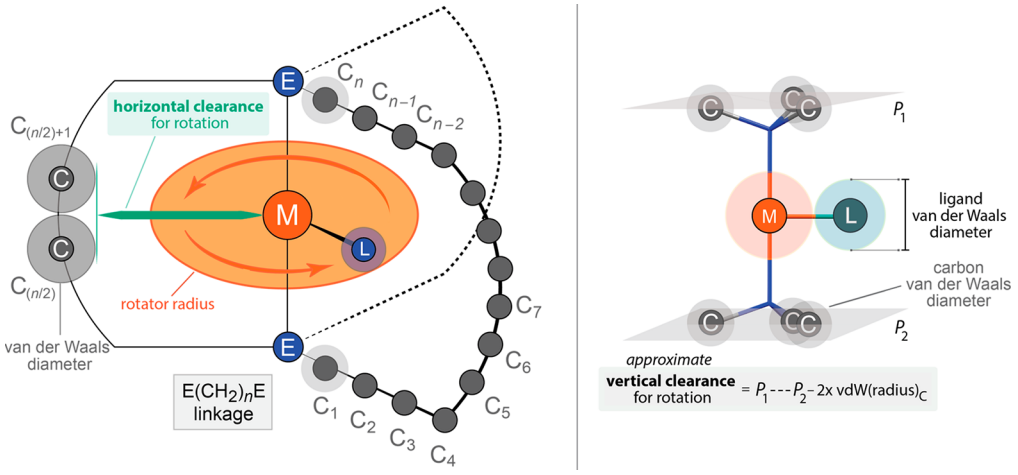

Figure 24. Structures illustrating the concepts of "horizontal clearance" and "vertical clearance" for complexes synthesized in the authors' laboratory.

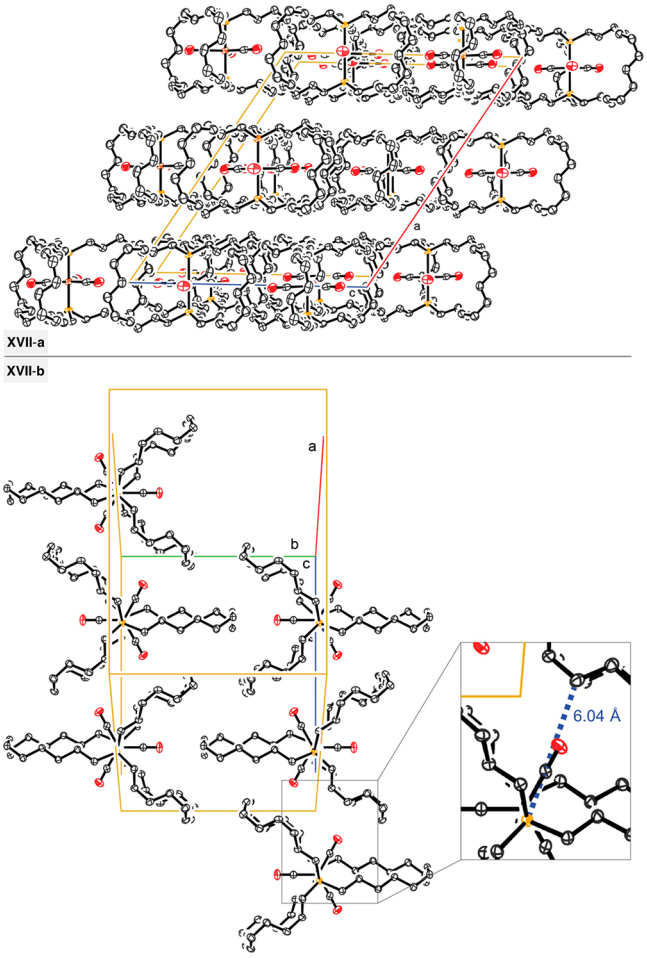

Figure 25. Crystal lattice of the $Fe(CO)_3$ complex **17c** viewed along the *b* axis (top) and perpendicular to the *b* axis (bottom); iron atoms are depicted in orange and oxygen atoms in red.

accompany rotator rotation in these three compounds, rotation remains fast on the NMR time scale. Thus, concurrent conformational processes that attenuate these interactions are presumably taking place (e.g., $P(CH_2)_nP$ bond rotations). This would be another contributor to the negative $\Delta S^{\ddagger}$ values in Table 1 (avg ca. −21 eu). In any case, a major portion of the activation energy must be due to poor vertical clearance. Possible means of ameliorating these interactions are discussed below.

Of course, under the solution phase conditions used to measure the rotational barriers in Table 1, the molecules are oriented randomly, and none of the approaches to functional molecular gyroscopes outlined in section 3 apply. Accordingly, the authors have sought crystalline samples of the preceding compounds in which the rotators (1) exhibit parallel axes, (2) have no *intermolecular* steric impediments to rotation, and (3) have significant dipole moments so that they can strongly interact with electric fields. Among the many square planar and octahedral complexes that have been structurally characterized, not one has crystallized with parallel rotator axes (although there are always subsets of molecules with parallel rotator axes).

However, both criteria 1 and 2 are fulfilled with all *neutral* trigonal bipyramidal complexes with $E(CH_2)_{14}E$ bridges and CO/NO/X ligands prepared to date, that is, species of the general formula *trans*-$M(L)(L')(L'')(E(CH_2)_{14}E)_2$.[97,106−108,110] These include $Fe(CO)_3$ rotators for E = P and As and $Os(CO)_3$, Fe(CO)(NO)Cl, Fe(CO)(NO)Br, and Fe(CO)(NO)(CN) rotators for E = P. For the last three rotators, DFT calculations indicate dipole moments of 2.68 to 1.38 D (decreasing as X = CN, Br, Cl).[146] These are in the range of dipolar rotators that have previously been driven by electrical fields.[132,147,148]

As summarized in Table 2, these six complexes crystallize in identical space groups ($C_{2/c}$) with very similar monoclinic lattice dimensions. Two perspectives of an abbreviated packing diagram for *trans*-$Fe(CO)_3(P(CH_2)_{14}P)_2$ (**17c**) are given in Figure 25. The upper view illustrates both the parallel rotator axes and a pronounced layering of molecules. The lower view illustrates the spacing between the $Fe(CO)_3$ rotators and neighboring molecules within the same layer. The individual CO ligands are directed at the stators of the neighbors. For all six complexes, it is a simple matter to calculate the distances between the metal atoms of one molecule and the closest stator atom of a neighboring molecule, which as easily inferred visually always turn out to be carbon atoms. The values range from 6.09 to 5.99 Å or 4.39 to 4.29 Å after subtracting the van der Waals radius of a carbon atom. In each case, this *intermolecular clearance* comes very close to accommodating the radius of the rotator (4.38−4.59 Å).

https://dx.doi.org/10.1021/acs.chemrev.0c01001
Chem. Rev. 2021, 121, 3701−3750

Table 2. Structural Data for Gyroscope-like Complexes of the Formula *trans*-$\overline{M(L)(L')(L'')(E(CH_2)_{14}E)_2}$

complex[a]	rotator	E	radius[b] [Å]	M···CH$_2$ [Å][b]	M···CH$_2$ − vdW$_C$ [Å][d]	*a* [Å]	*b* [Å]	*c* [Å]	*β* (deg)	ref
26c	Fe(CO)$_3$	As	4.45	6.01	4.31	21.438(3)	13.9810(17)	18.227(2)	121.3	107
17c	Fe(CO)$_3$	P	4.45	6.04	4.34	21.5104(8)	13.9765(6)	18.3436(8)	122.8	106
27c	Os(CO)$_3$	P	4.59	6.09	4.39	21.6848(5)	14.0336(2)	18.2091(4)	122.1	110
38c	Fe(CO)(NO)Cl	P	4.38	5.99	4.29	21.4367(4)	13.8586(4)	18.3518(5)	122.5	108
39c	Fe(CO)(NO)Br	P	4.47	6.06	4.36	21.2190(8)	13.9660(8)	18.1727(2)	121.0	108
41c	Fe(CO)(NO)(CN)	P	4.53	6.04	4.34	21.4114(6)	13.9998(2)	18.2960(5)	122.7	108

[a]All complexes crystallize in the space group $C_{2/c}$ as monoclinic crystal systems ($\alpha = \gamma = 90°$). [b]The distance from the metal to the terminal atom of each ligand is calculated, and the van der Waals radius of the terminal atom is added. The largest of the three values is taken as the radius. The distances used are from Skaper, D. doctoral thesis, Universität Erlangen-Nürnberg, 2010, Table 2-9. [c]The distance from the metal to the nearest carbon atom of a neighboring molecule in the crystal lattice (see example in Figure 25). [d]The previous distance minus the van der Waals radius of a carbon atom (intermolecular horizontal clearance).

6.7. Toward Molecular Gyroscopes

In assessing the crystalline forms of these complexes as candidates for molecular gyroscopes, the Fe(CO)(NO)Cl adduct **38c** would be preferred to the corresponding iodide species **40c** given the lower barrier to rotation in Table 1. However, the cyanide ligand in **41c** extends only slightly farther from iron than chloride (4.53 vs 4.38 Å; there is ample free volume in this dimension) and is slightly more "svelte" (3.40 vs 3.50 Å). The latter may help in the more congested vertical dimension, and as noted in section 6.6, the cyanide substituted rotator exhibits the highest dipole moment. Thus, the Fe(CO)(NO)Cl and Fe(CO)(NO)(CN) complexes **38c** and **41c** will serve as the leads in future experimental investigations. However, hydride or fluoride ligands would be smaller yet, and synthetic routes are currently under investigation.

The diantimony and dibismuth analogs of the trigonal bipyramidal iron complexes would also be attractive synthetic targets. Iron−heteroatom and heteroatom−carbon bonds progressively lengthen upon descending group 15. For example, in the crystallographically characterized series Fe(CO)$_4$(E(*t*-Bu)$_3$), the Fe−P, −Sb, and −Bi bonds lengthen from 2.364(1) to 2.547(1) to 2.6269(9) Å, and the P−, Sb−, and Bi−C bonds lengthen from 1.93 to 2.22 to 2.32 Å (averages; the Fe−E−C angles remain in the narrow range 107.2−106.0°).[149−151] The rotational barriers ($\Delta G^{\ddagger}_{298K}$) for the isostructural diphosphine and diarsine complexes **36b**$^+$ BF_4^- and **42b**$^+$ BF_4^- in Table 1 are 16.7 and 14.2 kcal/mol, respectively, a 2.5 kcal/mol reduction. Thus, longer Fe−E bond lengths appear to greatly relieve rotator/stator steric interactions in the vertical dimension.

Osmium analogs would also greatly improve the vertical clearance. However, as noted above, the authors have so far been unable to effect substitution reactions of the Os(CO)$_3$ complexes in Figure 17. It may also be advantageous to introduce some type of "belt" in the equatorial plane, connecting the spokes of the stators in a manner analogous to the stationary ring in Figure 1a. This would further shield the rotator from neighboring molecules and inhibit intercalation. A possible synthetic approach would be to construct the stator by alkyne instead of olefin metathesis[152] and then introduce linkers between the alkyne moieties.

With an eye on critical issues in realizing metal based molecular gyroscopes, Fekl and Schurko alertly pointed to H−M−H units as "low barrier rotators".[153] They studied the platinum dihydride complex **43** in Figure 26, which features two bulky *trans* disposed phosphine ligands. A variety of low temperature *solid state* NMR experiments were carried out and interpreted with the aid of a crystal structure and DFT

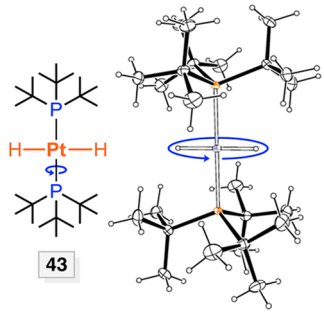

Figure 26. Bis(phosphine) platinum complex with a low barrier H−Pt−H rotator.

calculations. The rotational barrier, estimated as ca. 3 kcal/mol, is one of the lowest in this review. Interestingly, each energy minimum features an eclipsed H−Pt−P−C segment with a torsion angle of ca. 0°, as opposed to the 30° idealized torsion angles shown for the square planar complexes in Figure 22 (middle). But when one hydride ligand is replaced by a chloride ligand (affording a dipolar rotator), the solid state rotational barrier increases considerably.

7. SYSTEMS FROM THE SETAKA GROUP

7.1. Synthetic Strategies

The Setaka group has also been prolific with regard to embedding rotators within cage-like stators of 3-fold symmetry.[122−141] They have focused upon arenediyl rotators, denoted Q$_y$ in figures and tables herein, for which *p*-phenylene (*p*-C$_6$H$_4$) represents the parent case (Q$_1$). These are anchored by silicon or occasionally germanium atoms,[128] affording dibridgehead disilane (digermane) stators that are akin to the dibridgehead diphosphine stators in many of the transition metal containing rotors in section 6. The Setaka group often refers to their systems as "gyrotops".

Most of their syntheses feature 3-fold intramolecular ring closing olefin metathesis of species of the formula Q$_y$[E-((CH$_2$)$_m$CH=CH$_2$)$_3$]$_2$ (**L**; E = Si, Ge).[123−138] As depicted in Figure 27, two types of products are possible following hydrogenation: the gyroscope-like compounds **LI**, derived exclusively from metatheses of olefins tethered to different silicon atoms, and **LII**, derived in part from metatheses of olefins tethered to the same silicon atom. Per the convention in section 6, the former are given unprimed numbers and the latter primed ones (the alphabetical indices **a**, **b**, **c**, etc. for *m* and *n* are also kept constant). Compounds available by this route are

https://dx.doi.org/10.1021/acs.chemrev.0c01001
Chem. Rev. 2021, 121, 3701−3750

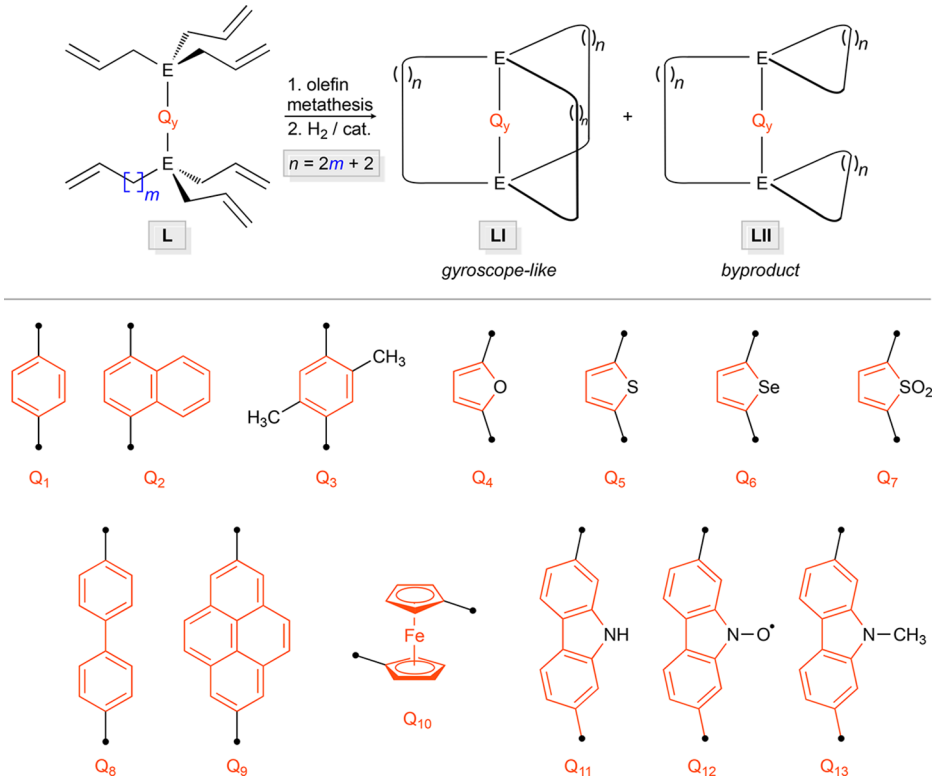

Figure 27. Gyroscope-like molecules prepared by the Setaka group by 3-fold ring closing metatheses of substrates of the type **L**.

summarized in Table 3. In about half of the cases, **LI** is the dominant product.

As shown in Figure 28, Setaka has considered the product distribution that would be expected if the rate constants at each branch point in the metathesis sequences leading to **LI** and **LII** were identical.[127] Interestingly, the latter is favored statistically, with an idealized 1:3 ratio (20% vs 60%, with 20% oligomer or incomplete metathesis). In Table 3, this ratio is realized (or exceeded) only for **50d′**, **52d′**, **54d′**, **58e′**, **59e′**, **60d′**, **61e′**, **61g′**, and **63e′**.

Thus, the rate constants for metatheses involving olefins tethered to different silicon atoms generally appear to be greater. However, for **50c** and **50c′**, the dominant product depends upon the temperature at which metathesis is carried out (**LI**/**LII** 1.0:0.8, 0 °C; 1.0:1.0, 20 °C; 1.0:1.7, 40 °C).[127] This suggests that, at least in this case, some macrocyclization steps are reversible, with **50c′** (or the triolefin precursor **LVIII** in Figure 28) representing the thermodynamically more stable product.

Setaka has also been able to prepare starting substrates in which the two anchoring silicon atoms bear different substituents.[131,135] For example, an endgroup Si-$(((CH_2)_mCH{=}CH_2)_3)_2$ can be paired with one in which each silicon substituent has an additional methylene spacer, $Si(((CH_2)_{m+1}CH{=}CH_2)_3)_2$. This allows access to methylene bridges with an odd number of carbon atoms, that is, $Si(CH_2)_{2m-1}Si$. Such products are depicted in Figure 29 and are designated with a double index (**cd** or **de**), denoting an intermediate (odd) value of *n*.

Setaka has also employed other types of 3-fold macrocyclizations to access dibridgehead disilanes. That shown in Figure 30 involves stitching together the terminal hydrosilane moieties of substituents of the formula $(Si)CH_2CH_2Si(CH_3)_2CH_2CH_2\mathbf{Si}(CH_3)_2\mathbf{H}$ with aqueous NaOH to give bridges with siloxane ($\mathbf{Si}(CH_3)_2\mathbf{O}(CH_3)_2\mathbf{Si}$) linkages.[139−141] As in Figure 29, this protocol also affords an odd number of atoms in the spokes between the bridgehead silicon atoms. Another macrocyclization method that was used to install two bridges between the anchoring silicon atoms was depicted in Figure 7 in section 4.3.

All of the gyroscope-like compounds in Figures 27, 29, and 30 exhibit 6-fold rotational barriers, with six maxima and six minima as the rotator is rotated through 360° (see section 6.4). Those with symmetrically substituted or nondipolar rotators like *p*-phenylene share many features with the square planar complexes with ML_2 rotators from the authors' laboratory (e.g., **18c−g,k** in Figure 11). Those with less symmetrical or dipolar rotators such as 2,3-dichloro-*p*-phenylene (**66** in Figure 30) would be conceptually related to square planar complexes with MLL′ rotators (e.g., **20c** in Figure 11 or **35c,e** in Figure 20).

7.2. Dynamic Properties in Solution

For several of his compounds, Setaka has probed the barriers to rotator rotation in solution by variable temperature NMR. Consider first the *p*-phenylene adduct **50c**, which features 14 methylene groups in each spoke connecting the bridgehead silicon atoms. Given the symmetry and the analysis in Figure 22 (middle panel), two sets of $^{13}C\{^1H\}$ NMR signals would be expected (ca. 2:1 area ratio). However, only a single set is observed in $CDCl_3$ at ambient probe temperature, indicative of rapid rotation on the NMR time scale.[123]

Such phenomena can be qualitatively analyzed in a manner analogous to Figure 24. However, one difference is that for most *p*-arylene rotators, the atoms that must pass through the macrocycles, for example, the HC⋯CH units derived from *ortho* carbon and hydrogen atoms of *p*-phenylene, are no longer in the equatorial plane. In any case, the crystal structure of **50c** provides important reference points. Several views of the lowest

https://dx.doi.org/10.1021/acs.chemrev.0c01001
Chem. Rev. 2021, 121, 3701−3750

Table 3. Data for the Reactions Represented in Figure 27

Q_y	E	n	product type **LI**	yield (%)[a]	product type **LII**	yield (%)[a]	ref
Q_1	Si	12	**50b**	*b*	**50b′**	*b*	129
Q_1	Si	14	**50c**	24	**50c′**		123,125,129
Q_1	Si	16	**50d**	10	**50d′**	43	129
Q_1	Si	18	**50e**	23[c]	**50e′**	39	127,129
Q_1	Ge	14	**51c**	24	**51c′**	8	128
Q_2	Si	14	**52c**	29	**52c′**	27	126,131
Q_2	Si	15	**52cd**	14	**52cd′**	29	131
Q_2	Si	16	**52d**	7	**52d′**	32	126,131
Q_2	Si	17	**52de**	13	**52de′**	28	131
Q_2	Si	18	**52e**	18	**52e′**	15	126,131
Q_3	Si	14	**53c**	7	**53c′**		123
Q_4	Si	14	**54c**	5	**54c′**	2	138
Q_4	Si	16	**54d**	4	**54d′**	19	132
Q_5	Si	14	**55c**	25	**55c′**	2	124
Q_5	Si	16	**55d**	15	**55d′**	24	132
Q_5	Si	17	**55de**	17	**55de′**	18	135
Q_6	Si	16	**56d**	18	**56d′**	38	132
Q_7	Si	16	**57d**	66	**57d′**		135
Q_7	Si	17	**57de**	60[d]	**57de′**		135
Q_8	Si	18	**58e**	3	**58e′**	45	133
Q_9	Si	18	**59e**	5	**59e′**	51	130
Q_{10}	Si	14	**60c**	8	**60c′**	19	134
Q_{10}	Si	16	**60d**	12	**60d′**	44	134
Q_{10}	Si	18	**60e**	15	**60e′**	17	134
Q_{10}	Si	22	**60g**	12	**60g′**	15	134
Q_{11}	Si	18	**61e**	5	**61e′**	46	136
Q_{11}	Si	22	**61g**	9	**61g′**	28	136
Q_{12}	Si	18	**62e**	*e*	**62e′**	*e*	136
Q_{12}	Si	22	**62g**	*e*	**62g′**	*e*	136
Q_{13}	Si	18	**63e**	3	**63e′**	34	137

[a]Isolated yields following metathesis and hydrogenation. [b]No disilicon products could be detected. [c]The highest yield among several conditions screened. [d]This yield is for the oxidation of **55de** using *m*-CPBA. [e]Due to the short half-life of these radical species, yields could not be established.

temperature modification are depicted in Figure 31 (the rotator is disordered in higher temperature modifications).

In **50c**, the average distance between the *ortho* carbon atoms on opposite sides of the rotator axis is 2.38 Å, and that for the corresponding hydrogen atoms is 3.92 Å. These relationships are depicted in Figure 32 (top; d_1 and d_2). When twice the van der Waals radius of a hydrogen atom is added, a wingspan of 5.73 Å (d_3) is obtained. This is halved to obtain the corresponding radius or "horizontal steric demand", 2.87 Å. For reference, the radius is much shorter than that of the iron or osmium rotator in the trigonal bipyramidal complexes in Table 2 (4.38−4.59 Å).

In the vertical dimension, the average distance between the two pairs of HC⋯CH hydrogen atoms is 2.28 Å (d_5), as shown in Figure 32 (top). When twice the van der Waals radius of a hydrogen atom is added, a "vertical steric demand" of 4.10 Å is obtained (d_6).

As in Figure 24, the horizontal and vertical "clearance" afforded by the stator is estimated from the crystal structure (Figure 31). For the former, the distance from the centroid of the *p*-phenylene ring to the two innermost CH_2 groups of each $(CH_2)_n$ bridge (here $(CH_2)_{14}$) is calculated, and the van der Waals radius of carbon is subtracted. The shortest of the six resulting distances is then used as the most conservative estimate, which for **50c** is 4.74 Å as compared to an average of 5.42 Å. Thus, the radius of the *p*-phenylene rotator can be comfortably accommodated within the spokes of the stator (2.87 Å vs 4.74 Å), as would be intuitively expected by viewing the crystal structure. As noted above, there are several alternative approaches to estimating horizontal clearances, but since all are intrinsically qualitative, the authors stick with Figure 24.

For the vertical clearance, it is a simple matter to define the two planes that contain the three $Si(CH_2)_3$ carbon atoms bound to each terminus of the rotator (Figure 32, bottom; cf. Figure 24, right). When these are not parallel, the plane/plane distance that runs through the silicon−silicon vector is calculated (7.87 Å). The van der Waals radii of two carbon atoms are then subtracted. For **50c**, the clearance so obtained (4.47 Å) is greater than the vertical steric demand of the *p*-phenylene rotator computed in Figure 32 (4.10 Å). Hence, in **50c** the rotator/stator steric interactions are greatly attenuated relative to the metal diphosphine complexes with $(CH_2)_{14}$ bridges in section 6. For comparison, the distance between the two $E(CH_2)_3$ planes of the analogous $Fe(CO)_3$ adduct **17c** is 6.00 Å versus 7.87 Å for **50c**.

In a tour-de-force, Setaka was able to synthesize and crystallographically characterize five dibridgehead disilicon compounds with 1,4-naphthalenediyl rotators and progressively longer $(CH_2)_n$ bridges (n = 14, **52c**; 15, **52cd**; 16, **52d**; 17, **52de**; 18, **52e**).[126,131] The structures of the compounds with bridges where n is an even number are shown in Figure 33. This rotator is much more sterically demanding than *p*-phenylene in both the horizontal and vertical dimensions.

To estimate the radius or horizontal steric demand, the centroid of the C_6H_2 ring that spans the bridgehead silicon atoms is first defined. As shown in Figure 32, the distance to the midpoint between the two remote hydrogen atoms of the C_6H_4 ring is then calculated. The van der Waals radius of a hydrogen atom is subsequently added to give the radius of the rotator (d_{AC}). As would be expected, very similar quantities are obtained for each compound (5.34−5.39 Å; average 5.37 Å).

The horizontal clearance associated with the stators is calculated as with **50c**, except that for **52cd** and **52de** (for which n in $(CH_2)_n$ is odd), the distances from the centroid of the C_6H_2 ring to a total of nine CH_2 groups (the three innermost of each bridge) are considered. After subtracting the van der Waals radius of a carbon atom, the shortest and average clearances are as follows: **52c**, 4.38/5.22 Å; **52cd**, 4.33/5.77 Å; **52d**, 5.39/6.43 Å; **52de**, 5.39/6.40 Å; **52e** 6.42/7.33 Å. With the three largest macrocycles, the values exceed the radius of the 1,4-naphthalenediyl moiety (5.34−5.39 Å), auspicious for rotation.

For the vertical steric demand, the distances between the *para* hydrogen atoms of the C_6H_4 rings are first calculated (4.66 Å). As depicted in Figure 32 (middle), the van der Waals radii of two hydrogen atoms are then added, giving 6.48 Å (d_7). The vertical clearances, calculated from the planes of the $Si(CH_2)_3$ carbon atoms as described for **50c** in Figure 32, average 4.57 Å (**50c**, 4.55 Å; **52cd**, 4.70 Å; **52d**, 4.53 Å; **52de**, 4.52 Å; **52de**, 4.55 Å). These values are significantly lower than the 6.48 Å vertical steric demand, impeding rotation.

Thus, rotation of the rotators will need to be correlated to conformational changes in the macrocycles that "open up" the vertical dimension. The crystal structures in Figure 33 allow one possible modus to be visualized. In **52c**, all six of the C_{ipso}−Si−CH_2−CH_2 linkages adopt *gauche* conformations. However, in

https://dx.doi.org/10.1021/acs.chemrev.0c01001
Chem. Rev. 2021, 121, 3701−3750

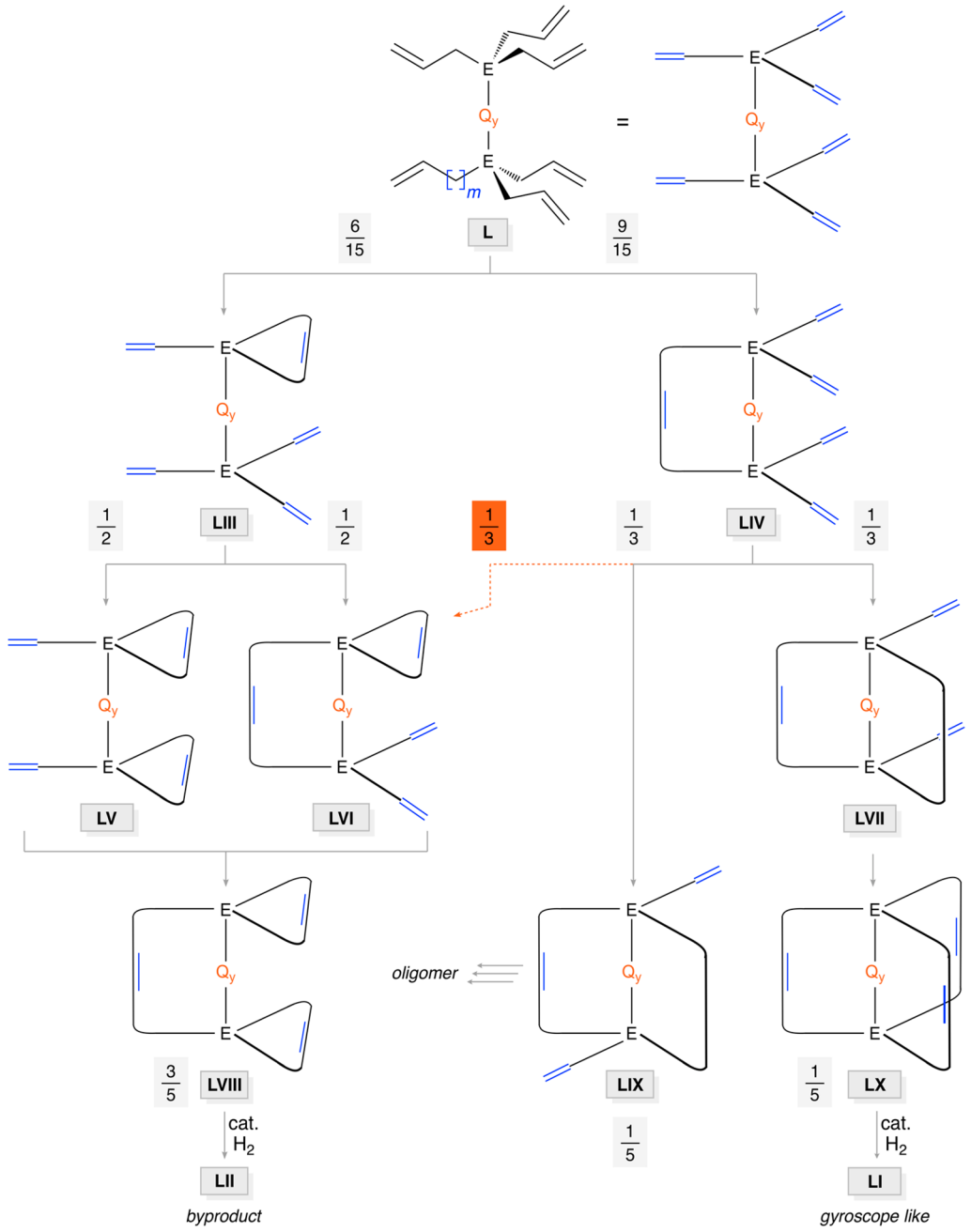

Figure 28. Predicted ratio of hydrogenated ring closing olefin metathesis products **LI** and **LII** (Figure 27) assuming equal rate constants for metathesis at every branch point (and no reversibility).[127]

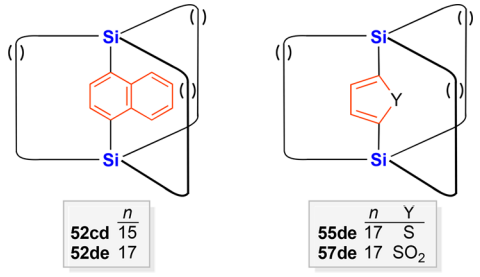

Figure 29. Gyroscope-like compounds synthesized by a variation of Figure 27 in which the number of methylene groups in the $P(CH_2)_m$ segments on the "top" and "bottom" in **L** differ by one [() indicates $(CH_2)_n$].[131,135]

52e there are two *anti* C_{ipso}–Si–CH_2–CH_2 linkages (one at each terminus), presumably facilitated by the longer methylene chain. The *anti* disposition widens the vertical dimension of the "hole" in the macrocycle.

Variable temperature NMR spectra of **52c**, **52cd**, **52d**, **52de**, and **52e** give results consistent with the preceding analyses. In the case of **52c**, $^{13}C\{^1H\}$ NMR spectra show two sets of $Si(CH_2)_{14}Si$ signals (ca. 2:1 area ratios) in toluene-d_8, both at ambient probe temperatures and upon heating to 340 K.[131] These data allow a lower limit of 15.4 kcal/mol to be set for $\Delta G^{\ddagger}_{340K}$ (calculated by the present authors from two non-coalescing $SiCH_2$ signals with a frequency difference of 202 Hz), as indicated in Table 4.

In the case of **52d**, the longer methylene chains allow the coalescence of ^{13}C NMR signals to be observed (260–280 K),

https://dx.doi.org/10.1021/acs.chemrev.0c01001
Chem. Rev. 2021, 121, 3701–3750

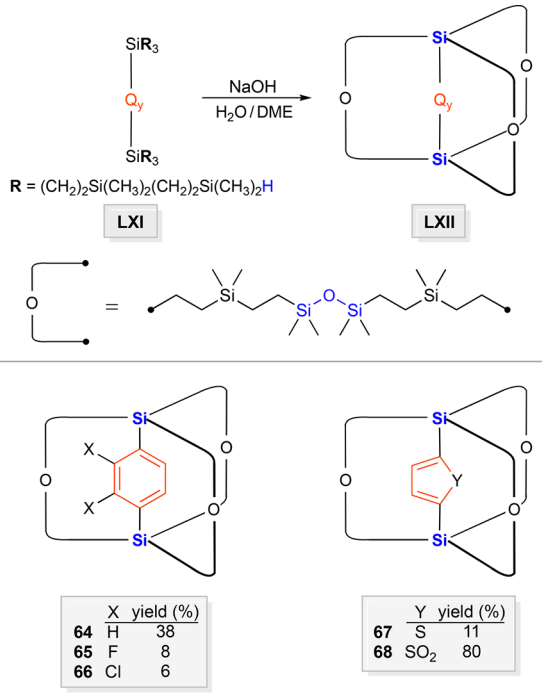

Figure 30. Gyroscope-like compounds from the Setaka group prepared by macrocyclizations other than olefin metathesis.[139−141]

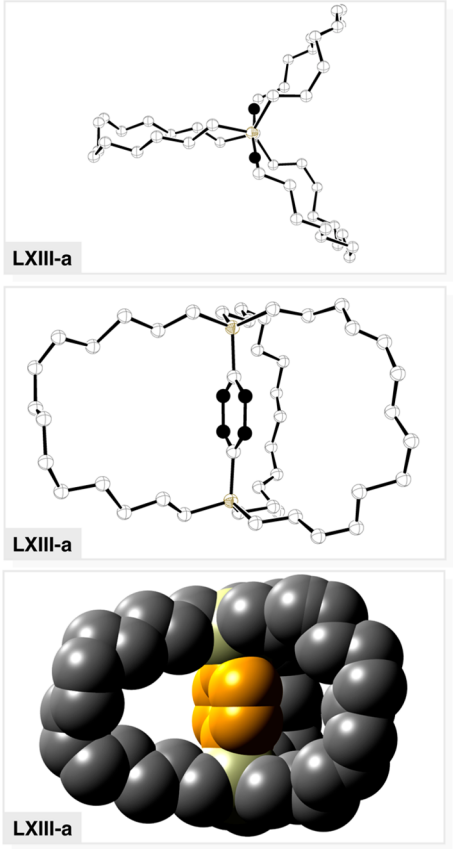

Figure 31. ORTEP and space filling representations of the crystal structure of **50c** (lowest temperature modification).

as shown in Figure 34.[126] The data give $\Delta H^{\ddagger}$ and $\Delta S^{\ddagger}$ values of 9.42 kcal/mol and −12.0 eu, respectively, as noted in Table 4. In the case of **52e**, the slow exchange limit cannot be realized,

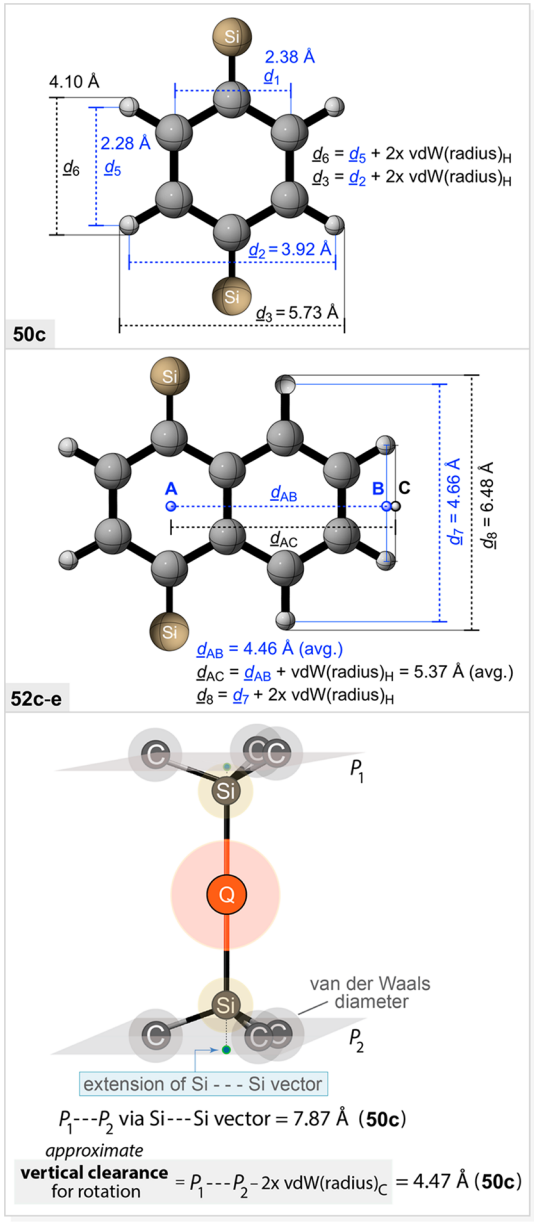

Figure 32. Geometric relationships involving the rotators and stators in the *p*-phenylene and 1,4-naphthalenediyl adducts **50c** and **52c−e**. In the five compounds **52c−e**, the distances d_{AB} and d_{AC} range from 4.43 to 4.48 Å and 5.34 to 5.39 Å, respectively.

even at 220 K. However, when toluene-d_8 solutions of the compound with an intermediate methylene chain length, **52de**, are cooled, decoalescence can be observed (230 K). The data give $\Delta H^{\ddagger}$ and $\Delta S^{\ddagger}$ values of 7.49 kcal/mol and −11.0 eu, respectively. Finally, **52cd** has been studied by $^{13}C-^{13}C$ EXSY, a technique that allows dynamic processes with a broader range of time scales to be characterized. The data give $\Delta H^{\ddagger}$ and $\Delta S^{\ddagger}$ values of 14.6 kcal/mol and −11.9 eu, respectively.

The activation parameter trends in Table 4 reflect the increasing abilities of the longer methylene chains to "open up" in the horizontal and vertical dimensions to accommodate the 1,4-naphthalenediyl rotators. In this context, an interesting feature can be seen in the top views of the crystal structures in Figure 33 (also with **52cd** and **52de**, which are not depicted). Namely, the rotators adopt conformations that maximize the distance of the sterically demanding C_6H_4 ring from the two

https://dx.doi.org/10.1021/acs.chemrev.0c01001
Chem. Rev. 2021, 121, 3701−3750

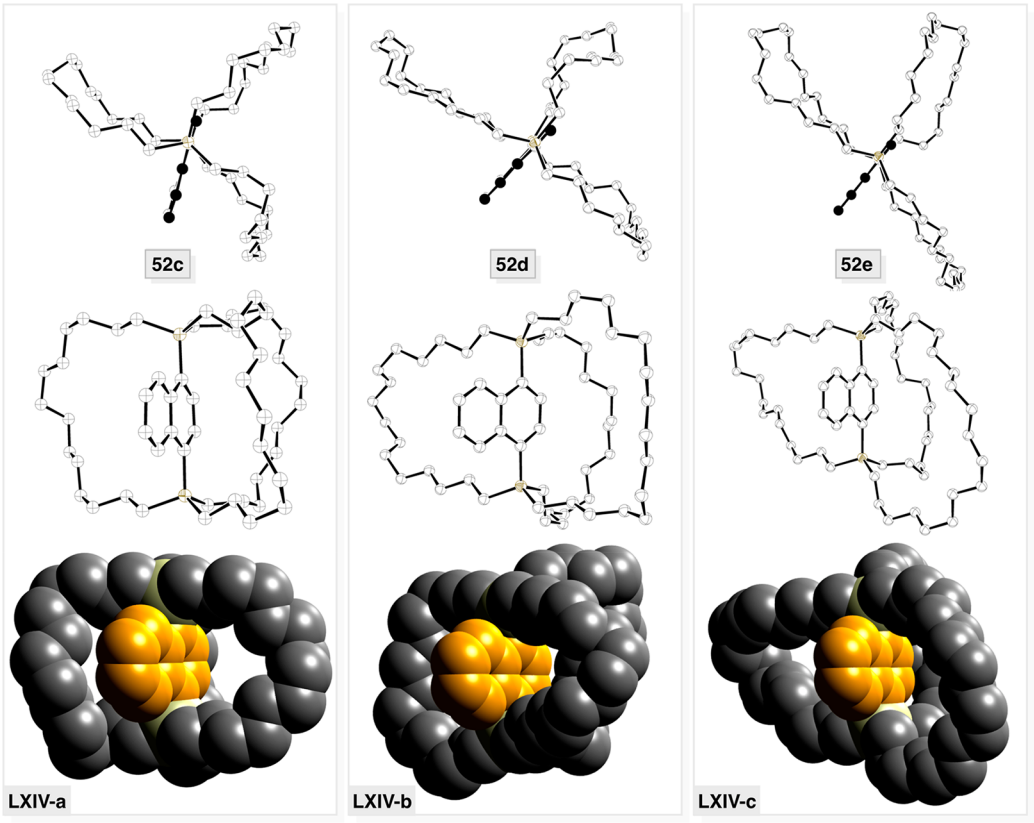

Figure 33. ORTEP and space filling representations of the crystal structures of **52c−e**.

Table 4. Activation Parameters for Rotation of 1,4-Naphthalenediyl Rotators in Toluene-d_8 Solution

compound	n	experiment	$\Delta H^{\ddagger}$ (kcal mol^{-1})	$\Delta S^{\ddagger}$ (eu)[a]	$\Delta G^{\ddagger}_{340K}$ (kcal mol^{-1})	ref
52c	14	^{13}C NMR	>14.6[b]		>15.4[c]	126,131
52cd	15	^{13}C−^{13}C EXSY NMR	14.6[d]	−11.9[d]	17.0	131
52d	16	^{13}C NMR (220−320 K)	9.42	−12.0	11.8	126,131
52de	17	^{13}C NMR (210−270 K)	7.49	−11.0	9.7	131
52e	18	estimate based on **52d**	<7.46[b]			126,131

[a]Units of cal·mol^{-1}·K^{-1}. [b]Estimated as described in the reference cited. [c]Limit calculated as described in the text. [d]These values were assigned appreciable error limits.

nearest macrocycles. This has the consequence of positioning the C_6H_2 ring within the cavity of the remaining macrocycle. Such eclipsing interactions are rarely observed in the crystal structures of the many other dibridgehead diheteroatom rotors in this review. Interestingly, there are intermolecular π stacking interactions between rotators in crystalline **52c**, **52d**, and **52e**, but not in **52cd** or **52de**.

Setaka has similarly studied a second series of compounds, this time varying the rotators. As shown in Figure 30 above, the *p*-phenylene, 2,3-difluoro-*p*-phenylene, and 2,3-dichloro-*p*-phenylene adducts **64−66** feature silicon atoms that are spanned by 13 atom bridges, each with four $SiMe_2$ groups. The additional methyl groups render the steric topology of these compounds much different from those discussed above. Thus, analyses of "clearances" and related properties are not attempted. Some views of the crystal structure of the dichloro species **66** are given in Figure 35.[140] The top representation shows that the rotator adopts a conformation that maximizes the distance the ClC⋯CCl moiety from the nearest macrocycles. In a phenomenon similar to that seen in Figure 33, this directs the smaller HC⋯CH moiety into a macrocycle cavity.

When NMR spectra of the *p*-phenylene compound **64** or difluoro analog **65** are recorded at 173−175 K in $CDCl_3$, only a single set of signals is observed. However, for the dichloro analog **66**, the $SiMe_2$ ^{1}H NMR signals decoalesce upon cooling as shown in Figure 36. Line shape analyses and application of a three site exchange model give $\Delta H^{\ddagger}$ and $\Delta S^{\ddagger}$ values of 12.8 kcal/mol and −4.6 eu, respectively.[139,140] The radii of the rotators in this series of compounds increase from 2.87 Å (**64**) to 3.84 Å (**65**, approximated from 1,2-difluorobenzene)[154] to 4.47 Å (**66**). A computational study of **64** suggests a miniscule barrier of 1.2 kcal/mol.[155]

7.3. Dynamic Properties in the Solid State

The Setaka group has also probed the rotation of the rotators of many of the preceding compounds in the solid state. There are several variable temperature solid state NMR methods that are widely applicable to the investigation of molecular dynamics within crystals, as reviewed by Garcia-Garibay, who first applied these techniques to gyroscope-like molecules.[35] In the Setaka group, the workhorse has been quadrupolar echo solid state ^{2}H NMR, which requires that the motional units be labeled with deuterium atoms. Most researchers concerned with dynamics in

https://dx.doi.org/10.1021/acs.chemrev.0c01001
Chem. Rev. 2021, 121, 3701−3750

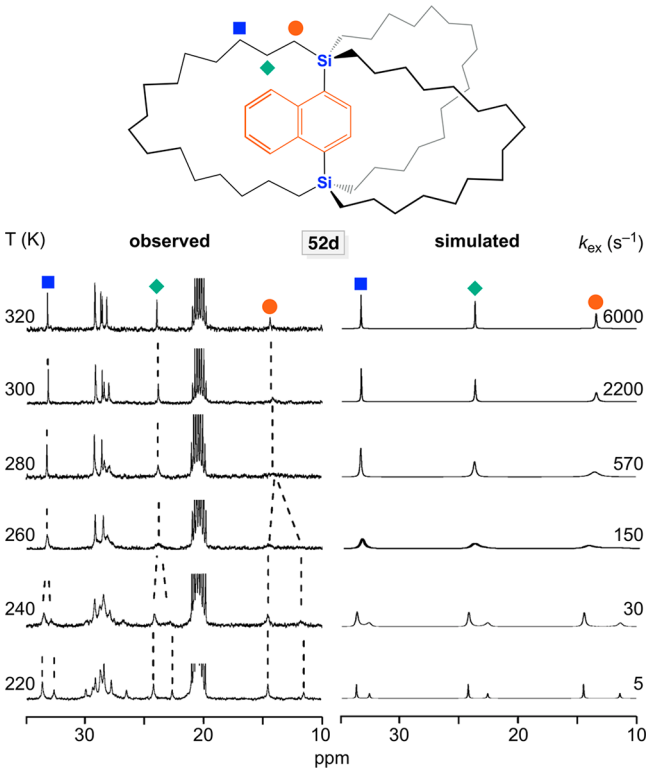

Figure 34. Temperature dependence of inverse gated decoupled ^{13}C NMR spectra of **52d** in toluene-d_8 (left) and simulated spectra (right, key signals only).[126]

crystals express barriers as E_a values (from Arrhenius plots), as opposed to $\Delta H^{\ddagger}$ or $\Delta G^{\ddagger}$ values (from Eyring plots). It is also common to speak of a group "flipping" as opposed to undergoing rotation.

As in section 7.2, the *p*-phenylene adduct **50c** provides a logical starting point. This compound crystallizes with all rotator axes (Si−*p*-C_6H_4−Si) parallel, and the C_6D_4 analog (**50c**-d_4) has been similarly synthesized.[123] When the entire crystal lattice is considered, the two DC⋯CD linkages occupy inequivalent sites (although the environments appear similar when a single molecule is viewed, as in Figure 31). Variable temperature quadrupolar echo ^2H NMR spectra give the Pake patterns depicted in Figure 37. Simulation of the line shapes for the data at 230−260 °C give rate constants that are used in an Arrhenius plot, affording an E_a of 10.3 kcal/mol for "flipping" the C_6D_4 moiety by 180°.

Above 270 °C, the narrower line widths indicate an additional oscillatory or librational degree of freedom. This is substantiated by crystal structures over a parallel temperature range, which reveal increased anisotropic thermal parameters followed by structural disorder. A reduced E_a of 9.0 kcal/mol could be computed from the data. Setaka also documented the temperature dependent birefringence of the crystals, a property exhibited by several other compounds below.

The analogous species with a dideuterated *p*-xylene based rotator (**53c**-d_2; see Figure 37) has been similarly studied. Although the radius of this rotator is significantly greater than that of *p*-phenylene (4.25 Å vs 2.87 Å), the crystal structures and lattices of the two compounds (as their non-deuterated analogs) are similar. As noted in section 7.2, a conservative estimate of the horizontal clearance in crystalline **50c** is 4.74 Å.

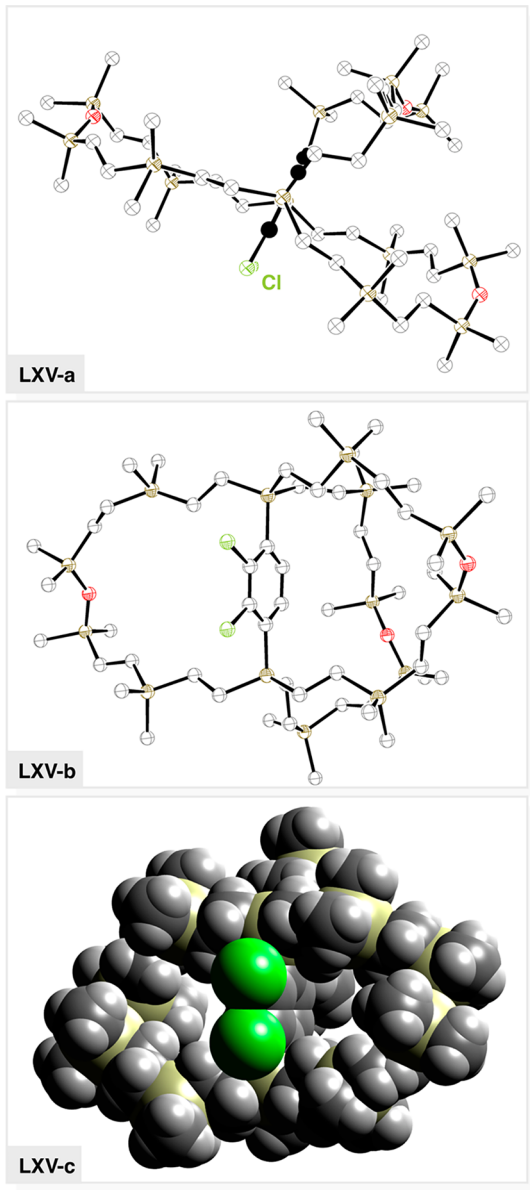

Figure 35. ORTEP and space filling representations of the crystal structure of the 2,3-dichloro-*p*-phenylene adduct **66** (see Figure 30).[140]

However, the ^2H NMR data indicate that the rotator in **53c**-d_2 is static within the crystal.

The digermanium analog of **50c**-d_4, **51c**-d_4, has also been synthesized.[128] Again, the molecular structures and crystal lattices (of the non-deuterated counterparts) are virtually identical. As expected, the Ge−C_{ipso} bond is longer than the Si−C_{ipso} bond (1.958(4) Å vs 1.885(4) Å, or 3−4%). Consistent with the vertically more spacious stator, the E_a for C_6D_4 rotation associated with the higher temperature dynamic regime decreases to 8.0 kcal/mol from 9.0 kcal/mol.

In another follow up to the NMR study of **50c**-d_4, Setaka examined the analog in which the saturated $(CH_2)_{14}$ bridges were replaced by monoolefinic (*E*)-$(CH_2)_6CH{=}CH(CH_2)_6$ bridges (**50c***-d_4).[125] The parent compound **50c*** (see Figure 38) proved isolable in 24% yield when the sequence in Figure 27 was worked up after olefin metathesis but prior to hydrogenation. It also crystallized with parallel rotator axes. In any case, ^2H NMR experiments (**50c***-d_4, 280−300 K)

https://dx.doi.org/10.1021/acs.chemrev.0c01001
Chem. Rev. 2021, 121, 3701−3750

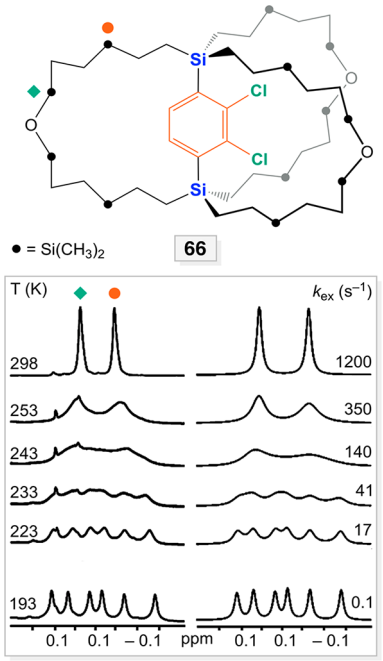

Figure 36. Variable temperature ^{1}H NMR spectra of **66** ($SiMe_2$ region): left, observed spectra; right, simulated spectra with rate constants for exchange.[140]

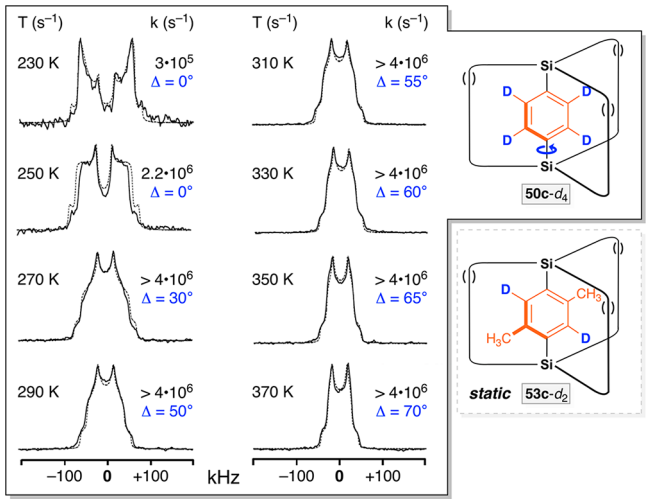

Figure 37. Variable temperature solid state quadrupolar echo ^{2}H NMR spectra of **50c**-d_4 showing characteristic Pake patterns. () indicates $(CH_2)_n$.[123]

established an E_a of 11.4 kcal/mol for a 180° flip of the rotator. The increase over that of **50c**-d_4 (10.3 kcal/mol under comparable conditions) was attributed to steric constraints imposed by the (*E*)-C═C linkages.

As with **50c**-d_4, a higher temperature dynamic regime (>300 K) distinguished by narrower line widths was also characterized. These data could be simulated by a six-site exchange model with the *p*-phenylene moiety populating three minima spaced by 120° about the rotator axis. The barrier dramatically decreased, and to help gain insight, crystal structures of **50c*** were determined at a series of temperatures. As shown in Figure 38, between 300 and 340 K the rotator became disordered over three positions (differing by 120° about the rotator axis; occupancies 0.24, 0.63, 0.29). In addition, the macrocycle

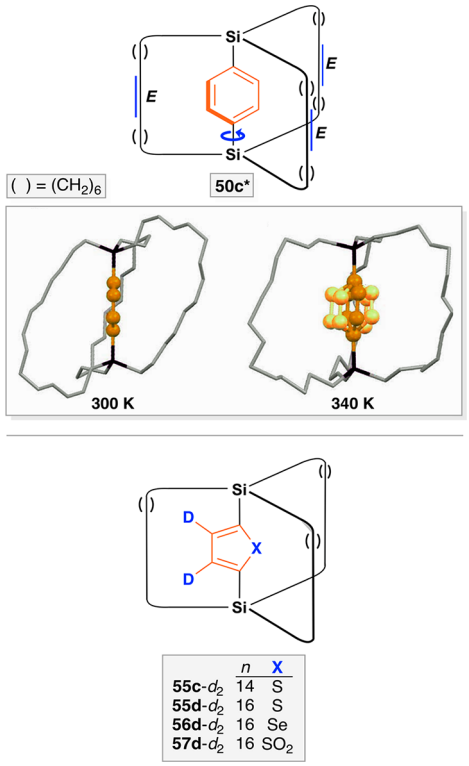

Figure 38. *p*-Phenylene adduct **50c*** (top), crystal structures at 300 and 340 K, with the latter showing *p*-C_6H_4 disorder (middle), and heterocycle adducts studied by solid state ^{2}H NMR (bottom, () indicates $(CH_2)_n$).[125]

conformations became more spherical or "horizontally extended". This could potentially be quantified in a number of ways, but only the data set collected at 100 K has been made available in the CCDC. These distortions were proposed to account for the faster *p*-phenylene rotation and provide a welcome "snapshot" of the "correlated conformational changes" frequently invoked above during rotator rotation.

The expansions of the macrocycles were also reflected in the unit cell dimensions, which were determined at closely spaced temperature intervals. All of these phenomena remained fully reversible below 355 K. Setaka likened the overall changes in macrocycle conformations to the inflation and deflation of a balloon.

Various compounds with heterocyclic rotators and saturated $(CH_2)_n$ bridges have also been studied by Setaka. For example, crystal structures of the dipolar 2,5-thiophenediyl rotor **55c** (see d_2 analog, Figure 38, bottom)[124] have been determined at a series of temperatures. Again, all rotator axes are parallel in the lattice. At 200 K, the rotators exhibit two orientations such that the molecular dipoles cancel. At 270 K, a different modification with two alternative dipole orientations is obtained, but the dipoles again cancel. At 300 K, a third modification is obtained in which the dipoles are randomly distributed between two orientations but with an overall 50:50 population. A number of ^{2}H NMR experiments have been carried out with **55c**-d_2. The thiophenediyl rotator is static in the low temperature crystalline form but undergoes slow and fast exchange in the higher temperature crystalline forms. However, it is not possible to obtain quantitative activation energies.

Setaka has also expanded this effort to the higher $(CH_2)_{16}$ homologue of **55c**-d_2, namely, **55d**-d_2[132] and the corresponding

https://dx.doi.org/10.1021/acs.chemrev.0c01001
Chem. Rev. 2021, 121, 3701−3750

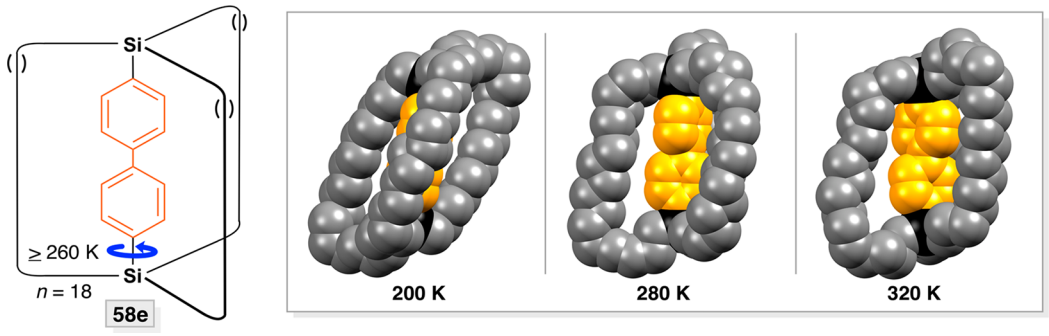

Figure 39. 4,4′-Biphenylene adduct **58e** [() indicates $(CH_2)_n$], and space filling representations of the crystal structures at 200 K (left), 280 K (center), and 320 K (right).

2,5-selenophenediyl species **56d**-d_2 in Figure 38.[132] Again, the nondeuterated analogs crystallize with parallel rotator axes. Once more, technical issues render quantitative activation energies elusive, but it is possible to establish a lower rotational barrier for the selenium compound. This counterintuitive result has been rationalized based upon subtle effects derived from Si−C(aryl) bonds, leading to a greater silicon−silicon separation in **56d** (6.31 Å vs 6.09 Å at 200 K).

However, it has proven possible to obtain E_a values for rotation of the heterocyclic rotator in the analogous 2,5-thiophene(dioxide)diyl species **57d**-d_n.[135] That determined by ^{2}H NMR is 9.0 kcal/mol, and that measured by dielectric spectroscopy is 9.1 kcal/mol. It seems likely that the barriers in the thiophenediyl analog **55d** would be lower. Interestingly, **57d** also crystallizes with parallel rotator axes.

The compound **58e** shown in Figure 39 features a 4,4′-biphenylene (p-C_6H_4−p-C_6H_4) rotator, which is among the longest studied by Setaka (see Figure 27).[133] Extended $(CH_2)_{18}$ chains are required to bridge the silicon atoms. Three crystalline phases could be characterized (Figure 39), all with parallel rotator axes and silicon−silicon distances of 10.68 Å, 10.88 Å, and 10.87 Å. The angles defined by the planes of the C_6H_4 rings increase from 42° in the lowest temperature modification to 66° in the higher temperature forms.

A variety of ^{2}H NMR experiments have been carried out with **58e**-d_4. The rotators in the lowest temperature modification are static at 220 K, but "flipping" can be detected at 260 K. In the higher temperature modifications, the macrocycles adopt more spherical (less ovoid) conformations, although not to the extent in Figure 38, and rotation becomes immeasurably fast. Interestingly, the data require that only one type of rotation is operational, either (1) synchronous rotation of the two p-phenylene moieties or (2) independent (asynchronous) rotation, but not both.

Finally, there have been some attempts to model the rotational dynamics of selected disilicon compounds by computational methods (**50c,d,e**;[129] **64**[155]). These initial efforts have been able to reproduce certain features in a qualitative sense (e.g., conformational energy minima), but have not given quantitatively reliable data. As noted above, the barrier computed for **64** is a very low 1.2 kcal/mol.

7.4. Toward Molecular Gyroscopes

Despite the steric interactions that attend rotation of the rotators in many of the above disilicon (and digermanium) compounds, there are also species that seemingly lack significant steric contacts (e.g., **50c**). Furthermore, most compounds crystallize in motifs with all rotator axes parallel, and dipolar rotators are easily accommodated. As such, this remains a very promising class of compounds for engineering very small barriers to rotator rotation, and application as molecular gyroscopes. Setaka's compounds also seem to be particularly prone to phase transitions in the solid state, affording multiple allotropes for study.

8. SYSTEMS FROM THE GARCIA-GARIBAY GROUP

8.1. Prefatory Comments

It hardly seems fitting that studies by the Garcia-Garibay group, which is responsible for so much intellectual and experimental leadership regarding molecular gyroscopes, are not treated in the leadoff section. Nonetheless, from a narrative standpoint it seemed more natural to transition from groups that have emphasized solution phase investigations to those that have emphasized solid phase investigations. Garcia-Garibay has also introduced the allied concept of "molecular compasses", in which dipolar rotators are oriented by static electric fields.[156−160] Unsurprisingly, he has reviewed some aspects of his work himself.[34−37]

The broad interests of the Garcia-Garibay group in molecular rotors and amphidynamic crystals present some complications. Some of these studies directly target molecular gyroscopes and others less so, although there remains an obvious relevance. Thus, most of the groups' work involving molecular rotors has been covered but with a few exclusions: (1) rotors that feature large biomolecules such as steroids as stators[161−167] are not treated, as these have generally been prepared with goals other than molecular devices in mind; (2) rotors that are restricted to crankshaft type motions[168] or are comprised of multiple nonparallel rotators[169,170] are likewise not treated.

Several design elements helped to drive these studies. In general, a svelte rotator with rod-like segments is paired with a bulky stator, usually in the form of two endgroups with appreciable radial extensions. The hope, aided by design elements familiar in crystal engineering, such as the "sextuple phenyl embrace",[171,172] is that the molecule will crystallize in a motif with all rotator axes parallel. It is furthermore hoped that the endgroups will enforce spacings between the axes that allow for facile rotation of the rotators in the solid state. One optimistic scenario is shown in **C** in Figure 40. However, as illustrated in **CI**, packing motifs remain in which the stator can sterically interact with the rotator of a neighboring molecule. This can be ameliorated by stators with enhanced shielding capabilities, as illustrated in **CII**.

Said differently, the objective is the creation of "free space" about a rotator with a "low volume demand". As this work has

https://dx.doi.org/10.1021/acs.chemrev.0c01001
Chem. Rev. 2021, 121, 3701−3750

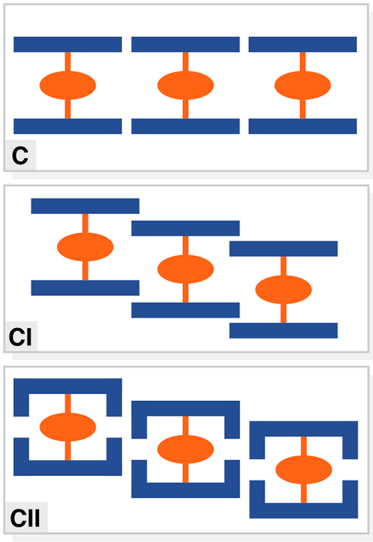

Figure 40. Combinations of different types of radially bulky stators (blue) and low-volume-demand rotators (orange) and possible packing motifs.

progressed, additional concepts such as "packing coefficients" (C_k; the van der Waals volumes of all molecules in the unit cell divided by the unit cell volume; typically 0.80−0.65 for organic molecules)[173] and "crystal fluidity" (the ability of the rotator surroundings to distort, creating transient cavities),[37] have been introduced. To fast-forward to where this line of inquiry winds up today, Garcia-Garibay concludes that the creation of free space alone does not always result in ultrafast dynamics.[37] In closed packed crystals (low free volumes), dynamics can also be rapid, but this requires substantial crystal fluidity.

One "wild card" in crystal engineering is the potential for solvent to occupy void spaces, so special attention must be paid to the composition of any crystal studied. Apropos to their chemical heritages, the authors refer to these as solvates, whereas Garcia-Garibay employs the more general term clathrates. Furthermore, polymorphism or pseudopolymorphism[174] can be observed, as seen in section 7 with a number of Setaka's molecular rotors.

As noted above, Garcia-Garibay has reviewed the NMR methods that are most widely applied to the study of molecular dynamics within crystals.[35] He most frequently employs variable temperature solid state ^{13}C CP/MAS NMR (cross-polarization/magic angle spinning) and quadrupolar echo ^{2}H NMR. Error limits are not quoted in the text for the resulting Arrhenius activation energies (E_a), but when these have been reported, they are incorporated into tabular summaries herein. The Arrhenius pre-exponential factors are also tabulated.

Well over half of the rotators studied by Garcia-Garibay incorporate -C≡C−(*p*-arylene)−C≡C- linkages. The individual sp carbon atoms are presumed to undergo barrierless rotation. In the case of *p*-phenylene, the distance between the C_{sp}/C_{sp} or -**C**≡C−(*p*-C_6H_4)−C≡**C**- termini is typically 8.06 Å. Thus, Garcia-Garibay's rotators are generally much longer than those studied by Setaka or the authors. The distance between the C_{sp^2}/C_{sp^2} termini of the 4,4′-biphenylene rotators in Setaka's compound **58e** (Figure 39) is 7.16−7.22 Å (depending upon modification).

Most of Garcia-Garibay's stators or endgroups feature C_3 symmetry axes. Many of the rotors used for solid state studies are assembled by similar sequences. Hence, to enhance continuity, their syntheses are grouped in a later section (section 8.4).

8.2. Rotors Studied in Solution

Garcia-Garibay has prepared a few molecular rotors with topologies evocative of those emphasized in the authors' and Setaka's groups, as opposed to the motifs depicted in Figure 40. These systems, **101** and **103** in Figure 41, consist of -C≡C−(*p*-C_6H_4)−C≡C- rotators capped by two trityl-based endgroups.[175,176] The endgroups are in turn connected, via one *meta* carbon atom of each aryl ring, by three ethereal spokes of the formulas $O(CH_2)_{10}O$ or OCH_2−(*p*-C_6H_4)−CO−(*p*-C_6H_4)CH_2O.

As shown in Figure 41, the best way to access **101** is from the tris(phenol) **100** via a 3-fold intramolecular Williamson ether synthesis. Attempts to effect a 6-fold variant from the hexaphenol **102** and the *α*,*ω*-dibromide $Br(CH_2)_{10}Br$ or a 3-fold *interligand* ring closing metathesis/hydrogenation sequence starting from the hexaalkene **104**, give instead **105**, derived from an alternative ring closing mode. However, under high dilution conditions, the hexaphenol **102** condenses with the appropriate dibenzylic *α*,*ω*-dibromide to give the target rotor **103**. A number of related species have been prepared in which the trityl endgroups were spanned by a single bridge.[175,176]

The rotators in **101** and **103** rapidly rotate in solution on the NMR time scale, so no quantitative data are available for these systems. The crystal structures of solvates of **101** and **103** have been determined, and space filling representations are provided in Figure 41 (**CIII**, **CIV**). In both cases, the interstices between the ethereal spokes are fully occupied by solvent molecules or the spokes of neighboring molecules. Due to the two C≡C linkages in the rotators of **101** and **103**, the "vertical clearance" is much greater than those in the systems studies by the authors and Setaka. As analyzed in Figure 32 above, the *p*-phenylene moiety has a rather modest "horizontal steric demand" (2.87 Å radius). Thus, the low rotational barriers in solution are not surprising.

8.3. Rotors Studied in the Solid State

8.3.1. Rotors Comprised of Covalent Bonds. Just as many of the molecular rotors studied by Setaka can be viewed as modifications of a benchmark compound with a *p*-phenylene rotator (**50c**, Figures 31 and 32), many rotors studied by Garcia-Garibay can be formally derived from **106** (Figure 42).[156,158,159,177,180,181] This relatively simple compound, which features a -C≡C−(*p*-C_6H_4)−C≡C- rotator and two trityl stators, was first reported in 2002.[156] Compound **102** in Figure 41 represents a hexahydroxylated derivative. In any case, **106** has spawned the large family of *p*-arylene or arenediyl analogs shown in Figure 42.[156,158,159,177,180,181]

Solvent free crystals of **106** could be grown from CH_2Cl_2, and a benzene disolvate (**106**·2C_6H_6) was obtained from benzene.[156,158] Their dynamic properties were probed by variable temperature ^{13}C CP/MAS NMR and quadrupolar echo solid state ^{2}H NMR. Per the measurements in section 7, the latter required the deuterated -C≡C−(*p*-C_6D_4)−C≡C- analog (**106**-d_4).[158] A more extensively deuterated species with two $(C_6D_5)_3C$ endgroups (**106**-d_{30}) was prepared to remove interfering signals in the ^{13}C CP/MAS NMR measurements.[178] Since representative solid state ^{2}H NMR spectra were depicted in Figure 37, partial ^{13}C CP/MAS NMR spectra of **106**-d_{30} are shown in Figure 43. The two main signals at low temperature are due to the *p*-phenylene CH carbon atoms.

https://dx.doi.org/10.1021/acs.chemrev.0c01001
Chem. Rev. 2021, 121, 3701−3750

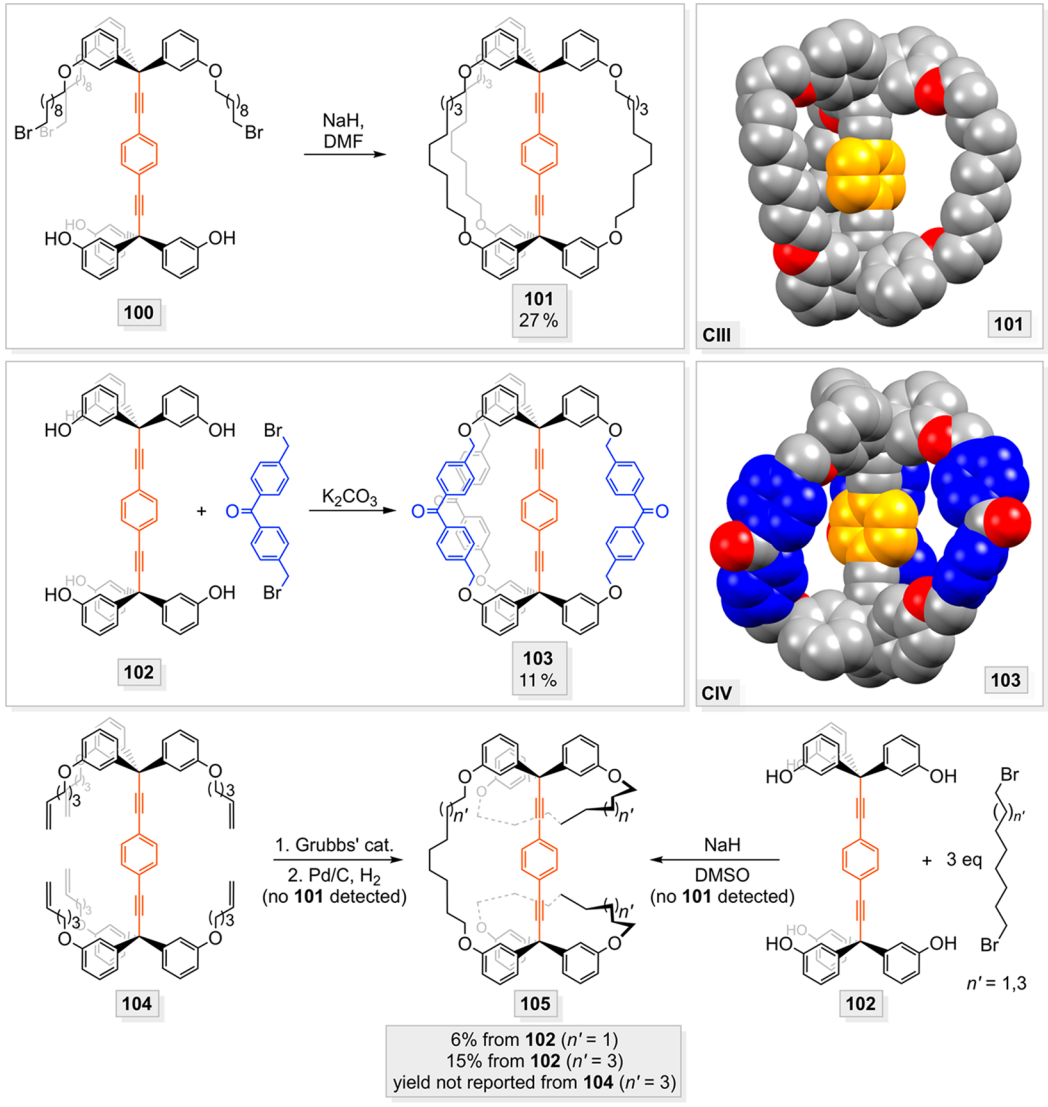

Figure 41. Synthetic approaches to gyroscope-like molecules **101** and **103** studied by Garcia-Garibay, and space filling representations of the molecular structures (with solvate molecules omitted; the rotator in **101** is disordered and only one conformation is depicted).

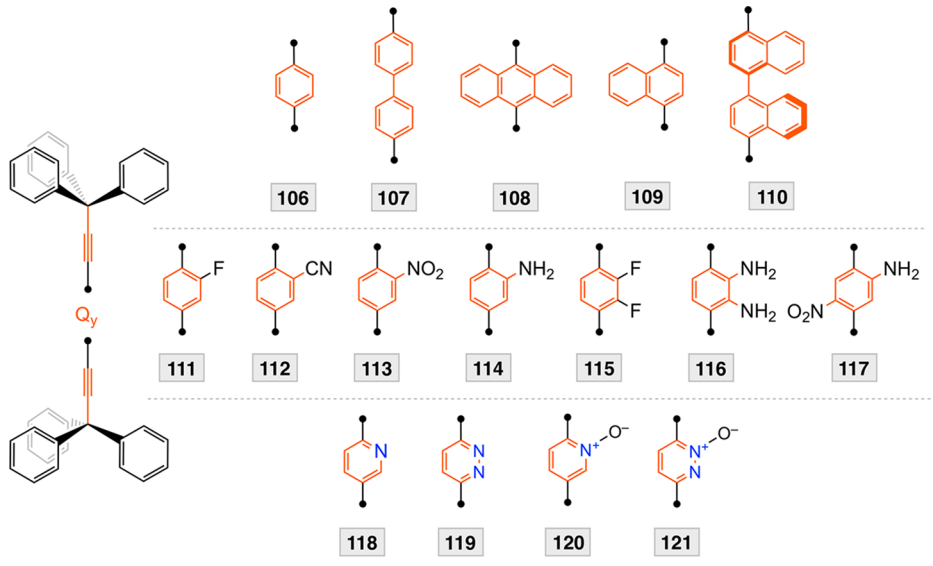

Figure 42. Molecular rotors consisting of -C≡C−(*p*-arylene)−C≡C- rotators and trityl stators studied by Garcia-Garibay.

https://dx.doi.org/10.1021/acs.chemrev.0c01001
Chem. Rev. 2021, 121, 3701−3750

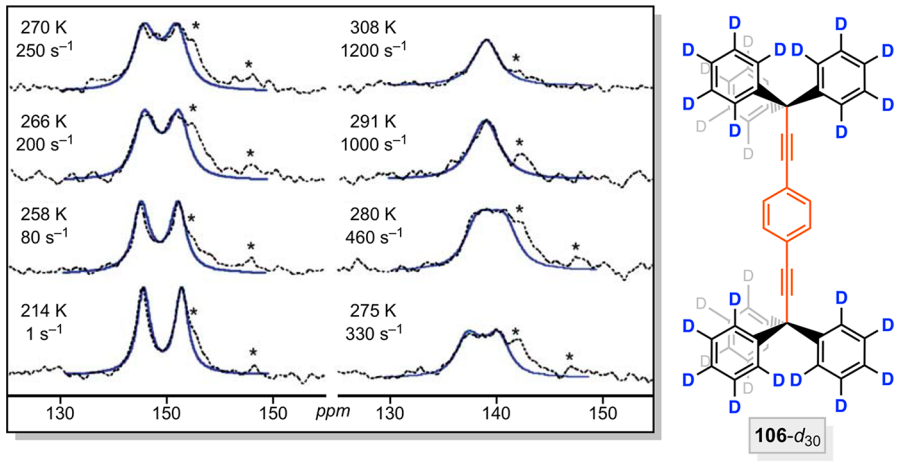

Figure 43. Variable temperature ^{13}C CP/MAS NMR spectra of **106**-d_{30} (*p*-phenylene CH signals) recorded with a contact time of 50 μs (black traces) and simulations (blue traces).[178] The asterisks denote residual signals due to the *ipso* *p*-phenylene carbon atoms and one of the trityl carbon atoms.

The NMR experiments clearly established 2-fold flipping of the *p*-C_6H_4 moiety. As summarized in Table 5, the data for solvent-free **106**-d_4 gave an E_a of 14.6 kcal/mol, and that for solvent-free **106**-d_{30} gave (from rate constants derived from the simulated spectra in Figure 43) an E_a of 11.3 kcal/mol. The 3.3 kcal/mol difference was attributed[178] to "the use of different temperatures, different isotopologues, or the accumulated errors of the two techniques." The principal component of the barrier involved interactions with neighboring molecules in the lattice.

The situation with **106**·2C_6H_6 was potentially more complex, as benzene molecules are capable of facile 6-fold rotation (discrete 6-fold flipping) in the solid state. There was the question as to whether this might be coupled to *p*-phenylene rotation, and the possibility for gearing was considered. To aid visualization, several views of the crystal lattice are given in Figure 44. Two (**CV-a**, **CV-c**) are reminiscent of motif **C** in Figure 40, with both trityl endgroups of neighboring rotor molecules in van der Waals contact. The benzene molecules help to fill the void space between the rotators. There are six arrayed around each, but in the interest of clarity, only two are depicted in Figure 44. Also, the space filling representation **CV-a** helps to visually calibrate readers as to what a packing coefficient (C_k) of ca. 0.7 can look like.

In depth NMR analyses did not provide any evidence for coupled rotation. Thus, independent *p*-phenylene rotation could be assigned an E_a of 12.8 kcal/mol (Table 5). Another investigator, Gardinier, has carried out similar studies with salts of the isoelectronic diboron compound $[Ph_3B{-}C{\equiv}C{-}(p\text{-}C_6H_4){-}C{\equiv}C{-}BPh_3]^{2-}$.[179] The accompanying cations result in packing motifs in which all rotator axes are no longer parallel. Although fewer details for this system are available, the rate of *p*-phenylene rotation appears to be somewhat faster.

Figure 42 also depicts compounds **107**–**110**, in which the *p*-phenylene moiety of **106** has been replaced by other unfunctionalized arylenes.[177] In the case of **107**, the 4,4′-biphenylene containing rotator would have the same radius as that in **106**. However, for the others (**108**–**110**), the radii are much greater. Hence, in the absence of new (favorable) crystal packing motifs, much higher rotational barriers would be expected. Indeed, the 9,10-anthracenediyl moiety in crystalline **108** is locked into a narrow pocket created by the stators of neighboring molecules.

Only the dynamic properties of the deuterated 4,4′-biphenylene systems **107**-d_8 and **107**-d_{30} have been studied in depth.[177] Solid state NMR experiments were carried out with (1) an *o*-xylene monosolvate in which the linked *p*-phenylene units were not quite coplanar and (2) a disordered solvent-free solid. Two-fold flipping processes were implicated with E_a values of 7.4 and 8.7 kcal/mol, respectively (Table 5). The data did not distinguish whether this was synchronous, involving both C_6D_4 rings or only one. With the *o*-xylene monosolvate, the data were best modeled when a barrier-free ±15° librational motion was included. Garcia-Garibay noted that the 7.4 kcal/mol barrier was 4–5 kcal/mol lower than that of the benzene solvate of **106**. However, there was no correlation to packing coefficients or any obvious geometric explanation. In response to other aspects of the data, it was speculated that rotational motion in solvated crystals may take advantage of long-range lattice vibrations that couple with molecular modes.

A number of derivatives of **106** have been prepared in which the *p*-phenylene rotator has been substituted with one or two heteroatom containing functional groups.[159,180] These are shown as **111**–**117** in Figure 42, and nearly all feature dipolar rotators. However, only the rotational dynamics of the two dipolar fluorinated compounds have been studied.

The monofluoro compound **111** crystallized analogously to **106**.[159] Either an unsolvated form or the benzene disolvate, **111**·2C_6H_6, could be obtained. In the latter, there was a belt of four benzene dimers about each rotator, somewhat akin to view **CV-a** of **106**·2C_6H_6 in Figure 44. In both cases, the fluorine atoms exhibited positional disorder (i.e., CH⋯CF/CH⋯CH exchange), which was initially fit to a 50:50 occupancy ratio.[159] Nonetheless, the possibility of domains in which the dipoles of neighboring molecules would be favorably aligned could not be excluded.

In any case, **111** and **111**·2C_6H_6 were studied both by dielectric spectroscopy and (following deuteration) solid state ^2H NMR.[147] Each probe indicated that the two fluoro-*p*-phenylene orientations were not isoenergetic but differed slightly. Thus, the crystal structure of **111** was redetermined at 296 K, and an 80:20 positional disorder was now found, corresponding to a difference of 0.7 kcal/mol. The E_a values, 13.7 and 13 kcal/mol, respectively (Table 5), represent the barriers for transiting from the higher energy to the lower

https://dx.doi.org/10.1021/acs.chemrev.0c01001
Chem. Rev. 2021, 121, 3701−3750

Table 5. Arrhenius Parameters for the Solid State Rotation of Rotators in Compounds Studied by Garcia-Garibay and Related Systems

compound	E_a[a] (kcal mol^{-1})	pre-exponential factor, A[a] (s^{-1})	variable temperature technique	ref
106-d_4·2C_6H_6	12.8		^{13}C CP/MAS NMR[b]	158,159
106-d_4	14.6 ± 2.5	7.96×10^{14}	quad. echo ^{2}H NMR[c]	37,158,159
106-d_{30}	11.3 ± 1	2.9×10^{11}	^{13}C CP/MAS NMR[b]	178
107-d_8·*o*-$C_6H_4(CH_3)_2$	7.4	2.5×10^{12}	quad. echo ^{2}H NMR[c]	177
107-d_{30}	8.7	4.9×10^9	^{13}C CP/MAS NMR[b]	177
111·2C_6H_6[d]	13.7 ± 0.9[d,e]		dielectric spectroscopy	37,147
111-d_3	13 ± 2[e]	$(1.0 \pm 0.7) \times 10^{14}$	quad. echo ^{2}H NMR[c]	37,147
115	14.1 ± 0.2 to 15.1 ± 0.5	$(4 \pm 1) \times 10^{13}$ to $(8 \pm 4) \times 10^{13}$	dielectric spectroscopy	148
115-d_2	14.8 ± 1	$(8 \pm 6) \times 10^{13}$	quad. echo ^{2}H NMR[c]	148
118-d_2·2THF	8.5	6.2×10^{12}	quad. echo ^{2}H NMR[c]	37,181
123-d_4	8.5 ± 2.5	1.07×10^{13}	quad. echo ^{2}H NMR[c]	37,182
124	3.55 ± 0.2	3.59×10^{10}	^{1}H spin−lattice relax.[f]	37,182
125	12.6 ± 2.5	9.63×10^{11}	^{13}C CP/MAS NMR[b]	37,182
126	3.0 ± 0.1	6.39×10^{10}	^{1}H spin−lattice relax.[f]	37,182
127-d_4	5.21	5.8×10^{10}	quad. echo ^{2}H NMR[c]	37,185
128-d_2	3.3−6.7	2.6×10^{11} to 3.6×10^8	quad. echo ^{2}H NMR[c]	186
131	4.1	2.2×10^{11}	^{1}H spin−lattice relax.[f]	37,187
131-d_{30}	13.7 ± 1.1	$(5.1 \pm 4.5) \times 10^{11}$	^{13}C CP/MAS NMR[b]	37,187
140-d_4·C_6H_6	11.6 ± 2.0	$(3.5 \pm 3.0) \times 10^{13}$	quad. echo ^{2}H NMR[c]	34,192
140·C_6H_6	11.7	1.7×10^{12}	^{13}C CP/MAS NMR[b]	34,192
140·C_6H_6	8.0−10.3		X-ray ADP[g]	192
148-d_4·8(solvent)[h,i]	15.7	3.5×10^{18}	quad. echo ^{2}H NMR[c]	37,191
148-d_{24}·8(solvent)[h,i]	15.5 (14.7)[j]	7.8×10^{17} (5.3×10^{13})[j]	quad. echo ^{2}H NMR[c]	37,191
148-d_{90}·8(solvent)[h,i]	13.7	7.8×10^{15}	quad. echo ^{2}H NMR[c]	37,191
149-d_4·2CH_2Cl_2[k]	<5[k]		quad. echo ^{2}H NMR[c]	34,160,210
150-d_4·2EtOAc[l]	5.0 (7.0)[l]	9.7×10^{11} (4.3×10^{10})[l]	quad. echo ^{2}H NMR[c]	37,194
156-d_4·2C_6H_5Br	4.4	1.6×10^{12}	quad. echo ^{2}H NMR[c]	37,195,196
159-d_4	7.9 ± 1.6	2.75×10^{11}	quad. echo ^{2}H NMR[c]	37,197
165-d_8·4$C_6H_5CH_3$	9.0	2.4×10^{13}	quad. echo ^{2}H NMR[c]	37,199
167-d_6	10.2	1.1×10^{10}	quad. echo ^{2}H NMR[c]	200
168-d_8	5.5	3.6×10^9	quad. echo ^{2}H NMR[c]	202
170a-e	2.4−4.8	1.1×10^{12} to 9.9×10^{12}	^{1}H spin−lattice relax.[f]	205
171	1.15 ± 0.04	$(1.3 \pm 0.3) \times 10^{12}$	^{1}H spin−lattice relax.[f]	206
172	0.71 ± 0.04	$(1.2 \pm 0.4) \times 10^{12}$	^{1}H spin−lattice relax.[f]	206
173	4.5	1.8×10^{12}	^{1}H spin−lattice relax.[f]	209
174	8 ± 2		^{1}H spin−lattice relax.[f]	209
174-d_{12}	9.5	4.2×10^{13}	quad. echo ^{2}H NMR[c]	209
175	2.63 (0.5)[m]	4.4×10^{12} (1.1×10^7)[m]	^{1}H spin−lattice relax.[f]	203
180-d_4	11.3	1.6×10^{12}	quad. echo ^{2}H NMR[c]	37,210
181	7.3	5×10^{11}	dielectric spectroscopy	37,212
182	5.0 ± 0.2	1.3×10^7	^{1}H spin−lattice relax.[f]	37,211
185-d_8	13.5	8.7×10^{15}	quad. echo ^{2}H NMR[c]	37,213
186	0.18	4.7×10^{10}	^{1}H spin−lattice relax.[f]	37,214
187-d_4	8.6	7×10^{11}	quad. echo ^{2}H NMR[c]	216
188-d_2	6.8 ± 0.1	5.4×10^{12}	quad. echo ^{2}H NMR[c]	215
188	7.1 ± 0.5	1.7×10^{14}	dielectric spectroscopy	215

[a]Error limits are given when provided in the paper cited. [b]^{13}C Cross-polarization magic angle spinning NMR. [c]Quadrupolar echo ^{2}H NMR, also referred to as spin−echo ^{2}H NMR. [d]The same barrier was obtained using a desolvated sample. [e]This value represents the barrier for conversion of the higher energy to the lower energy rotator conformation, which differ in energy by 0.7 kcal/mol. [f]^{1}H NMR spin−lattice relaxation (T_1). [g]Anisotropic displacement parameters from crystal structures. [h]In this series, the deuterium atoms are located on the central *p*-phenylene rotator, the six trityl based *p*-phenylene rotators, or the 12 phenyl rotators, respectively; the E_a values pertain to the deuterated rotator. [i]These crystals feature mixtures of 2,4,6-trimethylpyridine and 2,2,4-trimethylpentane solvent molecules. [j]This value is for an amorphous sample. [k]During sample preparation (grinding), desolvation occurred; due to this and other complications, the E_a value could only be estimated. [l]The two values are for two independent molecules of **150**-d_4 in the unit cell. [m]This value is for a high temperature phase.

energy well. Possible reasons for the ca. 1 kcal/mol discrepancy between the two techniques have been analyzed.[147]

The related 2,3-difluoro-*p*-phenylene compound **115** in Figure 42 could be crystallized in an unsolvated form that was isomorphous with those of **106** and **111**. The dynamic properties were analogously studied, and a very similar rotational potential with E_a values of 14−15 kcal/mol was obtained (Table 5).[37,148]

https://dx.doi.org/10.1021/acs.chemrev.0c01001
Chem. Rev. 2021, 121, 3701−3750

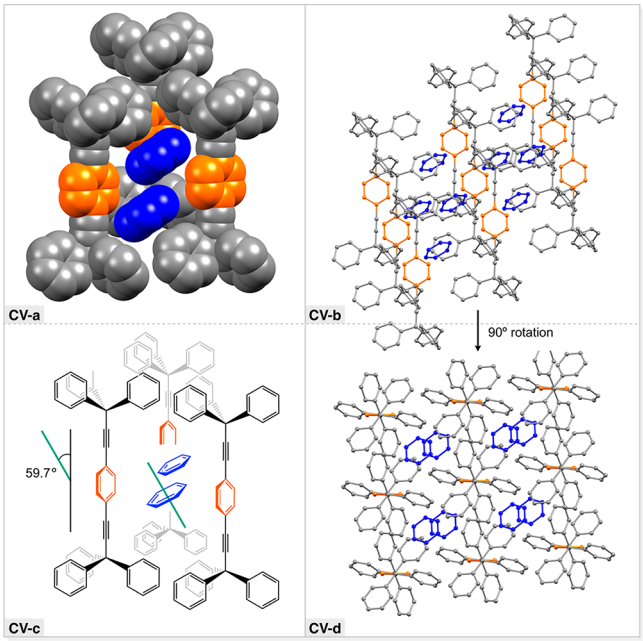

Figure 44. Representations of the crystal structure of the *p*-phenylene containing rotor **106**·2C_6H_6.

Several compounds with dipolar nitrogen heterocycle rotators are also depicted in Figure 42 (**118**−**121**).[181] In most of these, the dipole moments of the rotators are greater than those of the mono- and difluorinated *p*-phenylenes in **111** and **115**. Crystals of the 2,5-pyridinediyl (**118**·THF) and 3,6-pyridazinediyl (**119**, **119**·$CHCl_3$) adducts have been structurally characterized. The packing motifs are quite similar to those of **106**, **111**, and **115**, consistent with the similar dimensions of the rotators. Garcia-Garibay estimates the volumes of the *p*-arylene units in **118** and **119** as 0.5−1.1% less than that of **106**.[181]

Quantitative studies of dynamic properties are so far limited to the 2,5-pyridinediyl system **118**·THF.[181] Solid state ^2H NMR experiments (**118**-d_2·THF) afford an E_a of 8.5 kcal/mol for rotational site exchange. The higher E_a values for the monofluorine rotators in **111** and **111**·2C_6H_6 have been ascribed to the larger fluorine substituent, the lesser steric demand of the pyridinediyl moiety, and the smaller size of the occluded THF. The first two would also apply to the higher barrier in the difluorinated compound **115**.

Figure 45 collects other types of rotors examined by Garcia-Garibay. One subset (**123**−**126**) features triphenylsilyl endgroups.[182] The first compound, **123**, represents a disilicon analog of **106**. The *p*-phenylene segment is then replaced by a polycyclic hydrocarbondiyl moiety derived from either bicyclo[2.2.2]octane or cubane, both of which feature a C_3 symmetry axis, as shown by **124** or **125**. A *p*-carboranediyl moiety with an even higher symmetry axis (C_6) can be introduced, as shown by **126**.

Silicon−carbon bonds are typically 21% longer than carbon−carbon bonds,[183] and this is a potential factor when comparing the rotational barriers in these compounds to those of analogs with trityl endgroups. However, another property is in play in this series. Namely, rotators with higher rotational symmetry should generally exhibit diminished solid state rotational barriers. The reasoning is as follows.[182] First, note the geometric representations of the rotators in Figure 45. Those

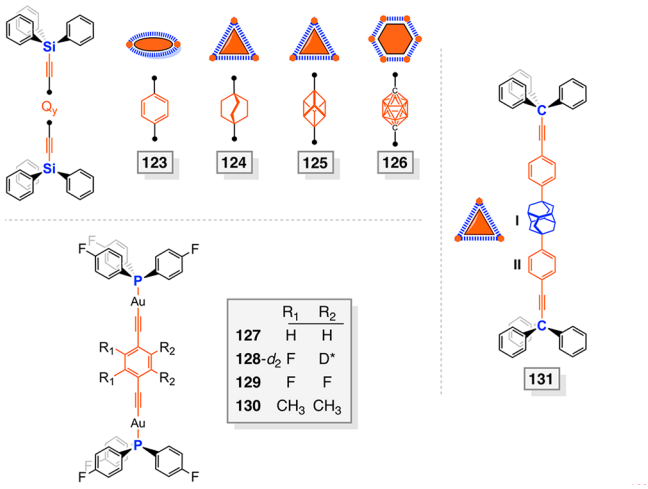

Figure 45. Additional molecular rotors studied by Garcia-Garibay, most with heteroatom containing endgroups.[182] For the significance of the geometric shapes, see the text and Figure 46. Deuterated compounds are normally not displayed, but **128**-d_2 has not been reported in nondeuterated form.

with C_3 symmetry axes are depicted as orange triangles, and those with C_2 and C_6 symmetry axes are depicted as orange ovals and hexagons, respectively. These shapes are repeated in Figure 46, together with some corresponding to rotators with other C_n symmetries.

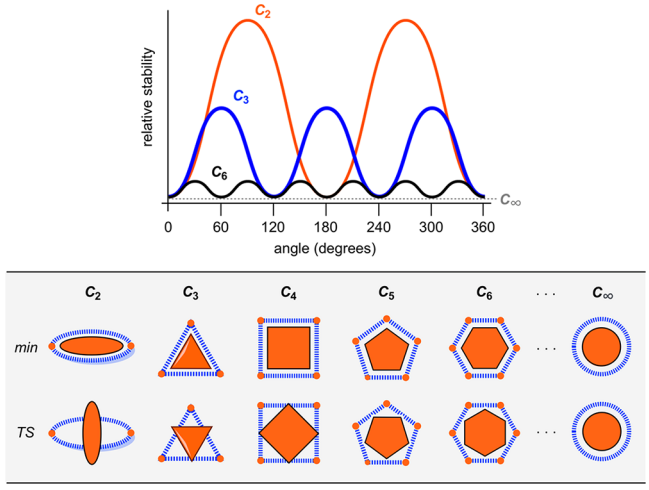

Figure 46. First row of structures: cross sections of rotators of C_n symmetries (solid orange) and packing motifs that saturate the van der Waals surface boundaries (dashed blue lines). Second row: packing environments that would be generated upon rotation of the rotators by 360°/2*n*. Top: idealized qualitative energy profiles.

Consider first the solid state environments of the C_∞ and C_6 rotators. One might expect that the neighboring molecules in the lattice would pack in a complementary, roughly cylindrically symmetrical manner about the C_∞ axis. In any event, rotation of the rotator by 30° or 60° or 90° (etc.) would not generate increased steric interactions. With the C_6 rotator, the adjacent molecules would pack with nearly cylindrical symmetry. A rotation of 30° (360°/2*n*) would likely lead to an energy maximum (TS in Figure 46), but the increased steric interactions would be moderate. A further rotation of 30° would restore the energy minimum.

https://dx.doi.org/10.1021/acs.chemrev.0c01001
Chem. Rev. 2021, 121, 3701−3750

Now consider a rectangular or ovoid rotator with C_2 symmetry. If the adjacent molecules pack about the rotator in a complementary manner, there is the likelihood of severe steric interactions upon a 90° rotation. Intermediate situations are obtained with C_3, C_4, or C_5 symmetric rotators. There are a number of conceptual parallels with the trends associated with *n*-fold rotational barriers detailed in section 6.4 (Figure 22). In any case, one would expect energy profiles with the relationships qualitatively expressed in Figure 46 (top) as the C_n symmetry of the rotator decreases.

The series of rotors **123**−**126** with varying rotator symmetries (Figure 45) crystallize without solvent.[182] Despite some differences in unit cell dimensions and crystal symmetries, they pack in relatively similar manners. Each crystal consists of long chains of molecules aligned by interactions between the aryl rings of the endgroups ($SiPh_3/Ph_3Si$). These entail attractive edge/face motifs and sextuple phenyl embraces. The structures are disorder-free, except for **124** in which the bicyclo[2.2.2]octane moiety occupies two positions (50:50) that differ by a 60° rotation.

The NMR properties of the disilyl analog of **106**, **123**, have been studied in detail.[182] Experiments with **123**-d_4 give an E_a of 8.5 kcal/mol (Table 5), somewhat lower than that of nonsolvated **106**-d_4 (11.6 kcal/mol) and intuitively in line with the longer silicon−carbon bonds. Much lower barriers are obtained for **124** and **126** (E_a 3.5 and 3.1 kcal/mol, respectively), consistent with expectations from the higher C_n-symmetries of their rotators. There is no correlation to the radii of the *p*-phenylene, bicyclo[2.2.2]octanediyl, and *p*-dicarboranediyl segments of the rotators (2.87, 3.05, and 3.42 Å, respectively, as estimated from their crystal structures including the van der Waals radii of the hydrogen atoms).

However, the barrier is much higher with the 1,4-cubanediyl adduct **125** (E_a = 12.6 kcal/mol), in which the radius of the rotator is 3.14 Å. This has been attributed to steric features of the tight rotator pocket formed by four neighboring molecules, as shown in Figure 47. The six cubane carbon atoms not connected to the -C≡C- units can be represented by a pair of triangles, as depicted in **CVI** and **CVII** (Figure 47; the dark background represents a van der Waals boundary). In particular, two phenyl hydrogen atoms (blue and orange semicircles in **CVI**) extend into the rotator pocket. As the six carbon atoms rotate, one hydrogen atom (orange) is poised to strongly interact with the atoms in the upper triangle, and the other (blue) in the lower triangle (see **CVII**).

The various geometric relationships embodied in **123**−**126** and their implications for rotational barriers have also been probed computationally by other investigators.[184] In general, good agreement with the experimental results were realized.

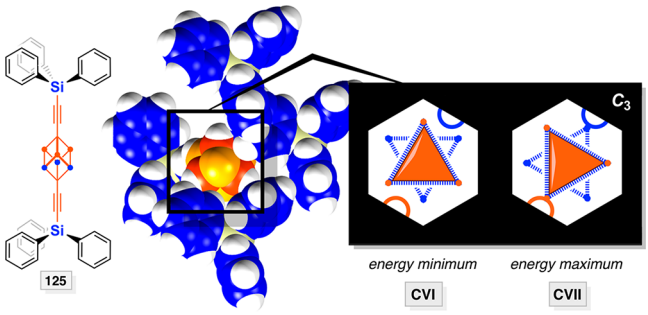

Figure 47. Steric interactions in the crystal structure of the 1,4-cubanediyl adduct **125** (see also text).[182]

A second subgroup of rotors in Figure 45 feature tri(*p*-fluorophenyl)phosphine endgroups as opposed to triphenylsilyl endgroups.[185,186] The phosphines in turn anchor digold rotators of the formula AuC≡C−(*p*-C_6R_4)−C≡CAu, with R_4 = H_4 (**127**), Me_4 (**130**), F_2D_2 (**128**-d_2), and F_4 (**129**). Outside of the MOF systems described below, these represent the only metal containing rotors studied in the Garcia-Garibay group, with one underlying goal being the modulation of phosphorescence emission. All of these adducts can be crystallized in solvent-free forms.[185,186] Aurophilic interactions between neighboring molecules are evident (Au−Au 2.95−3.36 Å) and are clearly a factor in the packing motifs.

In **127**, two of the *p*-phenylene hydrogen atoms exhibit weak CH···π interactions with the fluorophenyl groups from the triarylphosphine stators of neighboring molecules. Despite these attractive interactions, NMR experiments (**127**-d_4) indicate a low E_a of 5.2 kcal/mol. However, rotational site exchange could not be established for the sterically more demanding tetramethyl-*p*-phenylene rotator in **130**. The difluoro compound **128**-d_2 crystallizes analogously to **127** but with 2-fold rotationally disordered *p*-$C_6F_2D_2$ units. The packing motif of the tetrafluoro compound **129** is very similar.

The interpretation of the dynamic behavior of the difluoro compound **128**-d_2 was complicated by a nonlinear Arrhenius plot.[186] This was attributed to reversible expansion/compression of the distances between the axes, giving E_a values of 3.3−6.7 kcal/mol. There were additional challenges in the case of the tetrafluoro compound **129**, but solid state ^{19}F NMR experiments provided evidence for a similar dynamic range.

Finally, in the last and quite unique rotor **131** in Figure 45, a C_3 symmetric 4,9-diamantanediyl moiety has been inserted into the C_6H_4−C_6H_4 linkage of **107** (Figure 42).[187] The 4,9-diamantanediyl unit is conceptually related to the 1,4-cubanediyl unit of **125**, with the six four-membered rings of the latter now expanded to six-membered rings. This is the first compound in this review where there are two symmetry inequivalent components of the rotator that can independently rotate, the two *p*-phenylene groups (C_2) and the central 4,9-diamantanediyl group (C_3).

Solvent-free crystals of **131** could be obtained. NMR experiments with appropriately deuterated samples gave an E_a of 13.7 kcal/mol for two-site exchange of the *p*-phenylene groups. Consistent with the expectations from Figure 46, the E_a associated with three-site exchange of the 4,9-diamantanediyl moiety was much lower, 4.1 kcal/mol. Interestingly, the radii of the rotator segments trend in the opposite direction (*p*-phenylene, 2.87 Å; 4,9-diamantanediyl, 3.28 Å).

Another series of rotors studied by Garcia-Garibay is collected in Figure 48.[175,188] These feature (1) trityl endgroups with one or two oxygen-bound *meta* substituents (OH, OMe, OTIPS) and (2) *p*-phenylene, 2,3-difluoro-*p*-phenylene, or 2,5-pyridinediyl rotators. Solid state NMR experiments have been carried out with **132**, the difluorinated derivative **133**, and deuterated analogs.[188] The data indicate extremely slow rotation of the rotators, with E_a values much higher than 12−14 kcal/mol. The crystal structures of **132** and **133** have also been determined, and the isomorphous packing motifs were analyzed in detail. The high barriers could be ascribed to steric effects arising from the TIPS group and stabilizing edge/face interactions of the rotators with neighboring aryl groups.

https://dx.doi.org/10.1021/acs.chemrev.0c01001
Chem. Rev. 2021, 121, 3701−3750

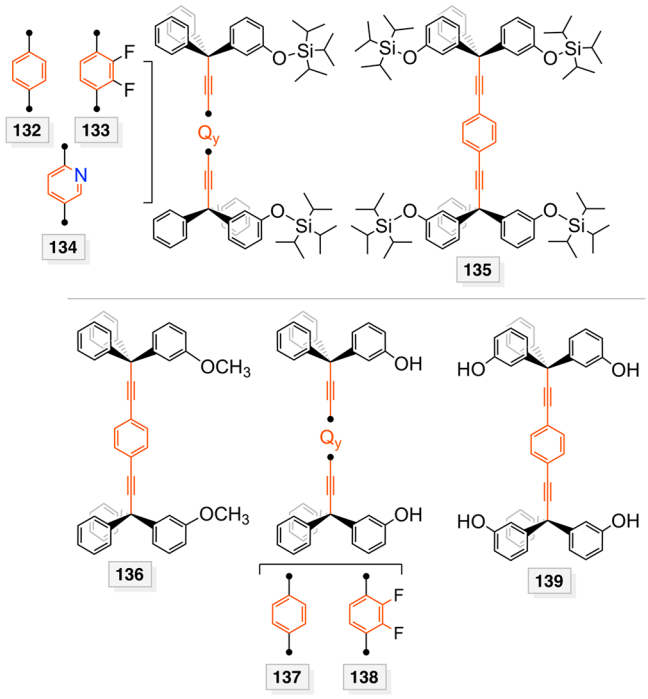

Figure 48. Molecular rotors with substituted trityl endgroups studied by Garcia-Garibay (part 1).

Some of the other compounds in Figure 48 represent stepping stones to more complicated species that were viewed as outside the scope of this review (see section 8.1).[175,188] Nonetheless, they are presented in the interest of a complete record. A related group of rotors is depicted in Figure 49. Each contains a -C≡C−(*p*-C_6H_4)−C≡C- rotator, and all except **145** and **146** have multiply substituted trityl endgroups of C_3 symmetry.[160,175,176,189−191,194]

One subset of rotors in Figure 49 features a single *meta* hydroxy or alkoxy substituent on each trityl aryl ring (**102**, **140**−**144**). Compound **140** has received particular attention as a candidate for a crystalline molecular gyroscope.[189,192,193] It is challenging to condense the full breadth of this study, as seven polymorphs have been characterized. Some of these arise from conformational degrees of freedom about the C−C−O−Me or C_{sp}−C_{sp^3}−C_{ipso}−C_{ortho} linkages, and others by incorporating different solvent molecules (pseudopolymorphs).[174]

The monobenzene solvate **140**·C_6H_6 has been extensively examined by the solid state NMR techniques described above. The data yield E_a values of 11.5−11.7 kcal/mol, close to those of the unsolvated and benzene solvated forms of the parent compound **106** (Table 5). In addition, a crystallographic approach to assaying rotational barriers has been investigated. This entails analyzing the anisotropic displacement parameters as a function of temperature, particularly with respect to librational motion and amplitudes. Readers are referred to the article for further details.[192] In any event, E_a values of 10.3, 10.1, and 8.0 kcal/mol could be derived from data collected at 100, 200, and 300 K, respectively. The lower value at 300 K has been attributed to an increased anharmonicity of the potential energy surface at higher temperature.

In another subset of rotors in Figure 49 (**145**−**147**), a *meta* $OSiPh_2tBu$ substituent can be found on one, two, or three of the aryl rings of each trityl endgroup.[190] The stator in the last compound is particularly bulky, but a crystal structure could not be determined. NMR experiments with **147**-d_4 provide evidence for very slow rotation of the *p*-phenylene moiety, but various issues preclude the determination of an E_a.

In the rotors **149** and **150** in Figure 49, *both* meta positions of all six aryl rings of the trityl endgroups are substituted with *t*-butyl or phenyl groups. In the latter, each endgroup can be viewed as having three *m*-terphenyl substituents. Both compounds can be seen as an effort to transition from packing motif **CI** to packing motif **CII** in Figure 40. The former crystallizes as the disolvate, **149**·2CH_2Cl_2, with one of the dichloromethane molecules located close to the *p*-phenylene group.[160] The solvent molecules could be removed without complete loss of crystalline order. Solid state NMR experiments with **149**-d_4 could attain both the fast (293 K) and slow exchange limits (≤193 K), but a number of complications prevent the quantitative measurement of the E_a value.

Compound **150** could be crystallized as the disolvate, **150**·2EtOAc.[194] The unit cell contained two independent molecules of **150**. Although the solid state NMR data (**150**-d_4·2EtOAc) and attendant modeling required complex analysis, it was possible to estimate the E_a values for rotation of the *p*-phenylene groups of the two molecules as 5 and 7 kcal/mol.[37] In the former, there were no close contacts involving the

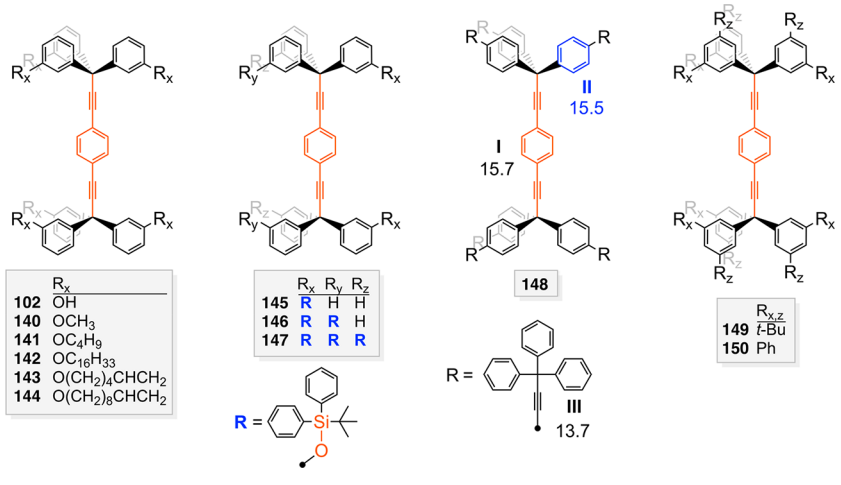

Figure 49. Molecular rotors with substituted trityl endgroups studied by Garcia-Garibay (part 2).

https://dx.doi.org/10.1021/acs.chemrev.0c01001
Chem. Rev. 2021, 121, 3701−3750

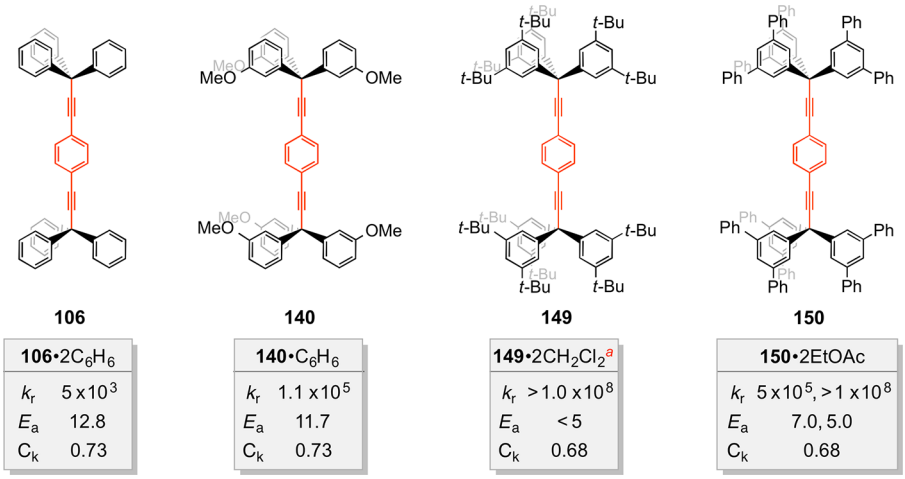

Figure 50. Comparison of packing coefficients (C_k) and E_a values (kcal/mol) for *p*-phenylene rotation in four molecules. [a]Consult the references in Table 5 for additional details regarding the composition of the solvate.

rotator, whereas in the latter sources of steric hindrance were apparent. Also, the *p*-phenylene units underwent essentially barrierless librations of ±15−20°.

Although Garcia-Garibay later integrated this analysis over a broader spectrum of compounds,[37] it is instructive to compare the four structurally related rotors in Figure 50, three of which come from Figure 49.[194] As the packing coefficients, C_k (which include the solvent molecules), decrease from 0.73 to 0.68, there is an overall (although not proportional) decrease in the E_a values. However, this relationship does not hold as well in other series of compounds, and additional relevant factors are treated below.

For the unique rotor **148** in Figure 49,[191] the *para* positions of all six trityl aryl groups have been substituted with bulky C≡CCPh$_3$ substituents, making for a dendrimer like adduct with a total of eight trityl moieties. Compound **148** could be crystallized from an unusual solvent mixture (2,4,6-trimethylpyridine/2,2,4-trimethylpentane) as a highly disordered tetrasolvate. The radius of the stator can be estimated as ca. 12 Å, which is unsurpassed in all of the preceding adducts. Ignoring the solvent molecules, the packing coefficient (C_k) is only 0.46. Accordingly, there are very few contacts involving the rotator.

Clearly, the hope was that there would be a low barrier to -C≡C−(*p*-C$_6$H$_4$)−C≡C- rotation in solid **148**. However, analysis of the NMR data proved complicated. Using **148**-d_4, Garcia-Garibay reported an *apparent* E_a of 15.7 kcal/mol,[191] greatly increased relative to that of **106** (12.8, 14.6, or 11.3 kcal/mol depending upon solvation; Table 5). However, other observations prompted him to adjust this value to 7.9 kcal/mol (253 K) and 6.9 kcal/mol (293 K). The temperature dependence was ascribed to crystal fluidity effects. The more heavily deuterated substrates **148**-d_{24} and **148**-d_{90} were used to probe the rotational barriers of the C$_{sp^3}$−(*p*-C$_6$H$_4$)−C≡C and C$_6$H$_5$ units. The apparent E_a values (15.5 and 13.7 kcal/mol) as well as the corrected values were similar to those obtained from **148**-d_4. The possibility of various types of correlated rotation or gearing was considered, but in the end it was concluded that rotation was primarily associated with a temperature induced softening of the packing structure.

For the series of rotors in Figure 51, one or both of the trityl endgroups in molecules treated earlier have been replaced by triptycyl or substituted triptycyl moieties.[157,195−197] These have

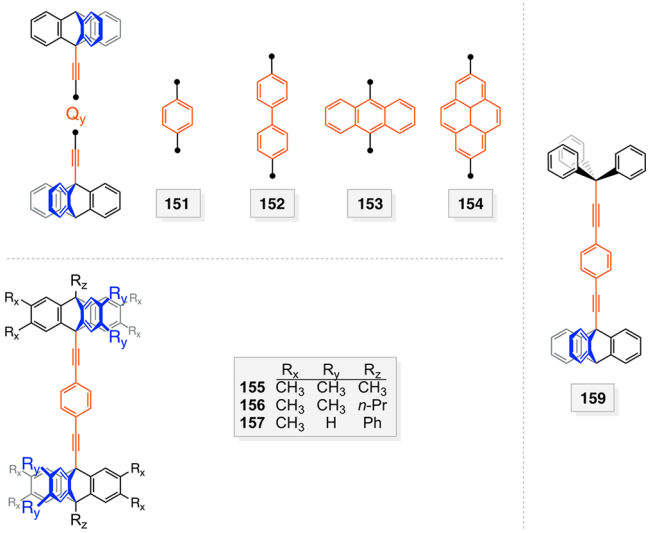

Figure 51. Additional molecular rotors studied by Garcia-Garibay, all with at least one triptycyl or substituted triptycyl endgroup.

fewer degrees of freedom and are incapable of propeller chirality, a feature that can play a role in crystal packing. The compounds **151**−**154**, two of which are homologues of **106** and **107** in Figure 42, were among the first studied by Garcia-Garibay.[157] Only solution phase NMR spectra were reported, and rotator rotation was always fast on the NMR time scale. In the crystalline *m*-xylene monosolvate **151**·C$_8$H$_{10}$, the protruding triptycene units of one molecule interdigitated into voids proximal to the *p*-phenylene unit of another, blocking rotation.[195]

Similar compounds have been prepared in which subsets of the triptycyl hydrogen atoms are replaced by methyl, *n*-propyl, or phenyl groups, as exemplified by **155**−**157**.[195−197] It was hoped that the additional substituents would hamper interdigitation. The *n*-propyl substituted compound **156** could be crystallized as a bromobenzene disolvate, **156**·2C$_6$H$_5$Br.[195] NMR experiments using **156**-d_4·2C$_6$H$_5$Br showed that the barrier to *p*-phenylene rotation was sharply reduced to 4.4 kcal/mol, the second lowest with respect to the other compounds described above. Garcia-Garibay noted that this is only 1.4 kcal/mol higher than the barrier to carbon−carbon

https://dx.doi.org/10.1021/acs.chemrev.0c01001
Chem. Rev. 2021, 121, 3701−3750

bond rotation in ethane in the gas phase.[195] The crystal structure of **156**·2C_6H_5Br revealed that the *p*-phenylene rotators were very well insulated from neighboring rotors, although in close proximity to six solvent molecules.

The rotor **159** in Figure 51 represents a mixed system with one trityl and one triptycyl endgroup[197] and constitutes a "hybrid" of **106** and **151**. It crystallizes as the monosolvate **159**·$CHCl_3$, but samples lose chloroform during solid state NMR measurements. However, it can be desolvated while retaining crystallinity at 110 °C. NMR data with **159**-d_4 indicate an E_a of 7.9 kcal/mol for *p*-phenylene flipping. Notably, this is 6 kcal/mol lower than that measured for solvent-free samples of **106**. Although the crystal structure of desolvated **159** is unknown, Garcia-Garibay observes that the packing coefficient of **159**·$CHCl_3$ (0.69) is lower than those of **106** (0.74) and **151** (0.85).

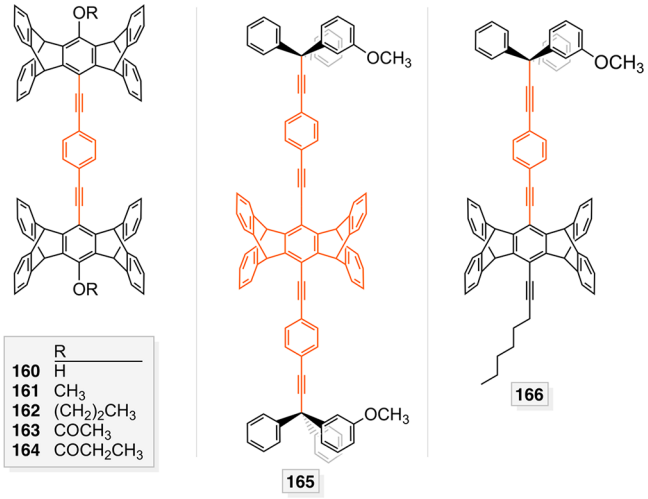

Figure 52. Additional molecular rotors studied by Garcia-Garibay, all of which incorporate a pentiptycene moiety.

Figure 52 depicts a series of compounds with -C≡C−(*p*-C_6H_4)−C≡C- rotators and substituted pentiptycene endgroups (**160**−**164**).[198] The wingspan associated with these endgroups is greater than those of triptycyl analogs such as **151** in Figure 51. However, in the three adducts that can be crystallized, it is obvious that intermolecular contacts strongly impede any rotation of the *p*-phenylene moiety. It has been suggested that bulky groups at the periphery of the pentiptycene stators would help prevent interdigitation.

The pentiptycene moiety has been moved to the "middle" in the adduct **165** in Figure 52.[199] Although this is the customary position for the rotator, the moment of inertia of the pentiptycene group is comparable to those of the triarylmethyl endgroups. Hence, **165** is better viewed as a "dirotor" with two -C≡C−(*p*-C_6H_4)−C≡C- rotators that have collinear axes. Although there are a number of interesting properties to appreciate in **165**, the bottom line is that NMR experiments with the toluene monosolvate **165**-d_8·C_7H_8 (C_k 0.71) establish an E_a of 9.0 kcal/mol for *p*-phenylene rotation. To the authors' knowledge, the rotor properties of **166** remain uninvestigated, although the photophysical properties of **165** and **166** have been studied in detail.[199]

Compound **167** in Figure 53 (top)[200] represents a return to the extremely bulky dendrimer like stators first encountered with **148** in Figure 49. The rotator features a central triptycenediyl moiety, flanked by two C≡C−*p*-phenylene

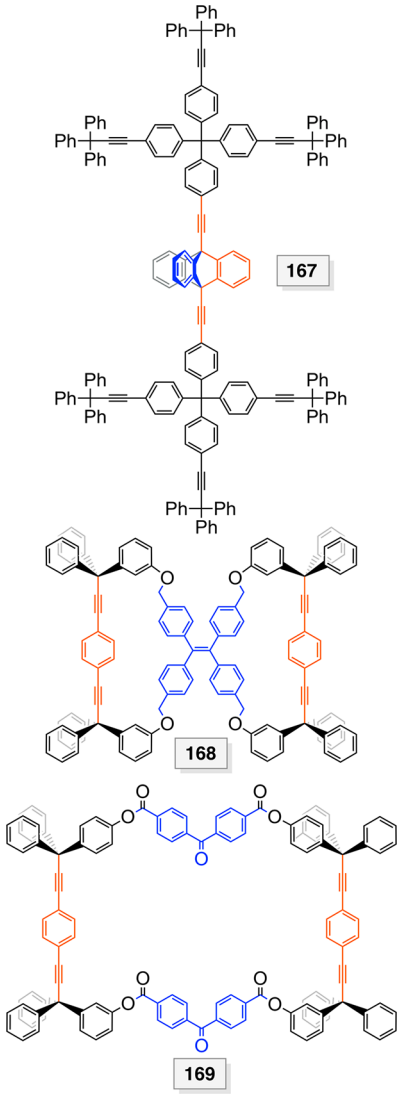

Figure 53. Additional molecular rotors studied by Garcia-Garibay.

domains. The radius of the triptycenediyl segment (ca. 5.52 Å, estimated from crystal structures of related molecules and including hydrogen atoms[201]) is much greater than those of the *p*-phenylene segments (2.87 Å, from Figure 32). Due to splintering and other problems, it has not proved possible to determine the crystal structure. However, solid state NMR studies of **167**-d_8 (deuterated on two of the three benzenoid triptycene rings) establish, following in depth analyses, an E_a of 10.2 kcal/mol for a 120° rotation of the triptycenediyl segment.

As noted above, compound **165** in Figure 52 features two rotators with collinear axes. Garcia-Garibay has also studied adducts that feature two rotators with parallel axes, as exemplified by **168** in Figure 53 (middle).[202] This compound was prepared with the idea that the fluorescence intensity of the tetraarylethylene core might be a function of the rotator mobilities. Solid state NMR experiments with **168**-d_8 indicate a low E_a, 5.5 kcal/mol, for *p*-phenylene rotation. However, a crystal structure could not be determined. Compound **169** in Figure 53 represents a byproduct in the synthesis of a monorotor precursor to **168**.[175] Compounds with more than one rotator for which the axes are not collinear or parallel[169] are considered beyond the scope of this review.

https://dx.doi.org/10.1021/acs.chemrev.0c01001
Chem. Rev. 2021, 121, 3701−3750

8.3.2. Rotors Based upon Supramolecular Assemblies or MOFs. *8.3.2.1. Supramolecular Systems.* Garcia-Garibay, sometimes together with collaborators, has also studied supramolecular rotators.[203−209] Although connections to gyroscopes are briefly mentioned in his papers, other investigators have emphasized potential relationships (section 9.2). One advantage of supramolecular rotors is that many can be synthesized by simple self-assembly of the rotator and stator components.[205]

Figure 54 (top) depicts a series of halogen bonded 1:2 adducts of DABCO and fluorinated phenyl iodides (**170a−e**).[205] The moments of inertia of the components are comparable, so the rotator and stator cannot be assigned by the criteria in section 1. Most of these crystallize as represented in Figure 54, although **170c** adopts an alternative connectivity. The crystal structures of **170a,e** have been studied in particular detail, and show numerous reversible phase transitions between 100 K and room temperature. The crystal packing motif remains intact throughout, but the DABCO moiety exhibits increasing rotational disorder over two positions differing by 60°. The rotator axes in **170a,e** are aligned in a parallel manner, as seen with virtually all of the rotors in section 8.3.1. However, this motif is not always observed in the halogen bonded rotors.

NMR experiments and other data confirm the preferential rotation of the C_3 symmetric DABCO moiety as opposed to the C_2 symmetric fluorinated aryl groups, consistent with the concepts embodied in Figure 46. The aryl groups can therefore be regarded as stators. The E_a values are quite low, ranging from 2.4 to 4.8 kcal/mol. A variety of properties have been analyzed, including the origin of the higher rotational barrier (8.2 kcal/mol) in pure crystalline DABCO.

In a subsequent study,[206] the 1:1 adducts **171** and **172** in Figure 54, derived from DABCO and the corresponding trityl substituted haloalkynes, were examined. Despite the absence of steric protection, NMR experiments established an E_a of only 0.71 kcal/mol for DABCO rotation in bromine containing **172**, aptly likened to "a spinning top on a tripod". At that time, this was the lowest rotational barrier measured in an amphidynamic crystal. A slightly higher E_a was found for iodine containing **171** (1.15 kcal/mol) and attributed to subtle differences in the crystal lattices that result in a more hindered DABCO cavity. Both potential energy surfaces consisted of six local minima and six local maxima. Garcia-Garibay also studied the solid state behavior of bis(alkynyl iodides) containing DABCO or *p*-phenylene rotators, for which halogen bonding between like molecules is possible.[204,207]

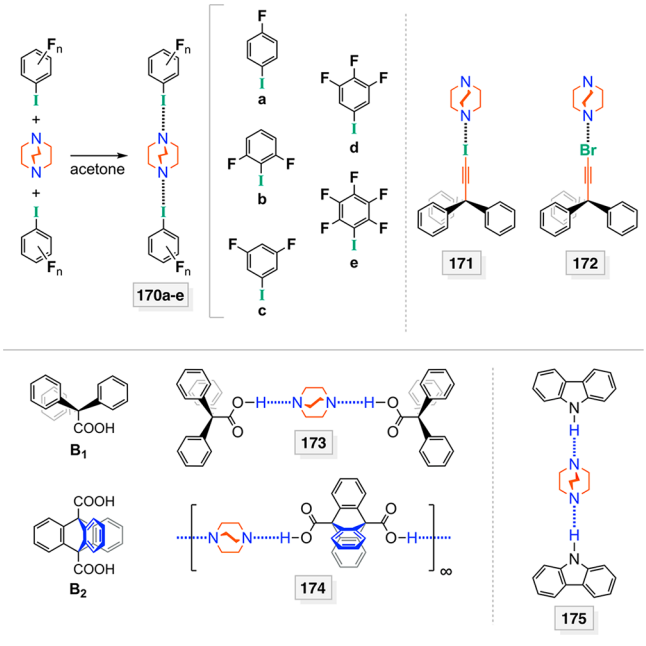

Figure 54. Supramolecular rotors studied by Garcia-Garibay and collaborators: top, halogen bonded DABCO adducts; bottom, hydrogen bonded DABCO adducts.

Hydrogen bonding is ubiquitous in supramolecular systems. As shown in Figure 54 (bottom), Garcia-Garibay has also employed DABCO as a component of (1) a 1:2 adduct with the monocarboxylic acid $\mathbf{B_1}$, affording **173**, and (2) a 1:1 adduct with the dibridgehead dicarboxylic acid $\mathbf{B_2}$, affording the one-dimensional polymer **174**.[209] These are structurally complex systems, with the crystallographic data indicating that the DABCO in **173** (1) is protonated on one nitrogen atom and hydrogen bonded on the other and (2) resides in a pseudo-4-fold symmetric cavity formed by aromatic residues from neighboring molecules. The mismatch with the C_3 symmetry axis of DABCO suggests the possibility of 12 nearly degenerate minima, which should help lower the rotational barrier. In contrast, in **174** the DABCO occupies a packing environment of pseudo-3-fold symmetry, which should enhance the rotational barrier.

NMR experiments (with d_{12} analogs) indicated rapid DABCO rotation in **173**, faster than 10^7/s at 148 K, but an exact E_a could not be obtained. In contrast, that for **174** was 9.2 kcal/mol (ca. 10^4/s at 243 K). However, the primary objective of this study concerned the prospects of exploiting dipoles generated by thermal proton transfer to attain transient ferroelectric domains. This undertaking also entailed a variety of dielectric measurements.

The 1:2 adduct of DABCO and carbazole, **175** in Figure 54 (bottom), has also been investigated.[203] Two crystalline phases can be characterized, with the symmetry of the crystal lattice and cavity hosting the C_3 rotator increasing at higher temperature. This leads to a reduction in the E_a value for DABCO rotation from 2.6 to 0.5 kcal/mol. However, due to a large decrease in the pre-exponential factor, the rate slows considerably at higher temperatures.

8.3.2.2. MOF Systems. Another obvious research direction would be to extend the preceding types of studies to MOFs and other porous materials. Of course, such assemblies would not qualify as *molecular* rotors or gyroscopes. However, the situation is not all that different from a crystal lattice of molecular rotors. Some of the MOFs studied by Garcia-Garibay and collaborators or close associates are given in Figure 55.

The first system studied by Garcia-Garibay was Yaghi's MOF-5 (**180**), also known as IMROF-1.[210] All horizontal and vertical connectors feature a *p*-phenylene rotator in the form of a terephthalate dianion. Each carboxylate is anchored to two zinc atoms (one for each oxygen atom). NMR experiments using **180** with deuterated rotators yield an E_a of 11.3 kcal/mol. This represents a relatively large barrier, especially in view of the void space (see **CVIII** or **CIX**, Figure 55) and miniscule packing coefficient (C_k 0.20). It has been attributed to an electronic effect, namely, to a loss of conjugation between the ideally coplanar *p*-phenylene and carboxylate groups, as depicted in **CX** in Figure 55.[210] Other probes of rotator dynamics are also surveyed in this work.

https://dx.doi.org/10.1021/acs.chemrev.0c01001
Chem. Rev. 2021, 121, 3701−3750

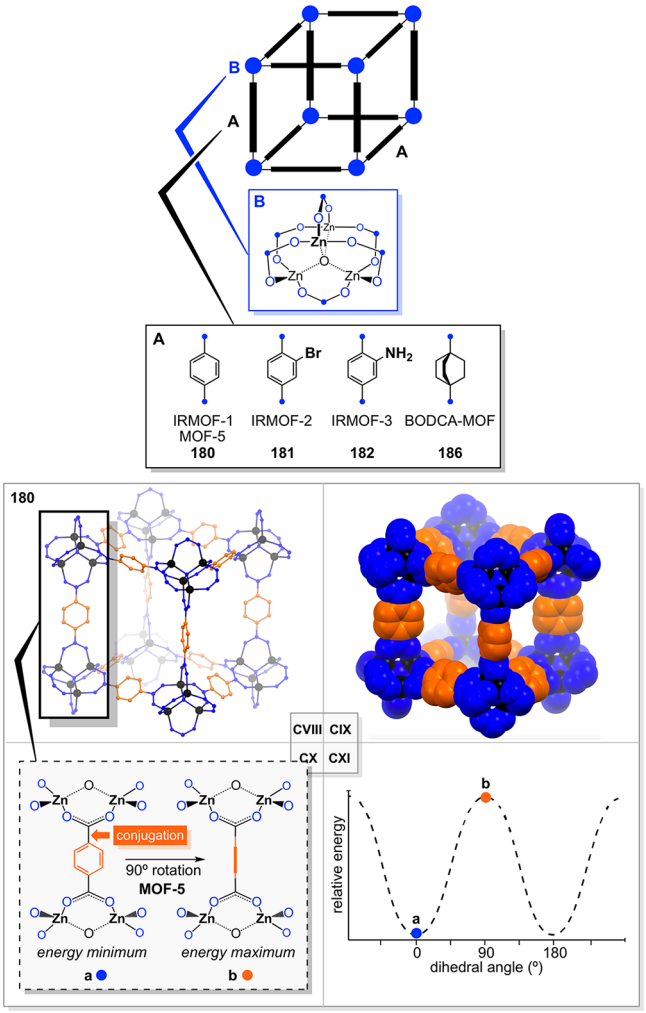

Figure 55. MOFs in which rotators have been incorporated into the connectors studied by Garcia-Garibay or others (part 1).

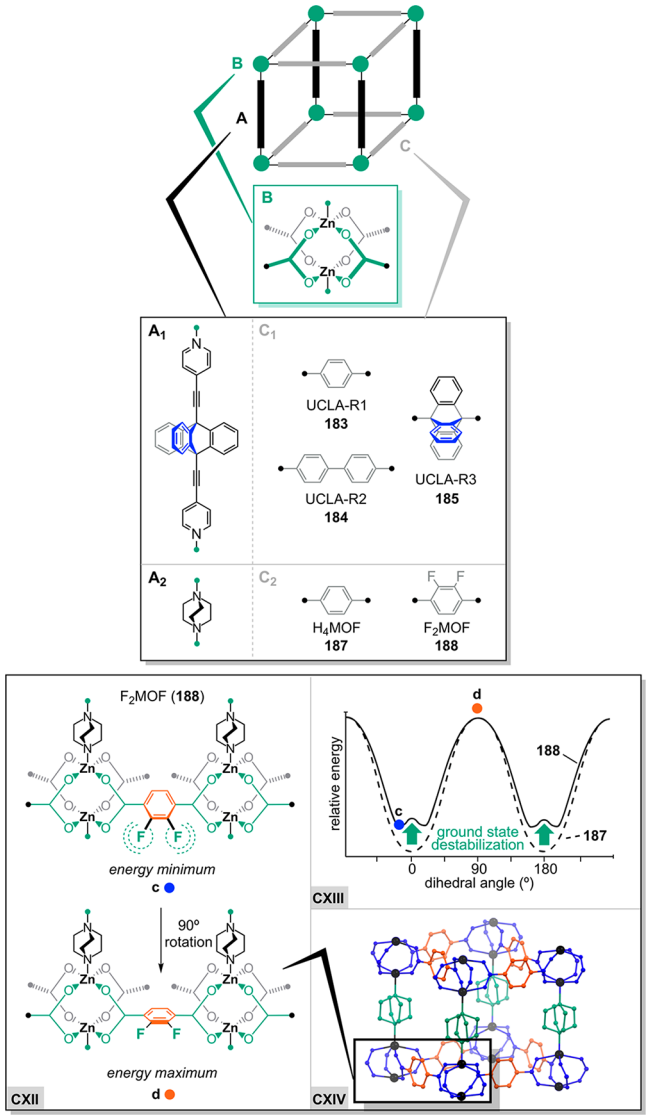

Figure 56. MOFs in which rotators have been incorporated into the connectors studied by Garcia-Garibay or others (part 2).

This effort was followed by studies of analogous MOFs with dipolar monosubstituted *p*-phenylene rotators, *p*-C_6H_3X.[211,212] In the case of bromo-*p*-phenylene (IMROF-2 or **181**), Price and Michl measured an E_a of 7.3 kcal/mol by dielectric spectroscopy.[212] In the case of amino-*p*-phenylene (IMROF-3 or **182**), Garcia-Garibay and Yaghi measured an E_a of 5.0 kcal/mol by ^{1}H spin−lattice relaxation.[211] Additional properties were characterized by further solid state ^{13}C and ^{15}N NMR experiments. The positions of the bromine atoms in **181** were disordered, and the dipole−dipole interactions were not strong enough to produce an observable polar ordering,[211] a topic further treated in section 9.3.

The trends in E_a values have been rationalized by Garcia-Garibay and Yaghi.[211] The larger bromine and amino substituents in **181** and **182** are thought to sterically destabilize the otherwise coplanar *p*-phenylene/carboxylate units in which conjugation is maximized (**CX**, Figure 55). This of course will lower barriers relative to that of **180**. Also, the NH_2 moiety, which undergoes independent rotation (E_a 1.8 kcal/mol), can hydrogen bond to the neighboring carboxylate group, and this is potentially a stronger interaction in the transition state.

Garcia-Garibay has also synthesized a series of three MOFs depicted in Figure 56, UCLA-R1 (**183**), UCLA-R2 (**184**), and UCLA-R3 (**185**).[213] These feature dizinc as opposed to tetrazinc junctions (**B**). The horizontal connectors (C_1) are the terephthalate dianion, the 4,4′-biphenyl analog, or the dibridgehead dicarboxylate of triptycene, respectively. The vertical connectors (A_1; pillars) are now capped by nitrogen donor atoms in the form of 9,10-bis(4-pyridylethynyl)-triptycene; these directly bind to zinc.

The first two MOFs crystallize in catenated motifs, such that what would be a cavity in the basic rectangular building block (top structure, Figure 56) is occupied by components of additional offset rectangular assemblies. The third, UCLA-R3 (**185**), crystallizes in an uncatenated motif with 10 DMF molecules in each cavity. It has been termed a pillared paddlewheel MOF. NMR experiments with deuterated analogs establish an E_a for rotation of 13.5 kcal/mol. A substantial portion of this barrier is attributed to interactions of the triptycene blades and the DMF molecules.

Applying insight from the studies in section 8.3.1, Garcia-Garibay designed the "BODCA MOF" (**186**) in Figure 55.[214] This can be viewed as an analog of MOF-5 (**180**) in which the *p*-phenylene unit of the terephthalate dianion has been replaced by a bicyclo[2.2.2]octanediyl moiety. There are two principal effects: (1) the destabilization associated with rotating the *p*-

https://dx.doi.org/10.1021/acs.chemrev.0c01001
Chem. Rev. 2021, 121, 3701−3750

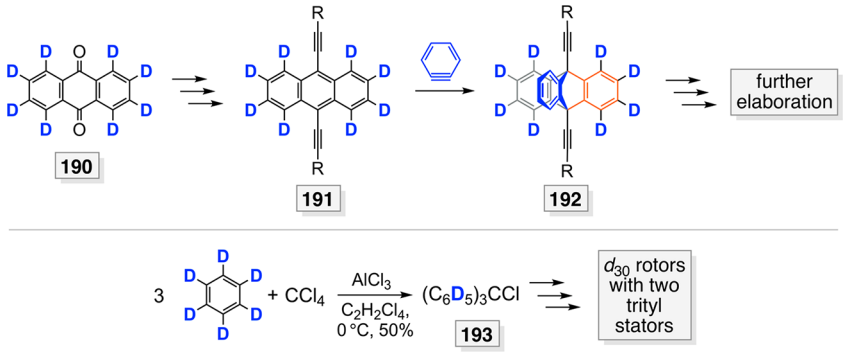

Figure 57. Reactions used to access molecular rotors with deuterated trityl or triptycyl groups.

Table 6. Syntheses of -C≡C−arylene−C≡C- Containing Rotors with Identical Trityl or Substituted Trityl Endgroups

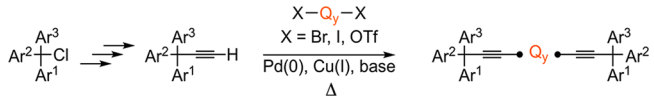

compound	Q_y	Ar_1[a]	Ar_2[a]	Ar_3[a]	yield (%)	ref
106	*p*-phenylene	Ph	Ph	Ph	15	156
107	4,4′-biphenylene	Ph	Ph	Ph	47	177
108	9,10-anthracenediyl	Ph	Ph	Ph	56	177
109	1,4-naphthalenediyl	Ph	Ph	Ph	68	177
110	4,4′-binaphthalenediyl	Ph	Ph	Ph	92	177
111	fluoro-*p*-phenylene	Ph	Ph	Ph	23	147
112	cyano-*p*-phenylene	Ph	Ph	Ph	10	159
113	nitro-*p*-phenylene	Ph	Ph	Ph	40	159
114	amino-*p*-phenylene	Ph	Ph	Ph	26	159
115	2,3-difluoro-*p*-phenyene	Ph	Ph	Ph	38	148,180
116	2,3-diamino-*p*-phenylene	Ph	Ph	Ph	22	159
117	2-amino-5-nitro-*p*-phenylene	Ph	Ph	Ph	12	159
118	2,5-pyridenediyl	Ph	Ph	Ph	22	181
119	3,6-pyridazinediyl	Ph	Ph	Ph	75	181
131	*p*-C_6H_4-X′-*p*-C_6H_4[b]	Ph	Ph	Ph	40	187
132	*p*-phenylene	*m*-TIPS	Ph	Ph	77	188
133	2,3-difluoro-*p*-phenyene	*m*-TIPS	Ph	Ph	82	188
134	2,5-pyridenediyl	*m*-TIPS	Ph	Ph	81	188
135	*p*-phenylene	*m*-TIPS	*m*-TIPS	Ph	86	188
136	*p*-phenylene	*m*-OCH_3	Ph	Ph	73	175
139	*p*-phenylene	*m*-OH	*m*-OH	Ph	92	188
140	*p*-phenylene	*m*-OCH_3	*m*-OCH_3	*m*-OCH_3	70	175,189
145	*p*-phenylene	*m*-TBDPS	Ph	Ph	74	190
146	*p*-phenylene	*m*-TBDPS	*m*-TBDPS	Ph	73	190
147	*p*-phenylene	*m*-TBDPS	*m*-TBDPS	*m*-TBDPS	75	190
148	*p*-phenylene	*p*-C≡CCPh_3	*p*-C≡CCPh_3	*p*-C≡CCPh_3	70	191
149	*p*-phenylene	3,5-(*t*-Bu)$_2$	3,5-(*t*-Bu)$_2$	3,5-(*t*-Bu)$_2$	64	160
150	*p*-phenylene	3,5-Ph_2	3,5-Ph_2	3,5-Ph_2	87	194

[a]Only the substituents are given for substituted phenyl groups. [b]X′ =

phenylene moiety "out of conjugation" is removed (**CX**, **CXI**; Figure 55); (2) a rotator with a local 2-fold symmetry axis is replaced by one with a local 3-fold symmetry axis. As analyzed above, this is conducive to lower rotational barriers.

Accordingly, solid state ^{1}H NMR measurements at 2.3−80 K establish the amazingly low E_a of 0.185 kcal/mol for rotation of the bicyclo[2.2.2]octanediyl segment. This is supported by ^{2}H NMR studies of deuterated analogs between 292 and 50 K, as well as molecular dynamics simulations. Garcia-Garibay notes that this represents the engineering of rotational dynamics in the solid state to a rapidity commensurate with a high density gas or low density liquid phase.

In his most recent efforts, Garcia-Garibay[215] has combined design elements from several of the above studies. As shown in Figure 56, the dizinc based MOFs **187** and **188** feature either the usual horizontal connector, the terephthalate dianion (H_4MOF), or the dipolar 2,3-difluorinated analog (F_2MOF). For the nitrogen donor pillars, DABCO is used, providing a much lower spacing than with the bis(pyridyl) units in UCLA-R3 (**185**).

https://dx.doi.org/10.1021/acs.chemrev.0c01001
Chem. Rev. 2021, 121, 3701−3750

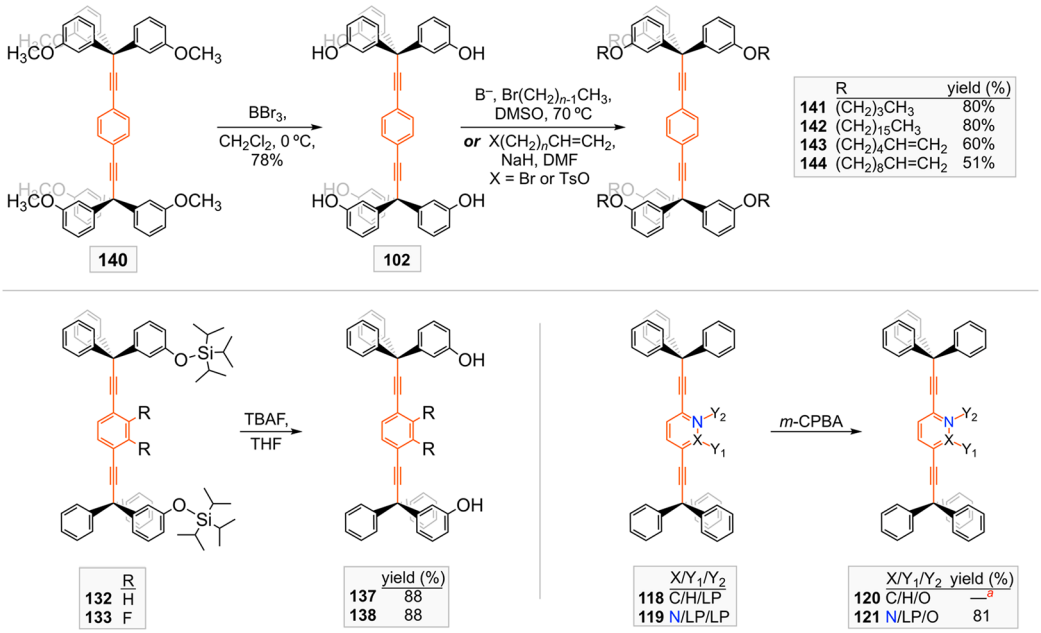

Figure 58. Molecular rotors accessed by postsynthetic modification of certain compounds in Table 6. [a]Rapidly decomposes in solution.

For **188**, NMR and dielectric spectroscopy measurements indicate E_a values of 6.8 and 7.1 kcal/mol, respectively, for rotation of the difluorinated *p*-phenylene rotators. NMR measurements with nonfluorinated **187** indicate a higher E_a, 8.6 kcal/mol.[215,216] Data from crystal structures and DFT calculations suggest that steric interactions involving the two fluorine substituents destabilize the planar conjugated conformations of the -O_2C−(*p*-$C_6H_2F_2$)−CO_2- units, leading to a lower barrier. Garcia-Garibay's representation of this phenomenon is sketched in **CXIII** in Figure 56. Similar interactions with bromine or amino substituents are invoked above to rationalize, at least in part, the lower barriers of **181** and **182** versus **180**.

8.4. Representative Syntheses of the Rotors in Section 8.3.1

Many of the molecular rotors studied by Garcia-Garibay in section 8.3.1, such as those in Figure 42, are of a modular structural nature. Thus, one would anticipate that modular syntheses would also be possible. For that reason, preparative routes have been collected into this separate section. As would be expected from the types of adducts in Figures 42, 45, and 48−53, the syntheses make particular use of coupling, addition, and displacement reactions of terminal alkynes. Appropriately substituted trityl, triptycyl, and pentiptycene building blocks are also required.

This section does not attempt to exhaustively treat the syntheses of deuterated rotors. However, accessing deuterated triptycyl and trityl groups is less routine, so the dominant routes are sketched in Figure 57. For example, 9,10-anthroquinone-d_8 (**190**) is commercially available and can be elaborated by addition/reduction sequences to various 9,10-bis(alkynyl) anthracenes (**191**). Subsequent reactions with benzyne afford triptycyl-d_8 species with bridgehead alkynyl substituents (**192**).[200] Alternatively, a 3-fold Friedel−Crafts reaction can be carried out with CCl_4, excess benzene-d_6, and $AlCl_3$.[177] The resulting perdeuterated product $(C_6D_5)_3CCl$ (**193**) is easily ethynylated and carried on to d_{30} rotor molecules.

All rotors with -C≡C−(*p*-arylene)−C≡C- rotators and identical trityl endgroups (Figure 42) or substituted trityl endgroups (Figures 48 and 49) have been synthesized via palladium catalyzed Sonogashira type reactions as summarized in Table 6.[147,148,156,159,160,175,177,180,181,187−191,194] The requisite X−(*p*-arylene)−X and $Ar^1Ar^2Ar^3CCl$ building blocks can be accessed by routine procedures. In several cases, the *p*-arylene moieties or endgroups have been subjected to postsynthetic functionalization.[175,176,181,188] These transformations are depicted in Figure 58.

The related disilicon and bis(triaryl phosphine) digold rotors in Figure 45 (**123−126** and **127−130**) have been accessed as shown in Figure 59.[182,185,186] In the final step in the disilicon series, the diconjugate dibase of a HC≡C−(*p*-arylene)−C≡CH species is treated with an excess of Ph_3SiCl. In the

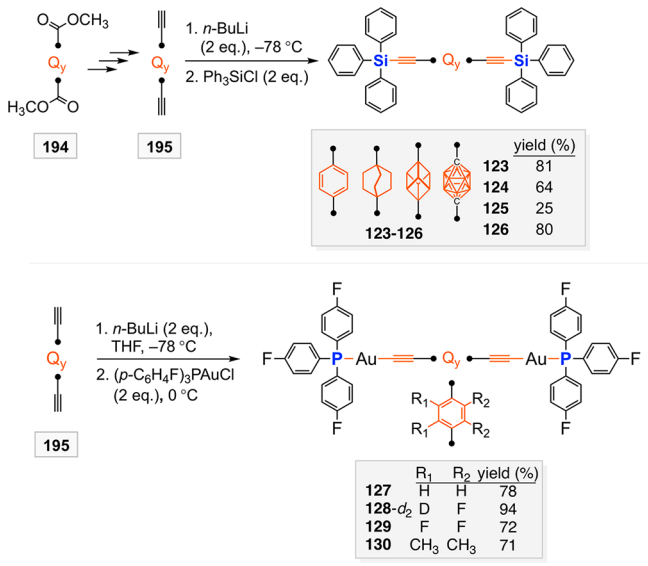

Figure 59. Syntheses of molecular rotors with silicon (**123−126**, top) or phosphorus (**127−130**, bottom) containing endgroups.

https://dx.doi.org/10.1021/acs.chemrev.0c01001
Chem. Rev. 2021, 121, 3701−3750

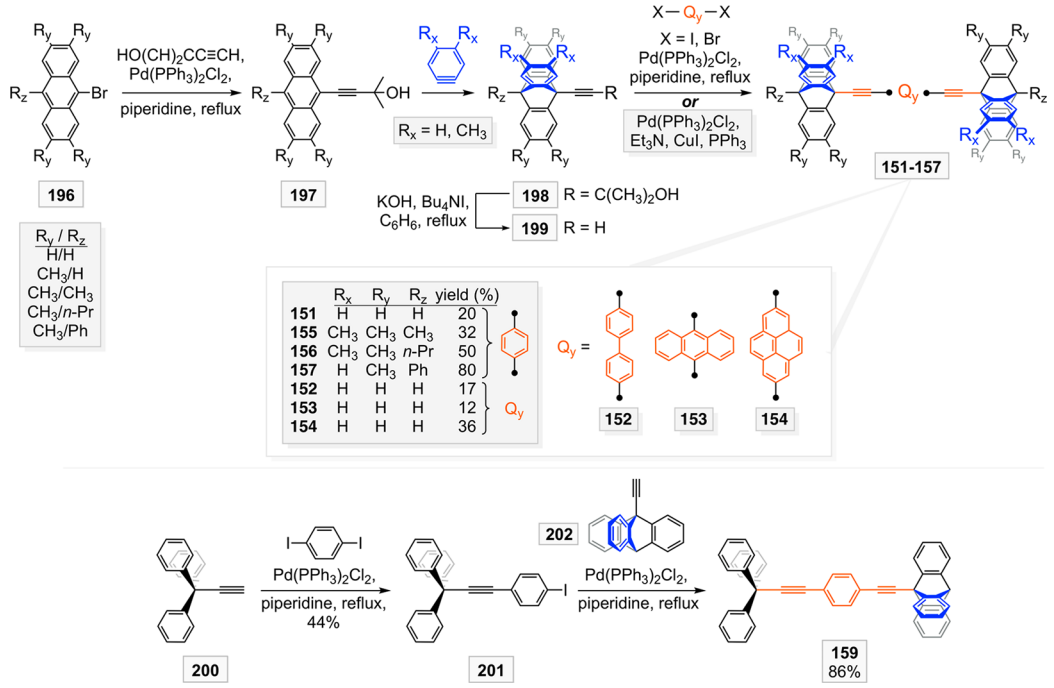

Figure 60. Syntheses of molecular rotors **151**−**157** (top) and **159** (bottom).

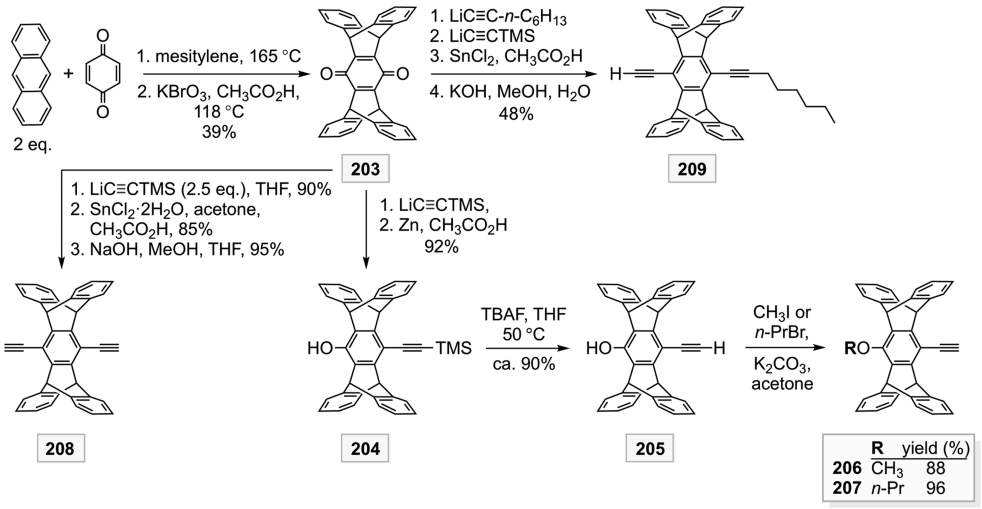

Figure 61. Syntheses of key precursors to the molecular rotors **160**−**166**.

diphosphorus series, the electrophile is switched to Ar_3PAuCl. Some of the α,ω-diynes required several steps to access, and readers are referred to the cited literature for further details.

Accessing rotors with triptycyl or substituted triptycyl endgroups requires somewhat more steps. As shown in Figure 60 (top), triptycyl precursors with bridgehead -C≡C−CMe_2OH substituents (**198**) are first prepared.[157,196] These syntheses involve benzyne additions similar to that introduced in Figure 57. In a standard protocol for generating terminal alkynes or transient conjugate bases, compounds **198** are treated with KOH. Subsequent Sonogashira couplings of the resulting alkynes **199** afford the target molecules **151**−**157**. As shown in Figure 60 (bottom), a stepwise approach involving *p*-diiodobenzene and two Sonogashira couplings is used for the mixed trityl/triptycyl adduct **159**.[197]

Some of the designer rotor architectures featured in Garcia-Garibay's later studies require somewhat more involved syntheses. Cases in point include the pentiptycene adducts **160**−**166** in Figure 52.[198,199] The final steps of the syntheses of **160**−**164** are analogous to those used for other -C≡C−(*p*-arylene)−C≡C- rotors in Table 6.[198] The trick is to prepare the requisite pentiptycene building blocks.

Figure 61 shows how these are accessed from **203**, derived from the 2-fold Diels−Alder adduct of anthracene and *p*-quinone.[198,199,217] Using LiC≡CTMS, an alkynyl group is first introduced, and reduction installs a *para* hydroxy group, giving **204**. The alkyne can be protodesilylated (→ **205**) and the hydroxy group can be replaced by methoxy or *n*-propoxy groups (**206**, **207**). Alternatively, two alkynyl groups can be introduced using excess LiC≡CTMS, with subsequent reduction and protodesilylation giving **208**. In a variant, two different alkynyl groups can be introduced, giving **209** via a parallel sequence.

These building blocks are then applied as depicted in Figure 62.[198,199] First, the monoethynyl compounds **205**−**207** are

https://dx.doi.org/10.1021/acs.chemrev.0c01001
Chem. Rev. 2021, 121, 3701−3750

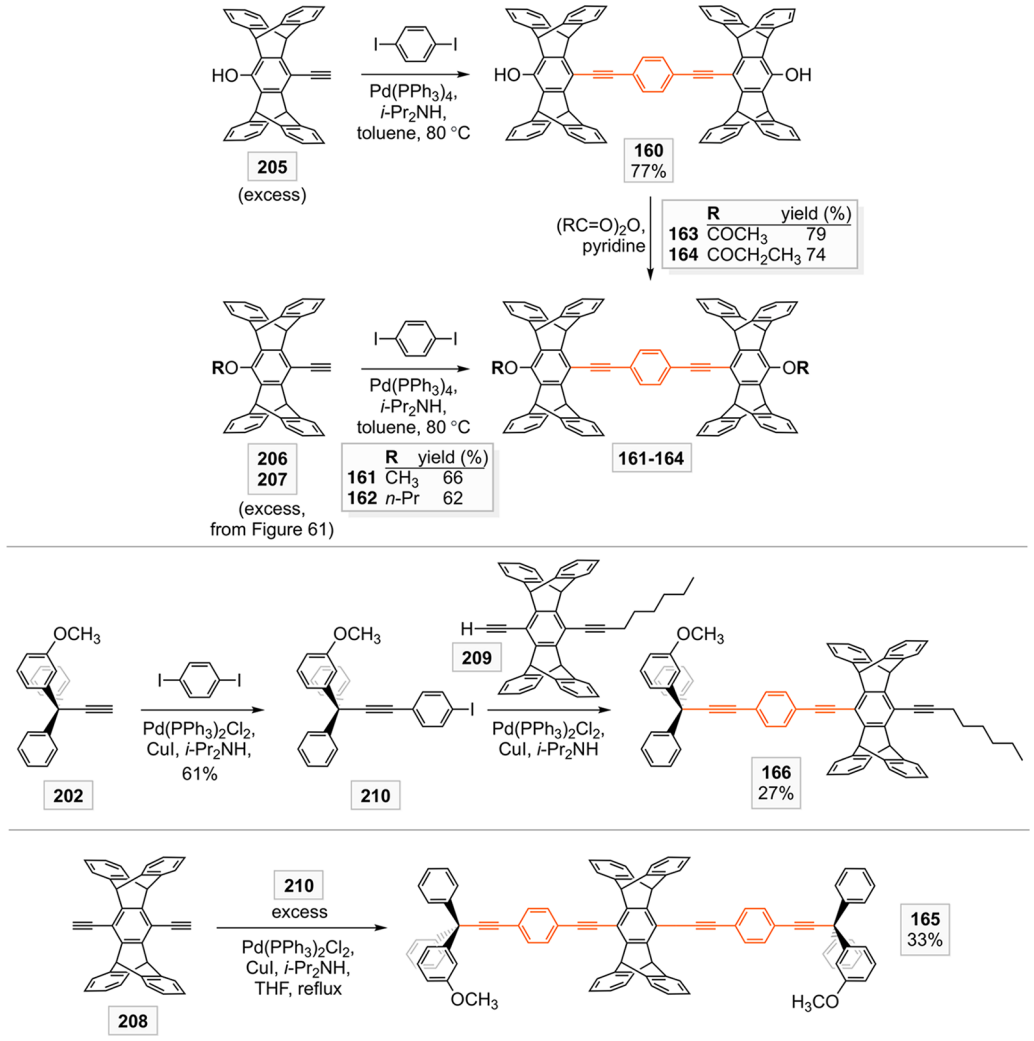

Figure 62. Final steps in the syntheses of molecular rotors **160**−**164** (top), **166** (middle), and **165** (bottom).

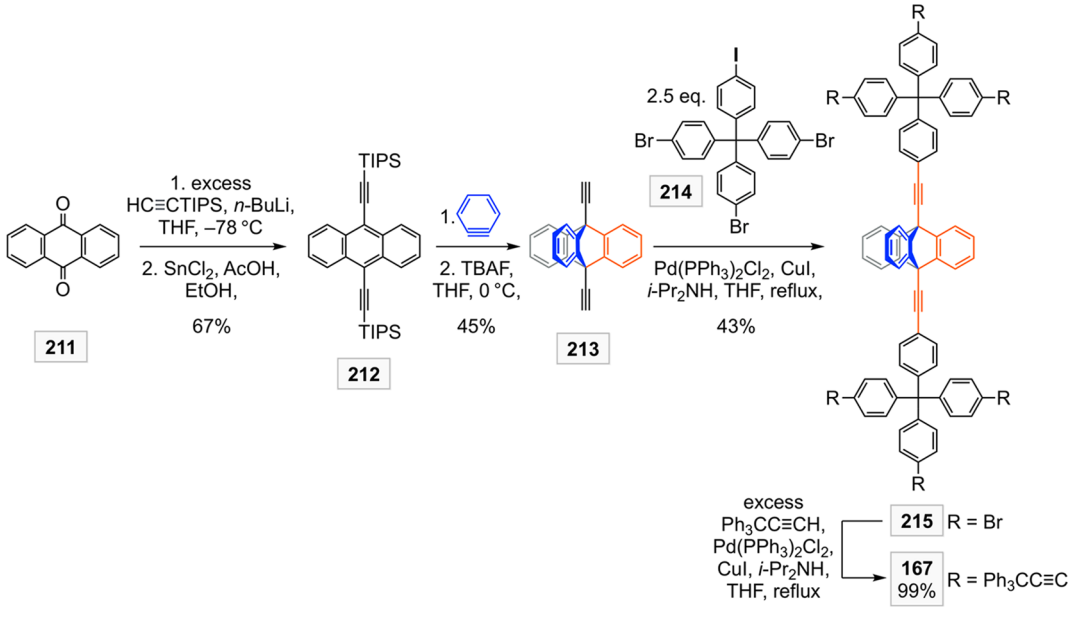

Figure 63. Synthesis of the dendrimer like molecular rotor **167**.

combined with *p*-diiodobenzene under Sonogashira conditions to give **160**−**162**. The hydroxyl groups in **160** can also be derivatized, for example, by acylation to give **163** and **164**. Second, the mixed ethynyl/octynyl compound **209** can be

https://dx.doi.org/10.1021/acs.chemrev.0c01001
Chem. Rev. 2021, 121, 3701−3750

combined with the iodoarene **210** under Sonogashira conditions. This affords **166**, which is comprised of a -C≡C−(p-C_6H_4)−C≡C- rotator and substituted trityl and pentiptycene endgroups. Third, an excess of **210** can be combined with the bis(ethynyl) compound **208** under Sonogashira conditions to give the bis(rotor) **165**, with a central pentiptycene unit.

Finally, as depicted in Figure 63, the dendrimer like rotor **167**, which features a triptycyl rotator, can be prepared in four linear steps from anthraquinone in quite high overall yield.[200] These utilize conditions similar to those applied in the preceding figures.

8.5. Toward Molecular Gyroscopes

The wide-ranging studies of the Garcia-Garibay group have provided a number of tantalizing leads with respect to molecular gyroscopes, especially within the context of amphidynamic crystals. Diverse types of rotors have been engineered with very low E_a values, and dipolar rotators, particularly fluorinated p-phenylenes, are easily introduced. For most any compound or crystal lattice, the principal factors affecting the rotational barriers can be identified. Certain generalizations, such as those embodied in Figure 46, have considerable applicability. However, exceptions can also be identified (e.g., Figure 47). These complicating factors render the realization of molecular gyroscopes more challenging, but the detailed road map provided by the preceding data should nevertheless facilitate future efforts.

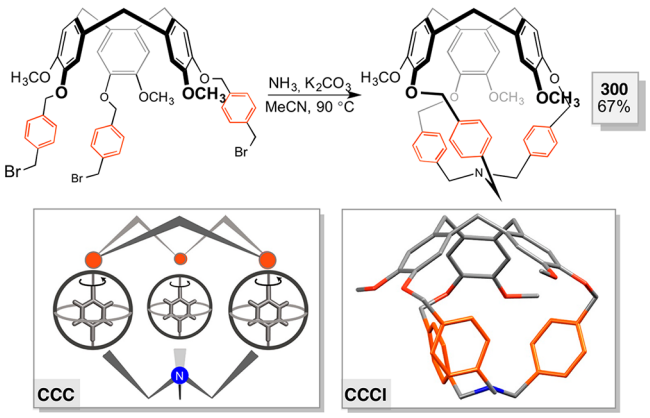

Figure 64. Synthesis and structural representations of a "gyroscope inspired" hemicryptophane (**300**).

9. SYSTEMS FROM OTHER RESEARCH GROUPS

This section collects other reports subsequent to the previous review[33] featuring molecules that have been described as gyroscopes or in some way related to gyroscopes. Since some readers or researchers have need of a comprehensive bibliography, this includes compounds where the connection to gyroscopes may be tenuous. The authors also note (1) a study where the investigators formulated targets viewed as molecular gyroscopes but then encountered synthetic obstacles[218] and (2) papers viewed as germane by reviewers, some of which represent expansions of the scope of this review and in an even handed treatment would necessitate many additional citations.[219,220]

9.1. Rotors Comprised of Covalent Bonds

In a study stated as "gyroscope inspired", the hemicryptophane **300** has been prepared by the 3-fold alkylation of ammonia as shown in Figure 64.[221] This molecule contains three p-phenylene rotators. Variable temperature NMR studies establish a ca. 10 kcal/mol activation energy for rotation in CD_2Cl_2. Rotation of the three rotators appears not to be strongly correlated (i.e., little or no gearing). In this context, compounds with multiple p-phenylene rotators are not intrinsically rare; all appropriately sized [$n.n$]paracyclophanes qualify.

A report with a title claim of molecular gyroscopes is excerpted in Figure 65.[222] The macrocycles **301** and **302**, each of which feature two 2,6-disubstituted aniline moieties, have been condensed with the *trans*-cyclohexane-1,4-dicarboxaldehyde **303** to give the bis(imines) or Schiff bases **304** and **305**. Rotation about the aryl−nitrogen bonds is rapid on the NMR time scale at 298 K in $CDCl_3$. The authors of this review see a closer relationship of **304** and **305** to molecular turnstiles (section 4.1).

9.2. Supramolecularly or Mechanically Bonded Systems and MOFs

Capsules or container molecules comprised of two hemispheric components linked by hydrogen bonds are now well-known.[223] These are often ovoid in shape, as exemplified by the empty capsule **306** in Figure 66.[224,225] Compound **306** can accommodate a single 1,4-acetoxybenzene guest (adduct **307**) or various disubstituted derivatives (**308**−**317**). The crystal structure of dimethoxy substituted **309** in Figure 66, as well as much supporting NMR data, establish that the acetoxy groups and disubstituted p-phenylene (p-$C_6H_2R_2$) rotators are oriented along the long axis of the ovoid capsule.

NMR studies show that for adducts with small 1,4-diacetoxybenzene substituents (R), rotation remains rapid on the NMR time scale even at 218 K (**307**, **308**, **316**, **317**), whereas in others with bulky substituents, rotation remains slow even at 323 K (**314**, **315**). For adducts where the guest substituents have intermediate sizes (**309**−**313**), $\Delta G^{\ddagger}_{298K}$ values of 11.3−17.4 kcal/mol have been determined. It is noteworthy that the adduct with a dipolar difluorinated rotor (**317**) falls into the low barrier group. However, interactions of these assemblies with electric fields will be complicated by the fact that the stator (capsule) is also dipolar, as the top and bottom hemispheres are not identical.

A crystalline supramolecular gyroscope has been claimed in another report.[226] The investigators were able to synthesize an adduct of 18-crown-6, the cation t-$BuNH_3^+$, and the anion $ZnCl_3(H_2O)^-$. Two crystalline phases could be obtained, and the one of most interest (200 K) is depicted in Figure 67. The oxygen atom of the water molecule binds to zinc, and the two hydrogen atoms hydrogen bond to two oxygen atoms of the crown ether that have a 1,3-relationship. At the opposite face of the crown ether, the three hydrogen atoms of the NH_3^+ moiety hydrogen bond to three oxygen atoms that have a 1,3,5-relationship.

The O···HOH···O hydrogen bonds are disordered over three symmetry related sites, suggesting that the water molecule is capable of rotation. Indeed, variable temperature dielectric spectroscopy, molecular dynamics simulations, and other experiments provide strong support for such behavior. An E_a of 10.1 kcal/mol could be established. The NH···O hydrogen bonds are said to remain static. In view of the "tilt" of the water

https://dx.doi.org/10.1021/acs.chemrev.0c01001
Chem. Rev. 2021, 121, 3701−3750

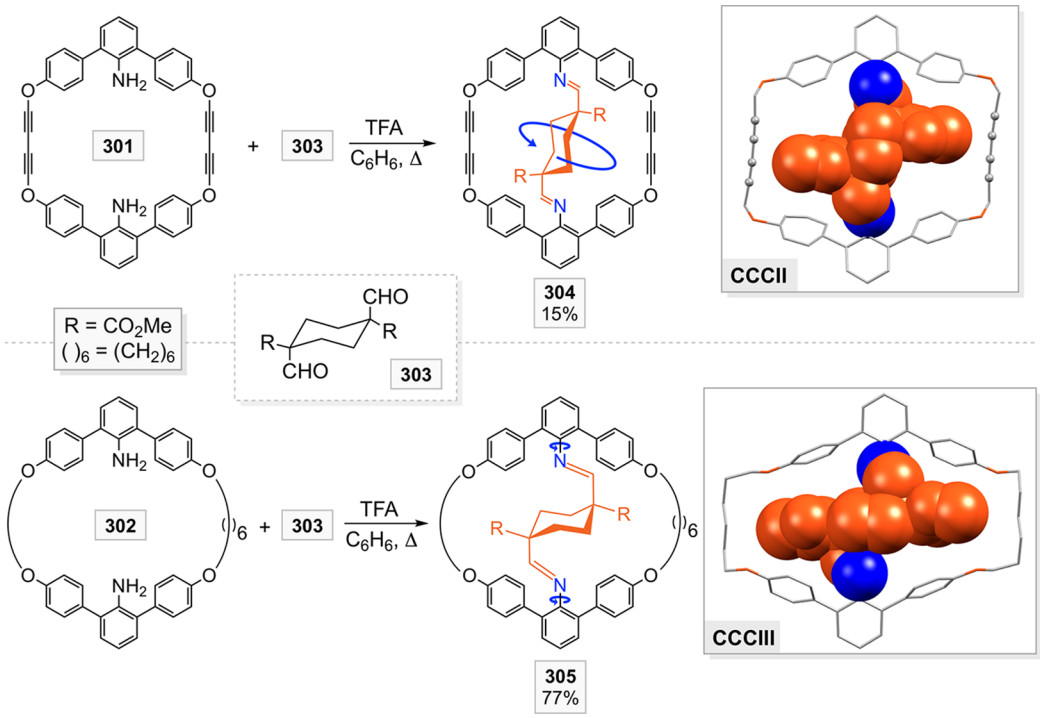

Figure 65. Syntheses and molecular structures of **304** and **305**, which were reported as molecular gyroscopes.

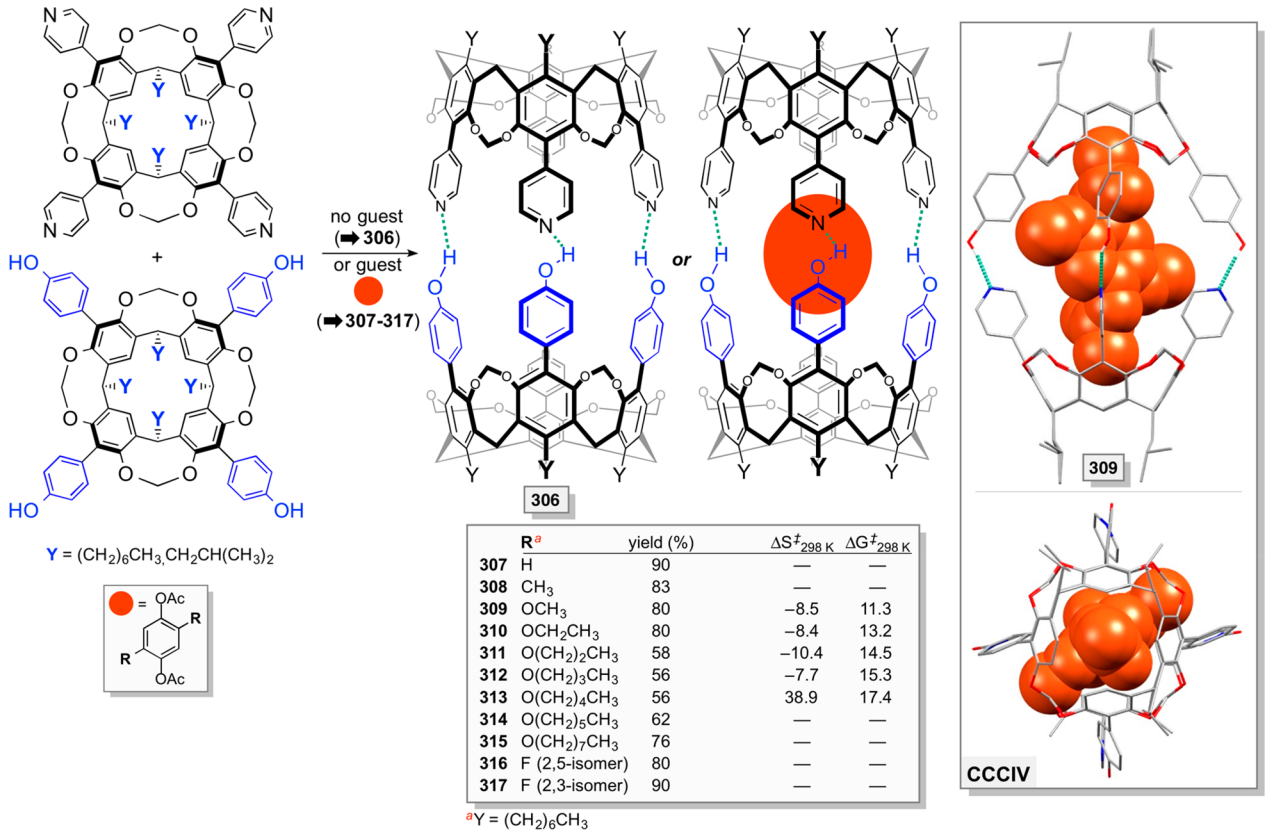

	R[a]	yield (%)	$\Delta S^{\ddagger}_{298\,K}$	$\Delta G^{\ddagger}_{298\,K}$
307	H	90	—	—
308	CH_3	83	—	—
309	OCH_3	80	−8.5	11.3
310	OCH_2CH_3	80	−8.4	13.2
311	$O(CH_2)_2CH_3$	58	−10.4	14.5
312	$O(CH_2)_3CH_3$	56	−7.7	15.3
313	$O(CH_2)_4CH_3$	56	38.9	17.4
314	$O(CH_2)_5CH_3$	62	—	—
315	$O(CH_2)_7CH_3$	76	—	—
316	F (2,5-isomer)	80	—	—
317	F (2,3-isomer)	90	—	—

[a]Y = $(CH_2)_6CH_3$

Figure 66. Self-assembly of gyroscope-like supramolecular systems **307**−**317**, rotational barriers of guest molecules, and crystallographic representations of the dimethoxy substituted adduct **309**.

molecule, **318** qualifies as a dipolar rotator. Similarly to the capsule molecules in Figure 66, the endgroups in **318** are inequivalent, thereby affording a dipolar stator.

Other supramolecular rotators have been reported in the literature, and selected references are supplied.[227,228] There is furthermore additional and often quite informative literature dealing with rotators imbedded in MOFs,[62] some of which is

https://dx.doi.org/10.1021/acs.chemrev.0c01001
Chem. Rev. 2021, 121, 3701−3750

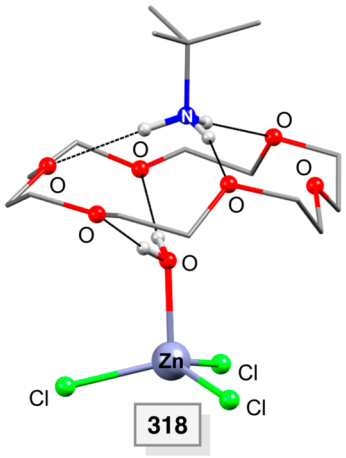

Figure 67. An assembly described as a supramolecular gyroscope (**318**) with a water molecule serving as a dipolar rotator.

cited in the references for section 8.3.2. However, as emphasized above, coverage is restricted to systems for which the authors have sought connections to molecular gyroscopes.

The solid endohedral fullerene $C_2Sc_2@C_{84}$ (**319**)[229] in Figure 68 represents a mechanically bonded system. In an experimental and computational study, the authors observe quantized rotational states for the C_2 unit and other attributes befitting a quantum gyroscope. In the quantum gyroscope literature, introduced in section 1,[23−28] most examples are not molecular in nature.

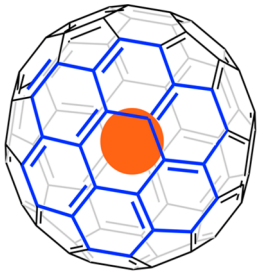

Figure 68. Solid endohedral fullerene $C_2Sc_2@C_{84}$ (**319**), considered an example of a quantum gyroscope.

9.3. Other Rotor Motifs

There has also been great interest in incorporating molecular rotors into porous materials.[220,230] In particular, Michl has explored the use of inclusion compounds to generate arrays of dipolar molecular rotors.[231−236] His workhorse systems are derived from tris(*o*-phenylenedioxy)cyclotriphosphazene (TPP) (**320**), the structure of which is provided in Figure 69. As illustrated by **CCCVI**, this compound can be crystallized with well-defined parallel channels of 4.5−5.0 Å internal diameter located ca. 11.5 Å apart.

Michl has synthesized a variety of complementary shaft like rotors, most of which are dipolar. Representative examples

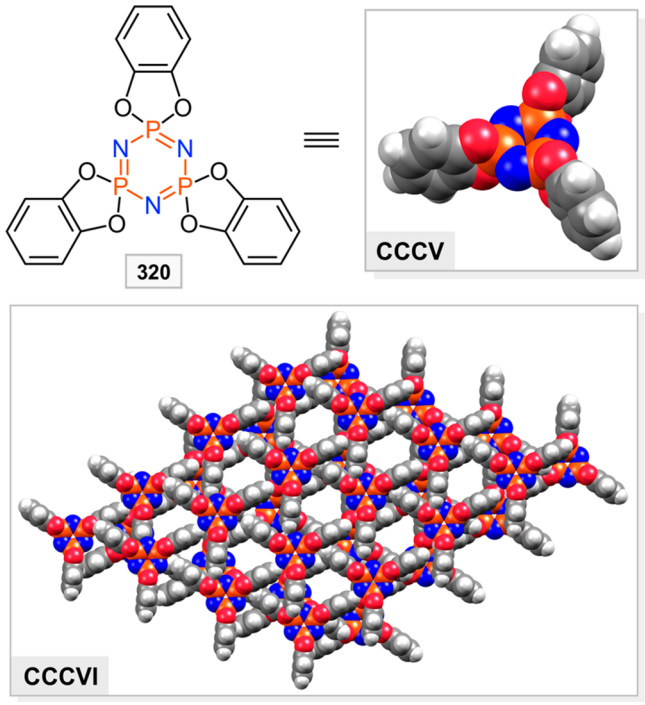

Figure 69. Tris(*o*-phenylenedioxy)cyclotriphosphazene (TPP; **320**), a space filling representation of the molecular structure (**CCCV**), and a top view of the crystal lattice (**CCCVI**).

include **321**−**326** in Figure 70. Some of these are designed to fully intercalate, whereas others have "stoppers" that limit the depth of penetration. The schematic representation **CCCVII** features the rotor **327**, and **CCCVIII** represents an interpretation of NMR and other data with the rotor **324**.

The overarching goal of this work is to characterize rotor dipole/rotor dipole interactions, with the hopes of achieving systems with ferroelectric ground states (dipoles of all rotators aligned). Such materials hold particular promise for certain types of ultrafast microelectronic devices. Dielectric spectroscopy measurements establish very low rotational barriers of 1.2 to 9 kcal/mol. Importantly, these values pertain only to the dipolar subunit of the guest molecules, other segments of which may remain static. In any event, the dipole moments of the embedded rotors respond to an oscillating electric field. Hence, they should also be responsive to a rotating electric field.

10. CONCLUSION

This review has outlined the considerable progress made during the period 2002−2020 toward the realization of functional molecular gyroscopes. A variety of general strategies for sterically protecting rotators and minimizing their rotational barriers have been identified, both in solution and the solid state. These in turn require significant degrees of molecular or crystal engineering. Toward these ends, an impressive underpinning of synthetic methodology has been developed. However, it should also be noted that a few rotors with very low barriers have more or less been identified by serendipity (e.g., **172** in Figure 54), and that fundamental, curiosity driven research may lead to unanticipated breakthroughs.

In the interest of providing readers with a full bibliography, this review has also included studies where an investigator has claimed to prepare a molecular gyroscope, or some related species, but has not fully substantiated or defined what is meant

https://dx.doi.org/10.1021/acs.chemrev.0c01001
Chem. Rev. 2021, 121, 3701−3750

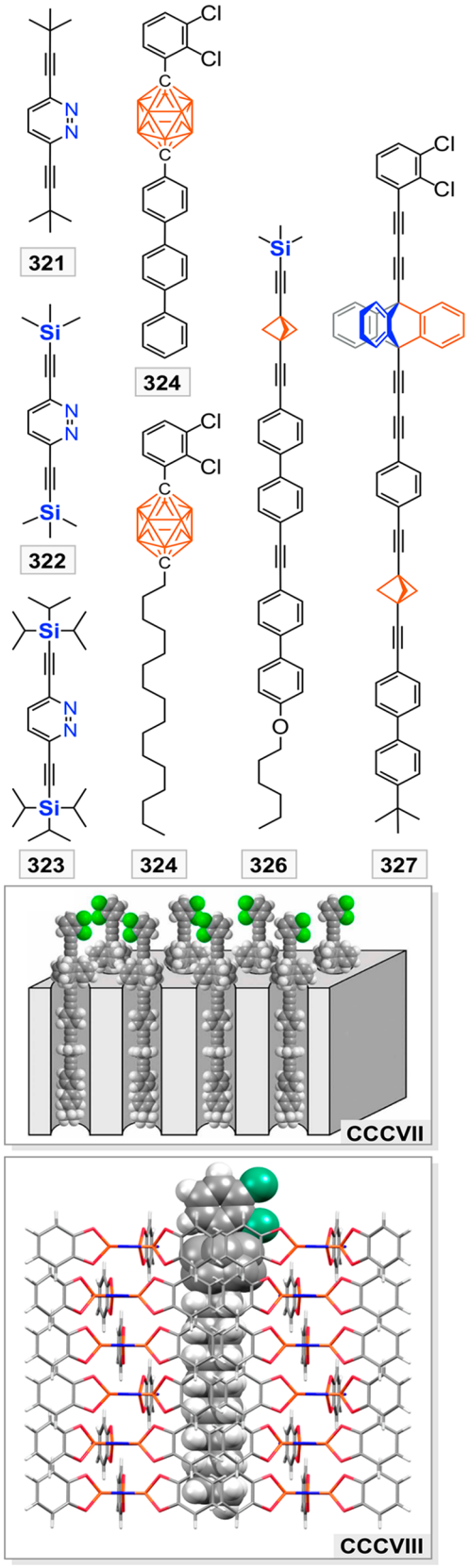

Figure 70. Typical molecular rotors (**321**–**327**) that have been intercalated into the channels of **CCCVI** (Figure 69) and representations of intercalated adducts of **327** (**CCCVII**, reproduced from ref 235. Copyright 2015 American Chemical Society) and **324** (**CCCIII**).

by the claim. For example, the authors have always applied "gyroscope-like" to the compounds from their laboratory highlighted in section 6. For some of the "faux gyroscopes" depicted above, a variety of similar compounds can be found in the literature, but it is beyond the scope of this review to treat them.

Appreciable numbers of the preceding dipolar molecules and assemblies have been studied by dielectric spectroscopy, in which an oscillating electric field is applied to "flip" the orientation of the dipole, or otherwise subjected to electric fields. However, extensions to rotating electric fields or alternative means of promoting unidirectional rotation (more demanding types of experiments)[31] have not yet been reported. This review represents the second installment of a projected trilogy,[33] and based upon the broad scope of progress and interest evident above, it is anticipated that the concluding article will be able to include examples of functional molecular gyroscopes. This will constitute a watershed event in the evolution of molecular devices.

AUTHOR INFORMATION

Corresponding Author

John A. Gladysz − *Department of Chemistry, Texas A&M University, College Station, Texas 77842-3012, United States;* orcid.org/0000-0002-7012-4872; Email: gladysz@mail.chem.tamu.edu

Author

Andreas Ehnbom − *Department of Chemistry, Texas A&M University, College Station, Texas 77842-3012, United States;* orcid.org/0000-0002-7044-1712

Complete contact information is available at: https://pubs.acs.org/10.1021/acs.chemrev.0c01001

Notes

The authors declare no competing financial interest.

Biographies

Andreas Ehnbom obtained his bachelor's and master's degrees in chemistry from Lund University, Sweden, in 2013. This work included studies with Prof. Ebbe Nordlander (Lund, 2009–2011), Prof. Graeme Hogarth (University College London, 2010), Prof. Selwyn Mapolie (Stellenbosch University, 2011), Prof. Suzanne A. Blum (UC Irvine, 2011–2012), Prof. Ola F. Wendt (Lund, 2013), and Prof. Peter Somfai (Lund, 2013–2015, photoredox catalysis). Since June of 2015, he has been exploring computational chemistry in the doctoral program at Texas A&M University (TAMU) in the laboratories of Profs. John A. Gladysz and Michael B. Hall. In 2018, Andreas received a predoctoral von Humboldt fellowship and visited Prof. Carsten Bolm at RWTH Aachen (Germany). Andreas received the CAS SciFinder Future Leader Award and the U.S. Senator Phil Gramm Doctoral Fellowship (TAMU) in 2019.

John A. Gladysz is a native of the Kalamazoo, Michigan, area and since receiving his doctoral degree (Stanford, 1974) has held academic appointments at UCLA, the University of Utah, the Universität Erlangen-Nürnberg, and Texas A&M University. He has received awards in organometallic chemistry from the ACS (1994) and the RSC (2013) and is a Fellow of the ACS (2009) and RSC (2014). From June 1984 through July 2010, he served as Associate Editor of *Chemical Reviews*. He then succeeded Dietmar Seyferth as the Editor in Chief of *Organometallics*, a position he held until January 2015. On the personal side, he is married to Janet Blümel, a Professor of Chemistry at Texas

https://dx.doi.org/10.1021/acs.chemrev.0c01001
Chem. Rev. 2021, 121, 3701−3750

A&M. They live on the Crow's Nest Ranch, which consists of 140 acres (57 hectares) a few miles east of College Station, Texas.

ACKNOWLEDGMENTS

The authors thank the US National Science Foundation (CHE-1153085, CHE-1566601, CHE-1900549) for support and a long-time co-worker on this project, Dr. Tobias Fiedler (2005–2020; deceased 28 October 2020) for the cover graphic, and for teaching one of the authors all there is to know about scientific artwork. Great appreciation and affection is also expressed to Josef Michl, a long-time Editor-in-Chief of this journal (1984–2014)[237] and a mentor of one of the authors for over 40 years.

REFERENCES

(1) See http://www.gyroscopes.org/uses.asp (accessed November 21, 2020). The authors are unaware of any books or peer-reviewed articles that match the diverse examples on the gyroscope.org website, which is maintained by G. Turner.
(2) Crabtree, H. *An elementary treatment of the theory of spinning tops and gyroscopic motion. Merchant Books, unrevealed location*, 2007, ISBN 1-933998-95-4 (http://merchantbooksonline.com).
(3) Armenise, M. N.; Ciminelli, C.; Dell'Olio, F.; Passaro, V. M. N. *Advances in gyroscope technologies*; Springer: Berlin, 2010. ISBN: 978-3-642-15493-5.
(4) This citation and refs 5 and 6 involve medical technologies: Najafi, B.; Aminian, K.; Loew, F.; Blanc, Y.; Robert, P. A. Measurement of stand-sit and sit-stand transitions using a miniature gyroscope and its application in fall risk evaluation in the elderly. *IEEE Trans. Biomed. Eng.* **2002**, *49*, 843–851.
(5) Lim, Y. P.; Brown, I. T.; Khoo, J. C. T. An accurate and robust gyroscope-based pedometer. *2008 30th Annual International Conference IEEE EMBS Conference* **2008**, 4587–4590.
(6) Kim, T. S.; Park, D. D. H.; Lee, B. Y.; Han, D. G.; Shim, J. S.; Lee, Y. J.; Kim, P. C. W. A study on the measurement of wrist motion range using the iPhone 4 gyroscope application. *Ann. Plast. Surg.* **2014**, *73*, 215–218.
(7) Delporte, B.; Perroton, L.; Grandpierre, T.; Trichet, J. Accelerometer and magnetometer based gyroscope emulation on smart sensor for a virtual reality application. *Sensors & Transducers Journal* **2012**, *14*, 32–47.
(8) Rajesh Desai, P.; Nikhil Desai, P.; Deepak Ajmera, K.; Mehta, K. A review paper on oculus rift-a virtual reality headset. *IJETT.* **2014**, *13*, 175–179.
(9) Broquetas, A.; Comerón, A.; Gelonch, A.; Fuertes, J. M.; Castro, J. A.; Felip, D.; López, M. A.; Pulido, J. A. Track detection in railway sidings based on MEMS gyroscope sensors. *Sensors* **2012**, *12*, 16228–16249.
(10) Aroganam, G.; Manivannan, N.; Harrison, D. Review on wearable technology sensors used in consumer sport applications. *Sensors* **2019**, *19*, 1983–2008.
(11) Kumar, N.; Dixit, A. Nanotechnology in futuristic warfare. *Nanotechnology for Defence Applications*; Springer; 2019; section 8.4.2, ISBN-13:978-3-030-29879-1.
(12) Gyroscope self-leveling pool table on the cruise ship *Radiance of the Seas*, (YouTube) https://www.youtube.com/watch?v=N-aE5oszXyQ (accessed November 21, 2020).
(13) Fictional characters are often useful in outreach lectures. The use of gyroscopic stabilizers in Iron Man's flying suit was first described in *Iron Man*, April 1976, Vol. *1*, #85 (see https://www.quora.com/How-do-Tony-Starks-Iron-Man-suits-generate-lift-for-horizontal-flight, accessed November 21, 2020).
(14) This BMW motorcycle balances itself. https://www.usatoday.com/story/money/2016/10/11/bmws-future-vision-includes-self-balancing-motorcycle/91908774/ (accessed November 21, 2020). This new motorcycle uses a gyroscope sensor that allows the rider to never have to put down a foot, even at a standstill.
(15) Butikov, E. Precession and nutation of a gyroscope. *Eur. J. Phys.* **2006**, *27*, 1071–1081.
(16) Kleppner, D.; Kolenkow, R. *An introduction to mechanics*; Cambridge University Press: Cambridge, UK, 2010; Chapters 7.3–7.5.
(17) Passaro, V. M. N.; Cuccovillo, A.; Vaiani, L.; De Carlo, M.; Campanella, C. E. Gyroscope technology and applications: a review in the industrial perspective. *Sensors* **2017**, *17*, 2284–2305.
(18) Yazdi, N.; Ayazi, F.; Najafi, K. Micromachined inertial sensors. *Proc. IEEE* **1998**, *86*, 1640–1659.
(19) See https://en.wikipedia.org/wiki/Vibrating_structure_gyroscope (accessed November 09, 2020). This site has a diverse set of applications of Coriolis Vibratory Gyroscopes (CVG).
(20) Wen, H.; Daruwalla, A.; Ayazi, F. Resonant pitch and roll silicon gyroscopes with sub-micron-gap slanted electrodes: breaking the barrier toward high-performance monolithic inertial measurement units. *Microsyst. & Nanoeng.* **2017**, *3*, 16092.
(21) Wen, H.; Daruwalla, A.; Liu, C. S.; Ayazi, F. A high-frequency resonant framed annulus pitch or roll gyroscope for robust high-performance single-chip inertial measurement units. *J. Microelectromech. Syst.* **2018**, *27*, 995–1008.
(22) Jin, L.; Qin, S.-Y.; Zhang, R.; Li, M.-W. High-sensitivity tunneling magneto-resistive micro-gyroscope with immunity to external magnetic interference. *Sci. Rep.* **2020**, *10*, 16441.
(23) This citation and refs 24–28 are provided as recent lead references: Landon-Cardinal, O.; MacKenzie, R. Decoherence of a quantum gyroscope. *Phys. Rev. A: At., Mol., Opt. Phys.* **2012**, *85*, 022333.
(24) Toro, C.; Liu, Q.; Echebiri, G. O.; Mullin, A. S. Inhibited rotational quenching in oriented ultra-high rotational states of CO2. *Mol. Phys.* **2013**, *111*, 1892–1901.
(25) Kok, P.; Dunningham, J.; Ralph, J. F. Role of entanglement in calibrating optical quantum gyroscopes. *Phys. Rev. A: At., Mol., Opt. Phys.* **2017**, *95*, 012326.
(26) Song, X.; Wang, L.; Diao, W.; Duan, C. Quantum gyroscope based on Berry phase of spins in diamond. *Proc. SPIE* **2018**, *10697*, 106974K.
(27) Song, X.; Wang, L.; Feng, F.; Lou, L.; Diao, W.; Duan, C. Nanoscale quantum gyroscope using a single ^{13}C nuclear spin coupled with a nearby NV center in diamond. *J. Appl. Phys.* **2018**, *123*, 114301.
(28) Tian, T.; Wang, Z.; Song, L. J. Rotation sensing in two coupled whispering-gallery-mode resonators with loss and gain. *Phys. Rev. A: At., Mol., Opt. Phys.* **2019**, *100*, 043810.
(29) Zhang, K.; Zhao, N.; Wang, Y.-H. Closed-loop nuclear magnetic resonance gyroscope based on Rb–Xe. *Sci. Rep.* **2020**, *10*, 2258.
(30) Jobs, S. *iPhone 4's new gyroscope* (YouTube) https://www.youtube.com/watch?v=ORcu-c-qnjg (accessed November 21, 2020).
(31) Kottas, G. S.; Clarke, L. I.; Horinek, D.; Michl, J. Artificial molecular rotors. *Chem. Rev.* **2005**, *105*, 1281–1376.
(32) Dattler, D.; Fuks, G.; Heiser, J.; Moulin, E.; Perrot, A.; Yao, X.; Giuseppone, N. Design of collective motions from synthetic molecular switches, rotors, and motors. *Chem. Rev.* **2020**, *120*, 310–433.
(33) Skopek, K.; Hershberger, M. C.; Gladysz, J. A. Gyroscopes and the chemical literature: 1852–2002. *Coord. Chem. Rev.* **2007**, *251*, 1723–1733.
(34) For reviews by Garcia-Garibay, see refs 35–37 and Garcia-Garibay, M. A. Crystalline molecular machines: encoding supramolecular dynamics into molecular structure. *Proc. Natl. Acad. Sci. U. S. A.* **2005**, *102*, 10771–10776.
(35) Karlen, S. D.; Garcia-Garibay, M. A. Amphidynamic crystals: structural blueprints for molecular machines. *Top. Curr. Chem.* **2005**, *262*, 179–227.
(36) Khuong, T.-A. V.; Nuñez, J. E.; Godinez, C. E.; Garcia-Garibay, M. A. Crystalline molecular machines: a quest toward solid-state dynamics and function. *Acc. Chem. Res.* **2006**, *39*, 413–422.
(37) Howe, M. E.; Garcia-Garibay, M. A. The roles of intrinsic barriers and crystal fluidity in determining the dynamics of crystalline molecular rotors and molecular machines. *J. Org. Chem.* **2019**, *84*, 9835–9849.

https://dx.doi.org/10.1021/acs.chemrev.0c01001
Chem. Rev. 2021, 121, 3701–3750

(38) Magnera, T. F.; Michl, J. Altitudinal surface-mounted molecular rotors. *Top. Curr. Chem.* **2005**, *262*, 63−97.
(39) Vacek, J.; Michl, J. Molecular dynamics of a grid-mounted molecular dipolar rotor in a rotating electric field. *Proc. Natl. Acad. Sci. U. S. A.* **2001**, *98*, 5481−5486.
(40) Arcenegui, J. J.; García-Sánchez, P.; Morgan, H.; Ramos, A. Electric-field-induced rotation of Brownian metal nanowires. *Phys. Rev. E* **2013**, *88*, 033025.
(41) Kopperger, E.; List, J.; Madhira, S.; Rothfischer, F.; Lamb, D. C.; Simmel, F. C. A self-assembled nanoscale robotic arm controlled by electric fields. *Science* **2018**, *359*, 296−301.
(42) Vacek, J.; Michl, J. Artificial surface-mounted molecular rotors: molecular dynamic simulations. *Adv. Funct. Mater.* **2007**, *17*, 730−739.
(43) Horansky, R. D.; Magnera, T. F.; Price, J. C.; Michl, J. Artificial dipolar molecular rotors. *Lect. Notes Phys.* **2007**, *711*, 303−330.
(44) Horinek, D.; Michl, J. Molecular dynamics simulation of an electric field driven dipolar molecular rotor attached to a quartz glass surface. *J. Am. Chem. Soc.* **2003**, *125*, 11900−11910.
(45) Zheng, X.; Mulcahy, M. E.; Horinek, D.; Galeotti, F.; Magnera, T. F.; Michl, J. Dipolar and nonpolar altitudinal molecular rotors mounted on an Au(111) surface. *J. Am. Chem. Soc.* **2004**, *126*, 4540−4542.
(46) Horinek, D.; Michl, J. Surface-mounted altitudinal molecular rotors in alternating electric field: single-molecule parametric oscillator molecular dynamics. *Proc. Natl. Acad. Sci. U. S. A.* **2005**, *102*, 14175−14180.
(47) Jian, H.; Tour, J. M. En route to surface-bound electric field-driven molecular motors. *J. Org. Chem.* **2003**, *68*, 5091−5103.
(48) Hutchison, J. A.; Uji-I, H.; Deres, A.; Vosch, T.; Rocha, S.; Müller, S.; Bastian, A. A.; Enderlein, J.; Nourouzi, H.; Li, C.; Herrmann, A.; et al. A surface-bound molecule that undergoes optically biased Brownian rotation. *Nat. Nanotechnol.* **2014**, *9*, 131−136.
(49) Mulcahy, M. E.; Bastl, Z.; Stensrud, K. F.; Magnera, T. F.; Michl, J. Mercury-mediated attachment of metal-sandwich-based altitudinal molecular rotors to gold surfaces. *J. Phys. Chem. C* **2010**, *114*, 14050−14060.
(50) Caskey, D. C.; Michl, J. Toward self-assembled surface-mounted prismatic altitudinal rotors. A test case: trigonal and tetragonal prisms. *J. Org. Chem.* **2005**, *70*, 5442−5448.
(51) Mulcahy, M. E.; Magnera, T. F.; Michl, J. Molecular rotors on Au(111): rotator orientation from IR spectroscopy. *J. Phys. Chem. C* **2009**, *113*, 20698−20704.
(52) Tierney, H. L.; Baber, A. E.; Jewell, A. D.; Iski, E. V.; Boucher, M. B.; Sykes, E. C. H. Mode-selective electrical excitation of a molecular rotor. *Chem. - Eur. J.* **2009**, *15*, 9678−9680.
(53) Jewell, A. D.; Tierney, H. L.; Baber, A. E.; Iski, E. V.; Laha, M. M.; Sykes, E. C. H. Time-resolved studies of individual molecular rotors. *J. Phys.: Condens. Matter* **2010**, *22*, 264006.
(54) Tierney, H. L.; Calderon, C. E.; Baber, A. E.; Sykes, E. C. H.; Wang, F. Understanding the rotational mechanism of a single molecule: STM and DFT Investigations of dimethyl sulfide molecular rotors on Au(111). *J. Phys. Chem. C* **2010**, *114*, 3152−3155.
(55) Murphy, C. J.; Smith, Z. C.; Pronschinski, A.; Lewis, E. A.; Liriano, M. L.; Wong, C.; Ivimey, C. J.; Duffy, M.; Musial, W.; Therrien, A. J.; et al. Ullmann coupling mediated assembly of an electrically driven altitudinal molecular rotor. *Phys. Chem. Chem. Phys.* **2015**, *17*, 31931−31937.
(56) Wasio, N. A.; Slough, D. P.; Smith, Z. C.; Ivimey, C. J.; Thomas, S. W., III; Lin, Y.-S.; Sykes, E. C. H. Correlated rotational switching in two-dimensional. *Nat. Commun.* **2017**, *8*, 16057.
(57) Balema, T. A.; Ulumuddin, N.; Murphy, C. J.; Slough, D. P.; Smith, Z. C.; Hannagan, R. T.; Wasio, N. A.; Larson, A. M.; Patel, D. A.; Groden, K.; et al. Controlling molecular switching via chemical functionality: ethyl vs methoxy rotors. *J. Phys. Chem. C* **2019**, *123*, 23738−23746.
(58) Vacek, J.; Chocholousova, J.; Michl, J. Calculations for a gas-flow driven molecular rotor. *IEEE* **2007**, 153−157.
(59) Prokop, A.; Vacek, J.; Michl, J. Friction in carborane-based molecular rotors driven by gas flow or electric field: classical molecular dynamics. *ACS Nano* **2012**, *6*, 1901−1914.
(60) Zhou, H.-C.; Long, J. R.; Yaghi, O. M. Introduction to metal-organic frameworks. *Chem. Rev.* **2012**, *112*, 673−674. This article represents the introduction to a thematic issue with many relevant reviews.
(61) Zhou, H.-C.; Kitagawa, S. Metal-organic frameworks (MOFs). *Chem. Soc. Rev.* **2014**, *43*, 5415−5418. This article represents the introduction to a thematic issue with many relevant reviews.
(62) Perego, J.; Bracco, S.; Negroni, M.; Bezuidenhout, C. X.; Prando, G.; Carretta, P.; Comotti, A.; Sozzani, P. Fast motion of molecular rotors in metal-organic framework struts at very low temperatures. *Nat. Chem.* **2020**, *12*, 845−851.
(63) von Hippel, A. R. *Dielectrics and waves*; John Wiley & Sons, New York, 1954.
(64) Daniel, V. V. *Dielectric relaxation*; Academic Press: London, 1967.
(65) McCrum, N. G.; Read, B. E.; Williams, G. *Anelastic and dielectric effects in polymeric solids*; John Wiley & Sons, New York, 1967.
(66) Bedard, T. C.; Moore, J. S. Design and synthesis of a "molecular turnstile". *J. Am. Chem. Soc.* **1995**, *117*, 10662−10671.
(67) Hirata, O.; Takeuchi, M.; Shinkai, S. Allosteric binding of anionic guests to a bicyclic host which imitates the action of a 'turnstile'. *Chem. Commun.* **2005**, 3805−3807.
(68) Carella, A.; Launay, J.-P.; Poteau, R.; Rapenne, G. Synthesis and reactivity of [penta(4-halogenophenyl)cyclopentadienyl][hydrotris-(indazolyl)borato]ruthenium(II) complexes: rotation-induced Fosbury flop in an organometallic molecular turnstile. *Chem. - Eur. J.* **2008**, *14*, 8147−8156.
(69) Weibel, N.; Mishchenko, A.; Wandlowski, T.; Neuburger, M.; Leroux, Y.; Mayor, M. Catechol-based macrocyclic rods: en route to redox-active molecular switches. *Eur. J. Org. Chem.* **2009**, *2009*, 6140−6150.
(70) Yu, C.; Ma, L.; He, J.; Xiang, J.; Deng, X.; Wang, Y.; Chen, X.; Jiang, H. Flexible, linear chains act as baffles to inhibit the intramolecular rotation of molecular turnstiles. *J. Am. Chem. Soc.* **2016**, *138*, 15849−15852.
(71) Wang, G.; Xiao, H.; He, J.; Xiang, J.; Wang, Y.; Chen, X.; Che, Y.; Jiang, H. Molecular turnstiles regulated by metal ions. *J. Org. Chem.* **2016**, *81*, 3364−3371.
(72) Le Pleux, L.; Kapatsina, E.; Hildesheim, J.; Häussinger, D.; Mayor, M. A molecular turnstile as an *E*-field-triggered single-molecule switch: concept and synthesis. *Eur. J. Org. Chem.* **2017**, *2017*, 3165−3178.
(73) Lang, T.; Guenet, A.; Graf, E.; Kyritsakas, N.; Hosseini, M. W. Porphyrin based molecular turnstiles. *Chem. Commun.* **2010**, *46*, 3508−3510.
(74) Lang, T.; Graf, E.; Kyritsakas, N.; Hosseini, M. W. Open and closed states of a porphyrin based molecular turnstile. *Dalton Trans.* **2011**, *40*, 3517−3523.
(75) Lang, T.; Graf, E.; Kyritsakas, N.; Hosseini, M. W. An oscillating molecular turnstile. *Dalton Trans.* **2011**, *40*, 5244−5248.
(76) Guenet, A.; Graf, E.; Kyritsakas, N.; Hosseini, M. W. Porphyrin-based switchable molecular turnstiles. *Chem. - Eur. J.* **2011**, *17*, 6443−6452.
(77) Lang, T.; Graf, E.; Kyritsakas, N.; Hosseini, M. W. Strapped-porphyrin-based molecular turnstiles. *Chem. - Eur. J.* **2012**, *18*, 10419−10426.
(78) Lang, T.; Graf, E.; Kyritsakas, N.; Hosseini, M. W. Zinc- and palladium-porphyrin based turnstiles. *New J. Chem.* **2013**, *37*, 112−118.
(79) Zigon, N.; Guenet, A.; Graf, E.; Kyritsakas, N.; Hosseini, M. W. A platinum turnstile with a palladium lock. *Dalton Trans.* **2013**, *42*, 9740−9745.
(80) Zigon, N.; Larpent, P.; Jouaiti, A.; Kyritsakas, N.; Hosseini, M. W. Optical reading of the open and closed states of a molecular turnstile. *Chem. Commun.* **2014**, *50*, 5040−5042.

https://dx.doi.org/10.1021/acs.chemrev.0c01001
Chem. Rev. 2021, 121, 3701−3750

(81) Zigon, N.; Larpent, P.; Jouaiti, A.; Kyritsakas, N.; Hosseini, M. W. A luminescent molecular turnstile. *Dalton Trans.* **2014**, *43*, 15779−15784.
(82) Zigon, N.; Kyritsakas, N.; Hosseini, M. W. Organometallic turnstiles: acid and base locking and unlocking. *Dalton Trans.* **2014**, *43*, 152−157.
(83) Zigon, N.; Hosseini, M. W. A bi-stable Pt(II) based molecular turnstile. *Chem. Commun.* **2015**, *51*, 12486−12489.
(84) Meshkov, I. N.; Bulach, V.; Gorbunova, Y. G.; Kyritsakas, N.; Grigoriev, M. S.; Tsivadze, A. Y.; Hosseini, M. W. Phosphorus(V) porphyrin-based molecular turnstiles. *Inorg. Chem.* **2016**, *55*, 10774−10782.
(85) Godde, B.; Jouaiti, A.; Fluck, A.; Kyritsakas, N.; Mauro, M.; Hosseini, M. W. Symmetrical or non-symmetrical luminescent turnstiles based on hydroquinone stators and rotors bearing pyridyl or *p*-dimethylaminopyridyl coordinating units. *Dalton Trans.* **2017**, *46*, 14897−14906.
(86) Godde, B.; Ritaine, D.; Jouaiti, A.; Mauro, M.; Hosseini, M. W. A pyridyl-benzimidazole based molecular luminescent turnstile. *New J. Chem.* **2018**, *42*, 7810−7815.
(87) Ng, P. L.; Lambert, J. N. Synthesis of macrocyclic inclusion complexes using olefin metathesis. *Synlett* **1999**, *1999*, 1749−1750.
(88) Zeits, P. D.; Rachiero, G. P.; Hampel, F.; Reibenspies, J. H.; Gladysz, J. A. Gyroscope-like platinum and palladium complexes with *trans*-spanning bis(pyridine) ligands. *Organometallics* **2012**, *31*, 2854−2877.
(89) Rochon, F. D.; Beauchamp, A. L.; Bensimon, C. Multinuclear NMR spectra of $[Pt(L)Cl_3]$- (L = pyridine derivatives) complexes and crystal structure of *trans*-Pt(2,6-di(hydroxymethyl)pyridine)$_2$Cl$_2$·H$_2$O. *Can. J. Chem.* **1996**, *74*, 2121−2130.
(90) Tessier, C.; Rochon, F. D. Multinuclear NMR study and crystal structures of complexes of the types *cis*- and *trans*-$Pt(Ypy)_2X_2$, where Ypy = pyridine derivative and X = Cl and I. *Inorg. Chim. Acta* **1999**, *295*, 25−38.
(91) Shima, T.; Bauer, E. B.; Hampel, F.; Gladysz, J. A. Alkene metatheses in transition metal coordination spheres: dimacrocyclizations that join *trans* positions of square-planar platinum complexes to give topologically novel diphosphine ligands. *Dalton Trans.* **2004**, 1012−1028.
(92) Steigleder, E.; Shima, T.; Lang, G. M.; Ehnbom, A.; Hampel, F.; Gladysz, J. A. Partially shielded $Fe(CO)_3$ rotors: syntheses, structures, and dynamic properties of complexes with doubly *trans* spanning diphosphines, *trans*-$Fe(CO)_3(PhP((CH_2)_n)_2PPh)$. *Organometallics* **2017**, *36*, 2891−2901.
(93) Joshi, H.; Kharel, S.; Bhuvanesh, N.; Gladysz, J. A. Synthesis, structure, and reactivity of doubly *trans*-spanning bis(dialkyl selenide) complexes; a new route to diselenamacrocycles via alkene metathesis in metal coordination spheres. *J. Organomet. Chem.* **2018**, *875*, 80−87.
(94) Stollenz, M.; Joshi, H.; Ehnbom, A.; Fiedler, T.; Kharel, S.; Reibenspies, J. H.; Bhuvanesh, N.; Hall, M. B.; Gladysz, J. A. Platinum complexes containing or derived from olefinic phosphines $P(X)((CH_2)_6CH{=}CH_2)_2$ (X = OH, Ph, $(CH_2)_6CH{=}CH_2$); ring closing metatheses, structures, and *trans*/*cis* isomerizations. *Polyhedron* **2019**, *158*, 325−333.
(95) Setaka, W.; Sato, K.; Ohkubo, A.; Kabuto, C.; Kira, M. Phenylene-bridged polysilaalkane macrocycles as framed molecular rotor. *Chem. Lett.* **2006**, *35*, 596−597.
(96) Phan, S. T.; Setaka, W.; Kira, M. Ring-closing metathesis for the synthesis of phenylene-bridged silamacrocycles. *Chem. Lett.* **2007**, *36*, 1180−1181.
(97) Shima, T.; Hampel, F.; Gladysz, J. A. Molecular gyroscopes: $\{Fe(CO)_3\}$ and $\{Fe(CO)_2(NO)\}^+$ rotators encased in three-spoke stators; facile assembly by alkene metatheses. *Angew. Chem., Int. Ed.* **2004**, *43*, 5537−5540; Molekulare Gyroskope: $\{Fe(CO)_3\}$- und $\{Fe(CO)_2(NO)\}^+$-Rotatoren in einem dreispeichigen Stator; einfache Synthese durch alkenmetathese. *Angew. Chem.* **2004**, *116*, 5653−5656.
(98) Nawara, A. J.; Shima, T.; Hampel, F.; Gladysz, J. A. Gyroscope-like molecules consisting of PdX_2/PtX_2 rotators encased in three-spoke stators: Synthesis via alkene metathesis, and facile substitution and demetalation. *J. Am. Chem. Soc.* **2006**, *128*, 4962−4963.
(99) Wang, L.; Hampel, F.; Gladysz, J. A. 'Giant' gyroscope-like molecules consisting of dipolar Cl−Rh−CO rotators encased in three-spoke stators that define 25−27-membered macrocycles. *Angew. Chem., Int. Ed.* **2006**, *45*, 4372−4375; 'Gyroskop-Giganten': dipolare Cl−Rh−CO-Rotatoren, umgeben von Statoren aus drei Speichen 25- bis 27-gliedriger Makrocyclen. *Angew. Chem.* **2006**, *118*, 4479−4482.
(100) Wang, L.; Shima, T.; Hampel, F.; Gladysz, J. A. Gyroscope-like molecules consisting of three-spoke stators that enclose "switchable" neutral dipolar rhodium rotators; reversible cycling between faster and slower rotating Rh(CO)I and $Rh(CO)_2I$ species. *Chem. Commun.* **2006**, 4075−4077.
(101) Hess, G. D.; Hampel, F.; Gladysz, J. A. Octahedral gyroscope-like molecules with $M(CO)_3(X)$ rotators encased in three-spoked diphosphine stators: Syntheses by alkene metathesis/hydrogenation sequences, structures, dynamic properties, and reactivities. *Organometallics* **2007**, *26*, 5129−5131.
(102) Skopek, K.; Gladysz, J. A. Syntheses of gyroscope-like molecules via three-fold ring closing metatheses of bis(phosphine) complexes *trans*-$L_yM(P((CH_2)_nCH{=}CH_2)_3)_2$, and extensions to bis(phosphite) complexes *trans*-$Fe(CO)_3(P(O(CH_2)_nCH{=}CH_2)_3)_2$. *J. Organomet. Chem.* **2008**, *693*, 857−866.
(103) Nawara-Hultzsch, A. J.; Skopek, K.; Shima, T.; Barbasiewicz, M.; Hess, G. D.; Skaper, D.; Gladysz, J. A. Syntheses and palladium, platinum, and borane adducts of symmetrical trialkylphosphines with three terminal vinyl groups, $P((CH_2)_mCH{=}CH_2)_3$. *Z. Naturforsch., B: J. Chem. Sci.* **2010**, *65b*, 414−424.
(104) Nawara-Hultzsch, A. J.; Stollenz, M.; Barbasiewicz, M.; Szafert, S.; Lis, T.; Hampel, F.; Bhuvanesh, N.; Gladysz, J. A. Gyroscope-like molecules consisting of PdX_2/PtX_2 rotators within three-spoke dibridgehead diphosphine stators: Syntheses, substitution reactions, structures, and dynamic properties. *Chem. - Eur. J.* **2014**, *20*, 4617−4637.
(105) Estrada, A. L.; Jia, T.; Bhuvanesh, N.; Blümel, J.; Gladysz, J. A. Substitution and catalytic chemistry of gyroscope-like complexes derived from Cl−Rh−CO rotators and triply *trans* spanning di(trialkylphosphine) ligands. *Eur. J. Inorg. Chem.* **2015**, *2015*, 5318−5321.
(106) Lang, G. M.; Shima, T.; Wang, L.; Cluff, K. J.; Skopek, K.; Hampel, F.; Blümel, J.; Gladysz, J. A. Gyroscope-like complexes based on dibridgehead diphosphine cages that are accessed by three-fold intramolecular ring closing metatheses and encase $Fe(CO)_3$, $Fe(CO)_2(NO)^+$, and $Fe(CO)_3(H)^+$ rotators. *J. Am. Chem. Soc.* **2016**, *138*, 7649−7663.
(107) Lang, G. M.; Bhuvanesh, N.; Reibenspies, J. H.; Gladysz, J. A. Syntheses, reactivity, structures, and dynamic properties of gyroscope-like iron carbonyl complexes based on dibridgehead diarsine cages. *Organometallics* **2016**, *35*, 2873−2889.
(108) Lang, G. M.; Skaper, D.; Hampel, F.; Gladysz, J. A. Synthesis, reactivity, structures, and dynamic properties of gyroscope like iron complexes with dibridgehead diphosphine cages: Pre- *vs.* post-metathesis substitutions as routes to adducts with neutral dipolar $Fe(CO)(NO)(X)$ rotors. *Dalton Trans.* **2016**, *45*, 16190−16204.
(109) Taher, D.; Nawara-Hultzsch, A. J.; Bhuvanesh, N.; Hampel, F.; Gladysz, J. A. Mono- and disubstitution reactions of gyroscope like complexes derived from Cl−Pt−Cl rotators within cage like dibridgehead diphosphine ligands. *J. Organomet. Chem.* **2016**, *821*, 136−141.
(110) Fiedler, T.; Bhuvanesh, N.; Hampel, F.; Reibenspies, J. H.; Gladysz, J. A. Gyroscope like molecules consisting of trigonal or square planar osmium rotators within three-spoked dibridgehead diphosphine stators: Syntheses, substitution reactions, structures, and dynamic properties. *Dalton Trans.* **2016**, *45*, 7131−7147.
(111) Hess, G. D.; Fiedler, T.; Hampel, F.; Gladysz, J. A. Octahedral gyroscope-like molecules consisting of rhenium rotators within cage-like dibridgehead diphosphine stators: Syntheses, substitution reactions, structures, and dynamic Properties. *Inorg. Chem.* **2017**, *56*, 7454−7469.

https://dx.doi.org/10.1021/acs.chemrev.0c01001
Chem. Rev. 2021, 121, 3701−3750

(112) Kharel, S.; Joshi, H.; Bhuvanesh, N.; Gladysz, J. A. Syntheses, structures, and thermal properties of gyroscope-like complexes consisting of $PtCl_2$ rotators encased in macrocyclic dibridgehead diphosphines $P((CH_2)_n)_3P$ with extended methylene chains (n = 20/22/30) and isomers thereof. *Organometallics* **2018**, *37*, 2991−3000.
(113) Joshi, H.; Kharel, S.; Ehnbom, A.; Skopek, K.; Hess, G. D.; Fiedler, T.; Hampel, F.; Bhuvanesh, N.; Gladysz, J. A. Three-fold intramolecular ring closing alkene metatheses of square planar complexes with *cis* phosphorus donor ligands $P(X(CH_2)_mCH{=}CH_2)_3$ (X = −, m = 5−10; X = O, m = 3−5): Syntheses, structures, and thermal properties of macrocyclic dibridgehead diphosphorus complexes. *J. Am. Chem. Soc.* **2018**, *140*, 8463−8478.
(114) Ruwwe, J.; Martín-Alvarez, J. M.; Horn, C. R.; Bauer, E. B.; Szafert, S.; Lis, T.; Hampel, F.; Cagle, P. C.; Gladysz, J. A. Olefin metatheses in metal coordination spheres: Versatile new strategies for the construction of novel monohapto or polyhapto cyclic, macrocyclic, polymacrocyclic, and bridging ligands. *Chem. - Eur. J.* **2001**, *7*, 3931−3950.
(115) Stahl, J.; Bohling, J. C.; Bauer, E. B.; Peters, T. B.; Mohr, W.; Martín-Alvarez, J. M.; Hampel, F.; Gladysz, J. A. sp carbon chains surrounded by sp^3 carbon double helices: A class of molecules that are accessible by self-assembly and models for "insulated" molecular-scale devices. *Angew. Chem., Int. Ed.* **2002**, *41*, 1871−1876; Von sp^3-Kohlenstoff-Helices umgebene sp-Kohlenstoffketten: eine Klasse von Molekülen, die durch Selbstorganisation zugänglich und Modellverbindungen für 'isolierte' molekulare Bauelemente sind. *Angew. Chem.* **2002**, *114*, 1951−1957.
(116) Horn, C. R.; Martín-Alvarez, J. M.; Gladysz, J. A. Olefin metatheses in metal coordination spheres: A new approach to steric shielding in dirhenium sp carbon chain complexes of the formula $(\eta^5\text{-}C_5Me_5)Re(NO)(PR_3)(C{\equiv}CC{\equiv}CC{\equiv}CC{\equiv}C)(R_3P)(ON)Re(\eta^5\text{-}C_5Me_5)$. *Organometallics* **2002**, *21*, 5386−5393.
(117) Bauer, E. B.; Hampel, F.; Gladysz, J. A. Alkene metatheses in transition metal coordination spheres: Effect of ring size and substitution on the efficiencies of macrocyclizations that join *trans* positions of square-planar platinum complexes. *Organometallics* **2003**, *22*, 5567−5580.
(118) Lewanzik, N.; Oeser, T.; Blümel, J.; Gladysz, J. A. Generation of *trans*-spanning diphosphine ligands via alkene metathesis: Synthesis, structure, and dynamic behavior of a missing link in a series of square-planar platinum complexes. *J. Mol. Catal. A: Chem.* **2006**, *254*, 20−28.
(119) Han, J.; Deng, C.; Fang, R.; Zhao, D.; Wang, L.; Gladysz, J. A. Square-planar palladium complexes with *trans* di- and tribenzylphosphine ligands bearing $O(CH_2)_4CH{=}CH_2$ substituents; two- and three-fold intramolecular ring-closing metatheses. *Organometallics* **2010**, *29*, 3231−3234.
(120) For a representative example of the additional content, see Kharel, S.; Joshi, H.; Bierschenk, S.; Stollenz, M.; Taher, D.; Bhuvanesh, N.; Gladysz, J. A. Homeomorphic isomerization as a design element in container molecules; binding, displacement, and selective transport of MCl_2 species (M = Pt, Pd, Ni). *J. Am. Chem. Soc.* **2017**, *139*, 2172−2175.
(121) Fiedler, T.; Gladysz, J. A. Multifold ring closing olefin metatheses in syntheses of organometallic molecules with unusual connectivities. In *Olefin metathesis - theory and practice*; Grela, K., Ed.; John Wiley & Sons: Hoboken, NJ, 2014; pp 311−328.
(122) Review: Setaka, W.; Inagaki, Y.; Yamaguchi, K. Chemistry of macrocage molecules with a bridged r-electron system as crystalline molecular gyrotops. *Yuki Gosei Kagaku Kyokaishi* **2019**, *77*, 813−822.
(123) Setaka, W.; Yamaguchi, K. Thermal modulation of birefringence observed in a crystalline molecular gyrotop. *Proc. Natl. Acad. Sci. U. S. A.* **2012**, *109*, 9271−9275.
(124) Setaka, W.; Yamaguchi, K. Order-disorder transition of dipolar rotor in a crystalline molecular gyrotop and its optical change. *J. Am. Chem. Soc.* **2013**, *135*, 14560−14563.
(125) Setaka, W.; Yamaguchi, K. A molecular balloon: Expansion of a molecular gyrotop cage due to rotation of the phenylene rotor. *J. Am. Chem. Soc.* **2012**, *134*, 12458−12461.
(126) Setaka, W.; Koyama, A.; Yamaguchi, K. Cage size effects on the rotation of molecular gyrotops with 1,4-naphthalenediyl rotor in solution. *Org. Lett.* **2013**, *15*, 5092−5095.
(127) Setaka, W.; Higa, S.; Yamaguchi, K. Ring-closing metathesis for the synthesis of a molecular gyrotop. *Org. Biomol. Chem.* **2014**, *12*, 3354−3357.
(128) Inagaki, Y.; Yamaguchi, K.; Setaka, W. A crystalline molecular gyrotop with germanium junctions between a phenylene rotor and alkyl spokes. *RSC Adv.* **2014**, *4*, 58624−58630.
(129) Setaka, W.; Inoue, K.; Higa, S.; Yoshigai, S.; Kono, H.; Yamaguchi, K. Synthesis of crystalline molecular gyrotops and phenylene rotation inside the cage. *J. Org. Chem.* **2014**, *79*, 8288−8295.
(130) Shionari, H.; Inagaki, Y.; Yamaguchi, K.; Setaka, W. A pyrene-bridged macrocage showing no excimer fluorescence. *Org. Biomol. Chem.* **2015**, *13*, 10511−10516.
(131) Nishiyama, Y.; Inagaki, Y.; Yamaguchi, K.; Setaka, W. 1,4,-naphthalenediyl-bridged molecular gyrotops: Rotation of the rotor and fluorescence in solution. *J. Org. Chem.* **2015**, *80*, 9959−9966.
(132) Masuda, T.; Arase, J.; Inagaki, Y.; Kawahata, M.; Yamaguchi, K.; Ohhara, T.; Nakao, A.; Momma, H.; Kwon, E.; Setaka, W. Molecular gyrotops with a five-membered heteroaromatic ring: Synthesis, temperature-dependent orientation of dipolar rotors inside the crystal, and its birefringence change. *Cryst. Growth Des.* **2016**, *16*, 4392−4401.
(133) Fujiwara, A.; Inagaki, Y.; Momma, H.; Kwon, E.; Yamaguchi, K.; Kanno, M.; Kono, H.; Setaka, W. A crystalline molecular gyrotop with a biphenylene dirotor and its temperature-dependent birefringence. *CrystEngComm* **2017**, *19*, 6049−6056.
(134) Takashima, H.; Inagaki, Y.; Momma, H.; Kwon, E.; Yamaguchi, K.; Setaka, W. Ferrocene-diyl bridged macrocages: Steric effects of the cage on the redox properties of ferrocene moiety. *Organometallics* **2018**, *37*, 1501−1506.
(135) Tsurunaga, M.; Inagaki, Y.; Momma, H.; Kwon, E.; Yamaguchi, K.; Yoza, K.; Setaka, W. Dielectric relaxation of powdered molecular gyrotops having a thiophene dioxide-diyl as a dipolar rotor. *Org. Lett.* **2018**, *20*, 6934−6937.
(136) Hashimoto, H.; Inagaki, Y.; Momma, H.; Kwon, E.; Setaka, W. Kinetic stabilization of carbazole nitroxides by inclusion in a macrocage and their electron spin resonance characterization. *J. Org. Chem.* **2019**, *84*, 11783−11789.
(137) Hashimoto, H.; Inagaki, Y.; Momma, H.; Kwon, E.; Yamaguchi, K.; Setaka, W. Polarized fluorescence of a crystal having uniaxially oriented molecules by a carbazole-diyl-bridged macrocage. *CrystEngComm* **2019**, *21*, 3910−3914.
(138) Inagaki, Y.; Ueda, S.; Yamaguchi, K.; Setaka, W. A furan-2,5-diyl bridged macrocage as a highly distorted molecular gyrotop. *Chem. Lett.* **2020**, *49*, 1291−1293.
(139) Setaka, W.; Ohmizu, S.; Kabuto, C.; Kira, M. A molecular gyroscope having phenylene rotator encased in three-spoke silicon-based stator. *Chem. Lett.* **2007**, *36*, 1076−1077.
(140) Setaka, W.; Ohmizu, S.; Kira, M. Molecular gyroscope having a halogen-substituted *p*-phenylene rotator and silaalkane chain stators. *Chem. Lett.* **2010**, *39*, 468−469.
(141) Setaka, W.; Ohmizu, S.; Kira, M. Kinetic stabilization against the oxidation reaction induced by a silaalkane cage in a thiophene-bridged molecular gyroscope. *Chem. Commun.* **2014**, *50*, 1098−1100.
(142) For crystallographically characterized examples, see ref 143 and Dixon, F. M.; Eisenberg, A. H.; Farrell, J. R.; Mirkin, C. A.; Liable-Sands, L. M.; Rheingold, A. L. Neutral macrocycles via halide-induced ring opening of binuclear condensed intermediates. *Inorg. Chem.* **2000**, *39*, 3432−3433.
(143) Koshevoy, I. O.; Sizova, O. V.; Tunik, S. P.; Lough, A.; Poë, A. J. A novel five-coordinate rhodium(I) complex. *Eur. J. Inorg. Chem.* **2005**, *2005*, 4516−4520.
(144) Anslyn, E. V.; Dougherty, D. A. *Modern physical organic chemistry*; University Science Books: Sausalito, CA, 2006; pp 97−98.
(145) Eliel, E. N.; Wilen, S. H. *Stereochemistry of organic compounds*; John Wiley & Sons: New York, 1994; pp 624−629 and 1142−1155.

https://dx.doi.org/10.1021/acs.chemrev.0c01001
Chem. Rev. 2021, 121, 3701−3750

(146) The dipoles approximately bisect the OC−Fe−NO angles, with the negative ends extending between the two oxygen atoms. See endnote 34 of ref 108.
(147) Horansky, R. D.; Clarke, L. I.; Price, J. C.; Khuong, T.-A. V.; Jarowski, P. D.; Garcia-Garibay, M. A. Dielectric response of a dipolar molecular rotor crystal. *Phys. Rev. B: Condens. Matter Mater. Phys.* **2005**, *72*, 014302.
(148) Horansky, R. D.; Clarke, L. I.; Winston, E. B.; Price, J. C.; Karlen, S. D.; Jarowski, P. D.; Santillan, R.; Garcia-Garibay, M. A. Dipolar rotor-rotor interactions in a difluorobenzene molecular rotor crystal. *Phys. Rev. B: Condens. Matter Mater. Phys.* **2006**, *74*, 054306.
(149) Pickardt, J.; Rösch, L.; Schumann, H. Die Kristallstruktur von Tetracarbonyl(tri-*t*-butylphosphin)eisen. *J. Organomet. Chem.* **1976**, *107*, 241−248.
(150) Rheingold, A. L.; Fountain, M. E. Tetracarbonyl(tri-*tert*-butylstibine)iron, $[Fe(CO)_4\{Sb(C_4H_9)_3\}]$. *Acta Crystallogr., Sect. C: Cryst. Struct. Commun.* **1985**, *C41*, 1162−1164.
(151) Breunig, H. J.; Borrmann, T.; Lork, E.; Moldovan, O.; Rat, C. I.; Wagner, R. P. Syntheses, crystal structures and DFT studies of $[Me_3EM(CO)_5]$ (E = Sb, Bi; M = Cr, W), *cis*-$[(Me_3Sb)_2Mo(CO)_4]$, and $[^tBu_3BiFe(CO)_4]$. *J. Organomet. Chem.* **2009**, *694*, 427−432.
(152) Bauer, E. B.; Hampel, F.; Gladysz, J. A. Alkyne metatheses in transition metal coordination spheres: Convenient tungsten- and molybdenum-catalyzed syntheses of novel metallamacrocycles. *Adv. Synth. Catal.* **2004**, *346*, 812−822.
(153) Prack, E.; O'Keefe, C. A.; Moore, J. K.; Lai, A.; Lough, A. J.; Macdonald, P. M.; Conradi, M. S.; Schurko, R. W.; Fekl, U. A Molecular rotor possessing an H−M−H "spoke" on a P−M−P "axle": A platinum(II) *trans*-dihydride spins rapidly even at 75 K. *J. Am. Chem. Soc.* **2015**, *137*, 13464−13467.
(154) Yogendra, S.; Hennersdorf, F.; Bauzá, A.; Frontera, A.; Fischer, R.; Weigand, J. J. Carbodiphosphorane mediated synthesis of a triflyloxyphosphonium dication and its reactivity towards nucleophiles. *Chem. Commun.* **2017**, *53*, 2954−2957.
(155) Marahatta, A. B.; Kanno, M.; Hoki, K.; Setaka, W.; Irle, S.; Kono, H. Theoretical investigation of the structures and dynamics of crystalline molecular gyroscopes. *J. Phys. Chem. C* **2012**, *116*, 24845−24854.
(156) Dominguez, Z.; Dang, H.; Strouse, M. J.; Garcia-Garibay, M. A. Molecular "compasses" and "gyroscopes". I. Expedient synthesis and solid state dynamics of an open rotor with a bis(triarylmethyl) frame. *J. Am. Chem. Soc.* **2002**, *124*, 2398−2399.
(157) Godinez, C. E.; Zepeda, G.; Garcia-Garibay, M. A. Molecular compasses and gyroscopes. II. Synthesis and characterization of molecular rotors with axially substituted bis[2-(9-triptycyl)ethynyl]-arenes. *J. Am. Chem. Soc.* **2002**, *124*, 4701−4707.
(158) Dominguez, Z.; Dang, H.; Strouse, M. J.; Garcia-Garibay, M. A. Molecular 'compasses' and 'gyroscopes.' III. Dynamics of a phenylene rotor and clathrated benzene in a slipping-gear crystal lattice. *J. Am. Chem. Soc.* **2002**, *124*, 7719−7727.
(159) Dominguez, Z.; Khuong, A.-T. V.; Dang, H.; Sanrame, C. N.; Nuñez, J. E.; Garcia-Garibay, M. A. Molecular compasses and gyroscopes with polar rotors: Synthesis and characterization of crystalline forms. *J. Am. Chem. Soc.* **2003**, *125*, 8827−8837.
(160) Khuong, T.-A. V.; Zepeda, G.; Ruiz, R.; Khan, S. I.; Garcia-Garibay, M. A. Molecular compasses and gyroscopes: Engineering molecular crystals with fast internal rotation. *Cryst. Growth Des.* **2004**, *4*, 15−18.
(161) Czajkowska-Szczykowska, D.; Aguilar-Granda, A.; Maj, J.; Wilczewska, A. Z.; Witkowski, S.; Santillan, R.; Garcia-Garibay, M. A.; Morzycki, J. W.; Rodríguez-Molina, B. Solid state characterization of bridged steroidal molecular rotors: Effect of the rotator fluorination on their crystallization. *Cryst. Growth Des.* **2016**, *16*, 1599−1605.
(162) Rodriguez-Molina, B.; Farfán, N.; Romero, M.; Méndez-Stivalet, J. M.; Santillan, R.; Garcia-Garibay, M. A. Anisochronous dynamics in a crystalline array of steroidal molecular rotors: Evidence of correlated motion within 1D helical domains. *J. Am. Chem. Soc.* **2011**, *133*, 7280−7283.
(163) Rodríguez-Molina, B.; Pérez-Estrada, S.; Garcia-Garibay, M. A. Amphidynamic crystals of a steroidal bicyclo[2.2.2]octane rotor: A high symmetry group that rotates faster than smaller methyl and methoxy groups. *J. Am. Chem. Soc.* **2013**, *135*, 10388−10395.
(164) Rodríguez-Molina, B.; Ochoa, M. E.; Romero, M.; Khan, S. I.; Farfán, N.; Santillan, R.; Garcia-Garibay, M. A. Conformational polymorphism and isomorphism of molecular rotors with fluoroaromatic rotators and mestranol stators. *Cryst. Growth Des.* **2013**, *13*, 5107−5115.
(165) Czajkowska-Szczykowska, D.; Rodríguez-Molina, B.; Magaña-Vergara, N. E.; Santillan, R.; Morzycki, J. W.; Garcia-Garibay, M. A. Macrocyclic molecular rotors with bridged steroidal frameworks. *J. Org. Chem.* **2012**, *77*, 9970−9978.
(166) Pérez-Estrada, S.; Rodríguez-Molina, B.; Xiao, L.; Santillan, R.; Jimenéz-Osés, G.; Houk, K. N.; Garcia-Garibay, M. A. Thermodynamic evaluation of aromatic CH/π interactions and rotational entropy in a molecular rotor. *J. Am. Chem. Soc.* **2015**, *137*, 2175−2178.
(167) Pérez-Estrada, S.; Rodríguez-Molina, B.; Maverick, E. F.; Khan, S. I.; Garcia-Garibay, M. A. Throwing in a monkey wrench to test and determine geared motion in the dynamics of a crystalline one-dimensional (1D) columnar rotor array. *J. Am. Chem. Soc.* **2019**, *141*, 2413−2420.
(168) Khuong, T.-A. V.; Zepeda, G.; Sanrame, C. N.; Dang, H.; Bartberger, M. D.; Houk, K. N.; Garcia-Garibay, M. A. Crankshaft motion in a highly congested bis(triarylmethyl)peroxide. *J. Am. Chem. Soc.* **2004**, *126*, 14778−14786.
(169) Stopin, A.; Garcia-Garibay, M. A. Crystals and aggregates of a molecular tetrarotor with multiple trityl embraces derived from tetraphenyladamantane. *Cryst. Growth Des.* **2012**, *12*, 3792−3798.
(170) Torres-Huerta, A.; Rodríguez-Molina, B.; Höpfl, H.; Garcia-Garibay, M. A. Synthesis and solid-state characterization of self-assembled macrocyclic molecular rotors of bis(dithiocarbamate) ligands with diorganotin(IV). *Organometallics* **2014**, *33*, 354−362.
(171) Scudder, M.; Dance, I. Dimorphic intra- and intermolecular aryl motifs in symmetrical hexafaceted molecules $(Ar_nX)_3Y-Z-Y-(XAr_n)_3$. *Chem. - Eur. J.* **2002**, *8*, 5456−5468.
(172) Dance, I.; Scudder, M. Crystal supramolecularity: Elaborate six-, eight- and twelve-fold concerted phenyl embraces in compounds $[M(PPh_3)_3]_z$ and $[M(PPh_3)_4]$. *New J. Chem.* **1998**, *22*, 481−492.
(173) Gavezzotti, A. The calculation of molecular volumes and the use of volume analysis in the investigation of structured media and of solid-state organic reactivity. *J. Am. Chem. Soc.* **1983**, *105*, 5220−5225.
(174) Nangia, A. Pseudopolymorph: Retain this widely accepted term. *Cryst. Growth Des.* **2006**, *6*, 2−4.
(175) Commins, P.; Nuñez, J. E.; Garcia-Garibay, M. A. Synthesis of bridged molecular gyroscopes with closed topologies: Triple one-pot macrocyclization. *J. Org. Chem.* **2011**, *76*, 8355−8363.
(176) Nuñez, J. E.; Natarajan, A.; Khan, S. I.; Garcia-Garibay, M. A. Synthesis of a triply-bridged molecular gyroscope by a directed meridional cyclization strategy. *Org. Lett.* **2007**, *9*, 3559−3561.
(177) O'Brien, Z. J.; Karlen, S. D.; Khan, S.; Garcia-Garibay, M. A. Solid-state molecular rotors with perdeuterated stators: Mechanistic insights from biphenylene rotational dynamics in ordered and disordered crystal forms. *J. Org. Chem.* **2010**, *75*, 2482−2491.
(178) Karlen, S. D.; Garcia-Garibay, M. A. Highlighting gyroscopic motion in crystals in ^{13}C CPMAS spectra by specific isotopic substitution and restricted cross polarization. *Chem. Commun.* **2005**, 189−191.
(179) Gardinier, J. R.; Pellechia, P. J.; Smith, M. D. Ionic rotors. Preparation, structure, and dynamic solid-state ^2D NMR study of the 1,4-diethynylbenzenebis(triphenylborate) dianion. *J. Am. Chem. Soc.* **2005**, *127*, 12448−12449.
(180) Santillán, R.; Karlen, S. D.; Dang, H.; Garcia-Garibay, M. A. Synthesis and characterization of natural abundance and isotopically labeled 1,4-bis(3,3,3-triphenylpropynyl)-2,3-difluorobenzene. A molecular gyroscope with a polar rotator. *J. Mex. Chem. Soc.* **2008**, *52*, 125−129.
(181) Rodriguez-Molina, B.; Ochoa, M. E.; Farfán, N.; Santillan, R.; Garcia-Garibay, M. A. Synthesis, characterization, and rotational

https://dx.doi.org/10.1021/acs.chemrev.0c01001
Chem. Rev. 2021, 121, 3701−3750

dynamics of crystalline molecular compasses with *N*-heterocyclic rotators. *J. Org. Chem.* **2009**, *74*, 8554−8565.
(182) Karlen, S. D.; Reyes, H.; Taylor, R. E.; Khan, S. I.; Hawthorne, M. F.; Garcia-Garibay, M. A. Symmetry and dynamics of molecular rotors in amphidynamic molecular crystals. *Proc. Natl. Acad. Sci. U. S. A.* **2010**, *107*, 14973−14977.
(183) Colvin, E. W. *Silicon in Organic Synthesis*; Butterworth: London, 1981; Table 2.1. ISBN 0-408-1083102.
(184) Akimov, A. V.; Kolomeisky, A. B. Molecular dynamics study of crystalline molecular gyroscopes. *J. Phys. Chem. C* **2011**, *115*, 13584−13591.
(185) Jin, M.; Chung, T. S.; Seki, T.; Ito, H.; Garcia-Garibay, M. A. Phosphorescence control mediated by molecular rotation and aurophilic interactions in amphidynamic crystals of 1,4-bis[tri-(*p*-fluorophenyl)phosphane-gold(I)-ethynyl]benzene. *J. Am. Chem. Soc.* **2017**, *139*, 18115−18121.
(186) Jin, M.; Yamamoto, S.; Seki, T.; Ito, H.; Garcia-Garibay, M. A. Anisotropic thermal expansion as the source of macroscopic and molecular scale motion in phosphorescent amphidynamic crystals. *Angew. Chem., Int. Ed.* **2019**, *58*, 18003−18010; *Angew. Chem.* **2019**, *131*, 18171−18178.
(187) Karlen, S. D.; Ortiz, R.; Chapman, O. L.; Garcia-Garibay, M. A. Effects of rotational symmetry order on the solid state dynamics of phenylene and diamantane rotators. *J. Am. Chem. Soc.* **2005**, *127*, 6554−6555.
(188) Arcos-Ramos, R.; Rodriguez-Molina, B.; Gonzalez-Rodriguez, E.; Ramirez-Montes, P. I.; Ochoa, M. E.; Santillan, R.; Farfán, N.; Garcia-Garibay, M. A. Crystalline arrays of molecular rotors with TIPS-trityl and phenolic-trityl stators using phenylene, 1,2-difluorophenylene and pyridine rotators. *RSC Adv.* **2015**, *5*, 55201−55208.
(189) Nuñez, J. E.; Khuong, T.-A. V.; Campos, L. M.; Farfán, N.; Dang, H.; Karlen, S. D.; Garcia-Garibay, M. A. Crystal phases and phase transitions in a highly polymorphogenic solid-state molecular gyroscope with *meta*-methoxytrityl frames. *Cryst. Growth Des.* **2006**, *6*, 866−873.
(190) Arcos-Ramos, R.; Rodríguez-Molina, B.; Romero, M.; Méndez-Stivalet, J. M.; Ochoa, M. E.; Ramírez-Montes, P. I.; Santillan, R.; Garcia-Garibay, M. A.; Farfań, N. Synthesis and evaluation of molecular rotors with large and bulky *tert*-butyldiphenylsilyloxy-substituted trityl stators. *J. Org. Chem.* **2012**, *77*, 6887−6894.
(191) Jiang, X.; O'Brien, Z. J.; Yang, S.; Lai, L. H.; Buenaflor, J.; Tan, C.; Khan, S.; Houk, K. N.; Garcia-Garibay, M. A. Crystal fluidity reflected by fast rotational motion at the core, branches, and peripheral aromatic groups of a dendrimeric molecular rotor. *J. Am. Chem. Soc.* **2016**, *138*, 4650−4656.
(192) Khuong, T.-A. V.; Dang, H.; Jarowski, P. D.; Maverick, E. F.; Garcia-Garibay, M. A. Rotational dynamics in a crystalline molecular gyroscope by variable-temperature ^{13}C NMR, ^{2}H NMR, X-ray diffraction, and force field calculations. *J. Am. Chem. Soc.* **2007**, *129*, 839−845.
(193) The E_a value quoted for the rotation of the *p*-phenylene unit of **140** in Figure 15 of ref 37, a perspective article (4.4 kcal/mol), is a typographical error (see Table 5 of this review for correct values from earlier papers).
(194) O'Brien, Z. J.; Natarajan, A.; Khan, S.; Garcia-Garibay, M. A. Synthesis and solid-state rotational dynamics of molecular gyroscopes with a robust and low density structure built with a phenylene rotator and a tri(*meta*-terphenyl)methyl stator. *Cryst. Growth Des.* **2011**, *11*, 2654−2659.
(195) Garcia-Garibay, M. A.; Godinez, C. E. Engineering crystal packing and internal dynamics in molecular gyroscopes by refining their components. Fast exchange of a phenylene rotator by ^{2}H NMR. *Cryst. Growth Des.* **2009**, *9*, 3124−3128.
(196) Godinez, C. E.; Zepeda, G.; Mortko, C. J.; Dang, H.; Garcia-Garibay, M. A. Molecular crystals with moving parts: Synthesis, characterization, and crystal packing of molecular gyroscopes with methyl-substituted triptycyl frames. *J. Org. Chem.* **2004**, *69*, 1652−1662.
(197) Karlen, S. D.; Godinez, C. E.; Garcia-Garibay, M. A. Improved physical properties and rotational dynamics in a molecular gyroscope with an asymmetric stator structure. *Org. Lett.* **2006**, *8*, 3417−3420.
(198) Escalante-Sánchez, E.; Rodríguez-Molina, B.; Garcia-Garibay, M. A. Toward crystalline molecular rotors with linearly conjugated diethynyl-phenylene rotators and pentiptycene stators. *J. Org. Chem.* **2012**, *77*, 7428−7434.
(199) Hughs, M.; Jimenez, M.; Khan, S.; Garcia-Garibay, M. A. Synthesis, rotational dynamics, and photophysical characterization of a crystalline linearly conjugated phenyleneethynylene molecular dirotor. *J. Org. Chem.* **2013**, *78*, 5293−5302.
(200) Jiang, X.; Rodríguez-Molina, B.; Nazarian, N.; Garcia-Garibay, M. A. Rotation of a bulky triptycene in the solid state: Toward engineered nanoscale artificial molecular machines. *J. Am. Chem. Soc.* **2014**, *136*, 8871−8874.
(201) Alameddine, B.; Baig, N.; Shetty, S.; Al-Sagheer, F.; Al-Mousawi, S. Microwave-assisted [4 + 2] Diels-Alder cycloaddition of 1,4-Diethynyl triptycene with various cyclopentadienone derivatives: Promising building blocks for polymer networks. *Asian J. Org. Chem.* **2018**, *7*, 378−382.
(202) Howe, M. E.; Garcia-Garibay, M. A. Fluorescence and rotational dynamics of a crystalline molecular rotor featuring an aggregation-induced emission fluorophore. *J. Org. Chem.* **2019**, *84*, 9570−9576.
(203) Colin-Molina, A.; Karothu, D. P.; Jellen, M. J.; Toscano, R. A.; Garcia-Garibay, M. A.; Naumov, P.; Rodríguez-Molina, B. Thermosalient amphidynamic molecular machines: Motion at the molecular and macroscopic scales. *Matter* **2019**, *1*, 1033−1046.
(204) Lemouchi, C.; Vogelsberg, C. S.; Zorina, L.; Simonov, S.; Batail, P.; Brown, S.; Garcia-Garibay, M. A. Ultra-fast rotors for molecular machines and functional materials via halogen bonding: Crystals of 1,4-bis(iodoethynyl)bicyclo[2.2.2]octane with distinct gigahertz rotation at two sites. *J. Am. Chem. Soc.* **2011**, *133*, 6371−6379.
(205) Catalano, L.; Pérez-Estrada, S.; Terraneo, G.; Pilati, T.; Resnati, G.; Metrangolo, P.; Garcia-Garibay, M. A. Dynamic characterization of crystalline supramolecular rotors assembled through halogen bonding. *J. Am. Chem. Soc.* **2015**, *137*, 15386−15389.
(206) Catalano, L.; Perez-Estrada, S.; Wang, H.-H.; Ayitou, A. J.-L.; Khan, S. I.; Terraneo, G.; Metrangolo, P.; Brown, S.; Garcia-Garibay, M. A. Rotational dynamics of diazabicyclo[2.2.2]octane in isomorphous halogen-bonded co-crystals: Entropic and enthalpic effects. *J. Am. Chem. Soc.* **2017**, *139*, 843−848.
(207) Simonov, S.; Zorina, L.; Wzietek, P.; Rodríguez-Fortea, A.; Canadell, E.; Mézière, C.; Bastien, G.; Lemouchi, C.; Garcia-Garibay, M. A.; Batail, P. Static modulation wave of arrays of halogen interactions transduced to a hierarchy of nanoscale change stimuli of crystalline rotors dynamics. *Nano Lett.* **2018**, *18*, 3780−3784.
(208) Lemouchi, C.; Mézière, C.; Zorina, L.; Simonov, S.; Rodríguez-Fortea, A.; Canadell, E.; Wzietek, P.; Auban-Senzier, P.; Pasquier, C.; Giamarchi, T.; et al. Design and evaluation of a crystalline hybrid of molecular conductors and molecular rotors. *J. Am. Chem. Soc.* **2012**, *134*, 7880−7891.
(209) Jiang, X.; Duan, H.-B.; Jellen, M. J.; Chen, Y.; Chung, T. S.; Liang, Y.; Garcia-Garibay, M. A. Thermally activated transient dipoles and rotational dynamics of hydrogen-bonded and charge-transferred diazabicyclo[2.2.2]octane molecular rotors. *J. Am. Chem. Soc.* **2019**, *141*, 16802−16809.
(210) Gould, S. L.; Tranchemontagne, D.; Yaghi, O. M.; Garcia-Garibay, M. A. Amphidynamic character of crystalline MOF-5: Rotational dynamics of terephthalate phenylenes in a free-volume, sterically unhindered environment. *J. Am. Chem. Soc.* **2008**, *130*, 3246−3247.
(211) Morris, W.; Taylor, R. E.; Dybowski, C.; Yaghi, O. M.; Garcia-Garibay, M. A. Framework mobility in the metal-organic framework crystal IRMOF-3: Evidence for aromatic ring and amine rotation. *J. Mol. Struct.* **2011**, *1004*, 94−101.
(212) Winston, E. B.; Lowell, P. J.; Vacek, J.; Chocholoušová, J.; Michl, J.; Price, J. C. Dipolar molecular rotors in the metal-organic

https://dx.doi.org/10.1021/acs.chemrev.0c01001
Chem. Rev. 2021, 121, 3701−3750

framework crystal IRMOF-2. *Phys. Chem. Chem. Phys.* **2008**, *10*, 5188−5191.
(213) Jiang, X.; Duan, H.-B.; Khan, S. I.; Garcia-Garibay, M. A. Diffusion-controlled rotation of triptycene in a metal-organic framework (MOF) sheds light on the viscosity of MOF-confined solvent. *ACS Cent. Sci.* **2016**, *2*, 608−613.
(214) Vogelsberg, C. S.; Uribe-Romo, F. J.; Lipton, A. S.; Yang, S.; Houk, K. N.; Brown, S.; Garcia-Garibay, M. A. Ultrafast rotation in an amphidynamic crystalline metal organic framework. *Proc. Natl. Acad. Sci. U. S. A.* **2017**, *114*, 13613−13618.
(215) Liepuoniute, I.; Huynh, C. M.; Perez-Estrada, S.; Wang, Y.; Khan, S.; Houk, K. N.; Garcia-Garibay, M. A. Enhanced rotation by ground state destabilization in amphidynamic crystals of a dipolar 2,3-difluorophenylene rotator as established by solid state ^{2}H NMR and dielectric spectroscopy. *J. Phys. Chem. C* **2020**, *124*, 15391−15398.
(216) Khudozhitkov, A. E.; Kolokolov, D. I.; Stepanov, A. G.; Bolotov, V. A.; Dybtsev, D. N. Metal-cation-independent dynamics of phenylene ring in microporous MOFs: A ^{2}H solid-state NMR study. *J. Phys. Chem. C* **2015**, *119*, 28038−28045.
(217) Yang, J.-S.; Swager, T. M. Fluorescent porous polymer films as TNT chemosensors: Electronic and structural effects. *J. Am. Chem. Soc.* **1998**, *120*, 11864−11873.
(218) Martin, J. R.; Hastings, S. D.; Freeman, J. L.; Gray, G. M. Synthesis, characterization and the thermal isomerization mechanism of a series of *trans*-tetracarbonyl-bis(phosphinite)molybdenum(0) complexes and an evaluation of their potential to form heterobimetallic compounds. *J. Organomet. Chem.* **2014**, *751*, 695−702.
(219) Huang, F.; Wang, G.; Ma, L.; Wang, Y.; Chen, X.; Che, Y.; Jiang, H. Molecular spur gears based on a switchable quinquepyridine foldamer acting as a stator. *J. Org. Chem.* **2017**, *82*, 12106−12111.
(220) Inukai, M.; Fukushima, T.; Hijikata, Y.; Ogiwara, N.; Horike, S.; Kitagawa, S. Control of molecular rotor rotational frequencies in porous coordination polymers using a solid-solution approach. *J. Am. Chem. Soc.* **2015**, *137*, 12183−12186.
(221) Khan, N. S.; Perez-Aguilar, J. M.; Kaufmann, T.; Hill, P. A.; Taratula, O.; Lee, O.-S.; Carroll, P. J.; Saven, J. G.; Dmochowski, I. J. Multiple hindered rotators in a gyroscope-inspired tribenzylamine hemicryptophane. *J. Org. Chem.* **2011**, *76*, 1418−1424.
(222) Sugino, H.; Kawai, H.; Fujiwara, K.; Suzuki, T. Molecular gyroscope with a *trans*-cyclohexane-1,4-diimine rotor unit: Isolation and characterization of a geometric isomer as a formal intermediate of hindered rotation. *Chem. Lett.* **2012**, *41*, 79−81.
(223) Conn, M. M.; Rebek, J., Jr. Self-assembling capsules. *Chem. Rev.* **1997**, *97*, 1647−1668.
(224) Kitagawa, H.; Kobori, Y.; Yamanaka, M.; Yoza, K.; Kobayashi, K. Encapsulated-guest rotation in a self-assembled heterocapsule directed toward a supramolecular gyroscope. *Proc. Natl. Acad. Sci. U. S. A.* **2009**, *106*, 10444−10448. The authors thank Prof. Kobayashi for a personal communication clarifying some of the yield data in Figure 66.
(225) See also Kobayashi, K.; Ishii, K.; Yamanaka, M. Orientational isomerism and binding ability of nonsymmetrical guests encapsulated in a self-assembling heterodimeric capsule. *Chem. - Eur. J.* **2005**, *11*, 4725−4734.
(226) Li, W.; He, C.-T.; Zeng, Y.; Ji, C.-M.; Du, Z.-Y.; Zhang, W.-X.; Chen, X.-M. Crystalline supramolecular gyroscope with a water molecule as an ultrasmall polar rotator modulated by charge-assisted hydrogen bonds. *J. Am. Chem. Soc.* **2017**, *139*, 8086−8089.
(227) Jose, D.; Datta, A. Molecular rotor inside a phosphonate cavitand: Role of supramolecular interactions. *J. Phys. Chem. Lett.* **2010**, *1*, 1363−1366. In their concluding paragraph, these authors speculated that structural modifications of their system could lead to (thermal) unidirectional rotation of the rotator.
(228) Huang, R.-K.; Xiao, Z.-F.; Liu, D.-X.; Zhang, W.-X.; Chen, X.-M. Unprecedented water-controlled rotator-stator conversion of supramolecular rotors in crystals. *Chem. Commun.* **2019**, *55*, 7159−7162.
(229) Krause, M.; Hulman, M.; Kuzmany, H.; Dubay, O.; Kresse, G.; Vietze, K.; Seifert, G.; Wang, C.; Shinohara, H. Fullerene quantum gyroscope. *Phys. Rev. Lett.* **2004**, *93*, 137403.
(230) Comotti, A.; Bracco, S.; Sozzani, P. Molecular rotors built in porous materials. *Acc. Chem. Res.* **2016**, *49*, 1701−1710.
(231) Zhao, K.; Dron, P. I.; Kaleta, J.; Rogers, C. T.; Michl, J. Arrays of dipolar molecular rotors in tris(*o*-phenylenedioxy)cyclotriphosphazene. *Top. Curr. Chem.* **2014**, *354*, 163−212.
(232) Kobr, L.; Zhao, K.; Shen, Y.; Comotti, A.; Bracco, S.; Shoemaker, R. K.; Sozzani, P.; Clark, N. A.; Price, J. C.; Rogers, C. T.; et al. Inclusion compound based approach to arrays of artificial dipolar molecular rotors. A surface inclusion. *J. Am. Chem. Soc.* **2012**, *134*, 10122−10131.
(233) Kobr, L.; Zhao, K.; Shen, Y.; Polívková, K.; Shoemaker, R. K.; Clark, N. A.; Price, J. C.; Rogers, C. T.; Michl, J. Inclusion compound based approach to arrays of artificial dipolar molecular rotors: Bulk inclusions. *J. Org. Chem.* **2013**, *78*, 1768−1777.
(234) Kobr, L.; Zhao, K.; Shen, Y.; Shoemaker, R. K.; Rogers, C. T.; Michl, J. Tris-*o*-phenylenedioxycyclotriphosphazene (TPP) inclusion compounds containing a dipolar molecular rotor. *Cryst. Growth Des.* **2014**, *14*, 559−568.
(235) Kaleta, J.; Dron, P. I.; Zhao, K.; Shen, Y.; Císařová, I.; Rogers, C. T.; Michl, J. Arrays of molecular rotors with triptycene stoppers: Surface inclusion in hexagonal tris(*o*-phenylenedioxy)-cyclotriphosphazene. *J. Org. Chem.* **2015**, *80*, 6173−6192.
(236) Dron, P. I.; Zhao, K.; Kaleta, J.; Shen, Y.; Wen, J.; Shoemaker, R. K.; Rogers, C. T.; Michl, J. Bulk Inclusions of pyridazine-based molecular rotors in tris(*o*-phenylenedioxy)cyclotriphosphazene (TPP). *Adv. Funct. Mater.* **2016**, *26*, 5718−5732.
(237) Michl, J. Farewell editorial. *Chem. Rev.* **2015**, *115*, 1−2.

https://dx.doi.org/10.1021/acs.chemrev.0c01001
Chem. Rev. 2021, 121, 3701−3750